Chemical Reactions at Nuclear Fuel-Clad Interfaces.

Submitted by

Ivan Hubert Robins

for the degree of Doctor of Philosophy

of the

University of Aston in Birmingham.

October 1976

SUMMARY.

This thesis presents a study of the chemical reactions that may occur at the fuel-clad interfaces of fuel elements used in advanced gas-cooled reactors (A.G.R.).

The initial investigation involved a study of the inner surfaces of irradiated stainless steel clad (20%Cr/25%Ni/niobium stabilised) and evidence was obtained to show that fission products, in particular tellurium, were associated with reaction products on these surfaces. An accelerated rate of oxidation was observed on the inner surfaces of a failed A.G.R. fuel pin. It is believed that fission product caesium was responsible for this enhancement.

A fundamental study of the reaction between 20%Cr/25%Ni/niobium stabilised stainless steel and tellurium was then undertaken over the range 350° - 850°C. Reaction occurred with increasing rapidity over this range and long term exposure at ≥ 750°C resulted in intergranular attack of the stainless steel and chromium depletion. The reaction on unoxidised steel surfaces involved the formation of an initial iron-nickel-tellurium layer which subsequently transformed to a chromium telluride product during continued exposure. The thermodynamic stabilities of the steel tellurides were determined to be chromium telluride > nickel telluride > iron telluride. Oxidation of the stainless steel surface prior to tellurium exposure inhibited the reaction. However reaction did occur in regions where the oxide layer had either cracked or spalled.

CONTENTS.

CHAPTER ONE. INTRODUCTION.

The generation of electricity in the United Kingdom relies on three major sources of energy; i.e. coal, oil and nuclear power. Electricity generation from nuclear fuels accounts for over one-tenth of all electricity produced by the Central Electricity Generating Board (C.E.G.B.) in England and Wales and in Scotland the proportion is even higher (i.e. over one-fifth).

Reactors based on the advanced gas-cooled system (A.G.R.) form the second generation of reactors to be built in the British nuclear power programme. Table 1 presents details of the A.G.R. stations in service as well as those still under construction. They have been developed from the earlier Magnox series of reactors that were instigated at the time of the Suez crisis in 1956. Although the Magnox power stations produce cheaper electricity than the best oil or coal fired power stations (Table 2) the metallurgical limitations of the fuel cladding material restricts the reactor operating temperature and thereby the overall efficiency to about 25%.

The A.G.R. is based on a fuel of enriched uranium dioxide clad in stainless steel, a carbon dioxide coolant and a graphite moderator. Fuel elements are concentrated in relatively few channels and the increase in rating and power density achieved results in higher carbon dioxide gas outlet temperatures and a thermal efficiency of approximately 40%.

The use of stainless steel as a fuel cladding has several advantages. It is relatively cheap, it can be

TABLE 1.

C.A.G.R. Stations in Operation or Under Construction within the U.K.

Station	Output (MW)	On load
Dungeness B	1200	1977
Hinkley Point B	1250	1976
Hunterston B	1250	1976
Hartlepool	1250	1979
Heysham	1250	1979

TABLE 2.

Generation Costs of C.E.G.B. Power Stations.

Fuel	Cost (pence per KW hour)			
	1972/73	1973/74	1974/75	1975/76
Coal	0.49	0.53	0.74	0.97
Oil	0.40	0.55	0.88	1.09
Nuclear	0.48	0.52	0.48	0.67

These values are those for power stations commissioned during the last 12 years and therefore exclude older, less efficient plant. (Eadie, 1975; The Times, 1976).

fabricated easily and it has adequate strength at high temperature. However because it has a relatively high neutron absorption cross-section it is necessary to use enriched fuel.

Uranium dioxide is used as the fuel because of its good corrosion resistance, its dimensional stability against radiation and its high melting point. It does, however, possess a lower thermal conductivity than uranium metal and is fairly brittle.

The principal life limiting feature of a nuclear fuel element is the integrity of its cladding; the cladding retains the fuel, protects it from any corrosive effect of the coolant and retains fission products. It must be able to maintain these properties under the operating conditions of the reactor and should therefore have suitable chemical, mechanical, nuclear and physical properties to withstand the operating temperature, any corrosive effect of the coolant, the induced stresses and the gamma and neutron radiation of its environment. Although the strain on the cladding due to a combination of internal pressure from fission gas release and forces from fuel swelling may limit the lifetime of the fuel element any chemical interaction between the fuel and the cladding material might accelerate these physical effects and ultimately cause failure of the cladding. In such cases this could result in a release of radioactivity to the coolant and the possible development of operational and environmental problems.

The steel chosen for the cladding is a 20%Cr/25%Ni/ niobium stabilised stainless steel; extensive oxidation studies within the United Kingdom Atomic Energy Authority (U.K.A.E.A.),

the C.E.G.B. and the Consortia have established that this material should perform satisfactorily at 850°C for up to 40,000 hours (Cowen and Webster, 1973). Above this temperature intergranular penetration occurs which is of particular concern when the fuel is power cycled, since propagation of the penetration would be anticipated leading to premature failure.

At the inner surface of the steel cladding there is some evidence to show that a reaction can occur between the fuel and the clad but this does not appear to contribute to failures observed to date. Nevertheless intergranular attack and reaction products have been observed at the clad inner surface of fast reactor fuels (see literature survey page 6). Thus the possibility of a fuel-clad reaction being a contributing or even an initiating parameter in fuel failure in A.G.R.'s has to be considered.

This thesis describes a study which examines the extent to which the A.G.R. fuel cladding might be affected by fuel-clad reactions. The literature regarding such reactions has been reviewed and shows that the majority of citations relate to the American fast breeder reactors where severe attack of the clad wall has been observed. A post irradiation examination of the inner surfaces of fuel cladding removed from the Windscale A.G.R. has been undertaken to identify the reaction products present and a basic study of the compatibility of a volatile fission product, tellurium, and 20%Cr/25%Ni/niobium-stabilised stainless steel has also been made. Finally the technical implications to the nuclear industry of the data obtained are discussed.

CHAPTER TWO. LITERATURE SURVEY.

2.1. Introduction.

In this section literature relevant to the compatibility of iron and nickel based alloys with uranium dioxide and mixed uranium/plutonium oxide fuels is reviewed to assess the importance of any reactions on fuel performance. Data on unirradiated uranium dioxide is examined as well as the more complex irradiated system. The latter contains fission products produced during the irradiation and the compatibility of these with the alloys is also considered.

2.2. Out-of-pile Uranium Dioxide-Alloy Compatibility Studies.

The compatibility of unirradiated uranium dioxide with various alloy steels or nickel based alloys has been examined for periods up to 5000 hours and at temperatures up to 1600°C by a number of workers (Cunningham, Beaver, Thurber and Waugh, 1958; Christensen, 1963; Pritchard, Johnson and Leary, 1963; Lauritzen and Comprelli, 1967; USAEC Report, 1967; Lauritzen, 1968; Smith, 1969b; Rosen, Simmons, Aitken, Frost, Tevebaugh and Sheely, 1971). The general conclusion from these studies is that a reaction between the uranium dioxide and the alloys does not occur. The studies of Götzmann and Thümmler (1968) showed that stoicheiometric and hypostoicheiometric uranium dioxide were both compatible with steel and nickel alloys up to 1300°C. However Götzmann (1969) observed that hyperstoicheiometric uranium dioxide was capable of causing the oxidation of high chromium steels and nickel

based alloys at 800°C. Lauritzen (1968) and workers at General Electric (Skavdahl and Zebroski, 1967a, 1967b, 1968) also observed reactions after 1000 hours at 760°C between both Incoloy 800* and stainless steel (types 304, 316, 321 and 347) and hyperstoicheiometric mixed oxide fuel; with type 347 stainless steel a reaction zone of up to 35μm was observed. It was implied from this work that the oxygen content of the fuel was important in producing an oxidising environment.

2.3. Post Irradiation Data.

The earliest data on reactions involving irradiated uranium dioxide and stainless steel were reported by Barney and Wemple (1958). The products formed were attributed to the presence of silicon in the steel and to the availability of oxygen which was released following uranium fission.

The majority of studies of fuel-clad reactions reported in the open literature originate from the American fast breeder reactor system. Unclassified British data on the Dounreay fast reactor (D.F.R.) summarised in a paper by Batey and Bagley (1974) shows that approximately a third of the irradiated oxide fuel pins examined had undergone sporadic attack of the inner surface of the cladding. Most of the available data relate to stainless steel clad fuels although there are also some references to the performance of nickel-chromium alloys.

---

*The basic composition of this and other alloys cited in this thesis is given in Appendix 1.

The effects which have been observed include:-

a) the development of surface reaction layers,

b) intergranular penetration

and c) the production of subsurface porosity.

The first two effects are the most common in steel clad fuels with the attack sometimes being enhanced at fuel pellet interfaces and cracks in the fuel. In addition some of the major elements in the clad have been observed along cracks and as inclusions in the fuel.

The evidence accumulating suggests that fuel-clad reactions could initiate a failure process. Post irradiation burst tests on 304, 304L and 316 stainless steels have shown that intergranular fracture occurs at drastically lower stresses than would normally be expected. There was a substantial reduction in ductility in cans suffering from this type of attack suggesting the clad would tolerate less deformation before failure (Fish, Holmes and Leggett, 1970; Ring, Challenger and Busboom, 1972). Hoechel (1971) has also shown that both Incoloy 800 and Inconel 625 clad fuel pins can fail due to a chemical interaction after burn-ups of 80,000 MWD/te in a thermal flux irradiation at temperatures just below 700°C.

Analysis of reaction layers has revealed the presence of fission products, fuel, fuel impurities and the major elemental components of the clad (USAEC Report, 1967; Perry and Craig, 1969; Andriessen, Hoppe, Tavernier and Soenen, 1970; Simon, Lindgren, Siltanen and Fitts, 1970; Fitts, Long and Leitnaker, 1971; Perry, Melde and Duncan, 1971; Perry, Melde, McCarthy and Duncan, 1971; Calais, Conte, Koroulas and Le Beuze,

1972; Keroulas, Le Beuze, Calais, Van Craeynest and Conte, 1972). However the distribution of the elements in the products does not appear to form a consistent pattern, which suggests that different mechanisms might exist depending on the operating conditions. There is also evidence which indicates that grain boundary penetration occurs only after a reaction product has formed on the surface (Fitts et al., 1971).

In many of the studies caesium, iodine and tellurium have been the fission products observed most frequently in reaction products and zones of intergranular penetration (Lauritzen, Novak and Davies, 1966; Adams, 1967; Neimark, Brown, Natesh, Petkus and Murphy, 1969; Perry and Craig, 1969; Andriessen et al., 1970; Bailey and Zebroski, 1970; Fitts et al., 1971; Johnson and Crouthamel, 1971a; McCarthy, Bennett, Hull and Perry, 1971; Niemark and Lambert, 1971; Weber and Jensen, 1971; Calais et al., 1972; Keroulas et al, 1972; Skinner and Newbigging, 1973; Batey and Bagley, 1974). Their roles in the reactions have not been established with certainty. Some evidence (Rubin and Perry, 1969; Maiya, 1971) indicates that the chromium from the steel could be present in the reaction product as a mixed oxide with alkali and alkaline earth fission products; it has also been suggested that the transfer of iron and nickel into the fuel matrix involves the formation and decomposition of ferrous and nickel iodides (Johnson and Crouthamel, 1970). Such a mechanism might account for the "rivers" of iron which have been detected along fuel cracks for distances up to approximately 500μm. (Fitts, Long and Cuneo, 1970; Simon et al., 1970; Fitts et al., 1971).

Reactions involving impurities in the fuel can be promoted by a high fuel centre temperature and thermal gradient in oxide fuels. Skinner and Newbigging (1973) have observed silicon in reaction zones of A.G.R. fuel pins. Also the formation of silicides of the major clad components has been observed at clad temperatures above 710°C (Batey and Bagley, 1974). It was suggested that the reaction involved the production of SiO, which is stable at high temperatures; this is then transported in the vapour phase along radial cracks in the fuel to the clad inner surface. Whereas reactions with silicon impurities have not been apparent in D.F.R., reactions with the carbon impurity in the fuel have been observed. Carbon levels in the clad have been raised from 0.05% to approximately 0.2% when the carbon impurity content of the fuel was not greater than 50ppm. It is believed that carbon was transported to the clad surface along fuel cracks as CO/CO_2. Batey and Bagley (1974) have also detected CrN in irradiated stainless steel cladding. This was attributed to diffusion of the nitrogen impurity in the fuel into the clad surface and reaction with the chromium constituent.

Perry et al., (1971) have shown a relationship between clad penetration and temperature and other workers suggest that the temperature threshold for a reaction to occur is in the region of 500° - 600°C (Fitts et al., 1971; McCarthy, Perry, Hull and Bennett, 1972). A correlation between clad penetration and burn-up has been observed by Kwast (1971); for fuel pins of similar temperature history an increasing attack with increasing burn-up was observed. In addition fuel density appears to be important with low

density fuel having a high level of clad attack and vice versa. However many workers now believe that the oxygen potential in the fuel pin, which is related to the fuel stoicheiometry, is the most important factor in initiating fuel-clad reactions (Cox, Olsen, Fitts and Long, 1971; Johnson and Crouthamel, 1971a and b; Weber and Jensen, 1971; Coquerelle, Cabolde, Lesser and Werner,1972). Thus the data presented by Weber and Jensen (1971) shows that above a threshold temperature of approximately 550°C initially hypostoicheiometric fuel undergoes less reaction with the cladding than stoicheiometric fuel (Figure 1). High burn-up irradiation experiments by Coquerelle et al., (1972) also confirm that with an initial oxygen/metal ratio of 1.94 no significant clad reaction occurs in mixed oxide fuel with a clad temperature of 650°C (in this case Inconel 625), whereas corrosion was observed with stoicheiometric fuel. Oxygen enhancement in irradiated cladding (approximately 3000ppm compared with 50 - 100ppm in the unirradiated material) has also been observed (Johnson, Crouthamel, Chen and Blackburn, 1969; Blackburn, Johnson, Battles, Johnson, Markin, Tetenbaum, Crouthamel, Tevebaugh and Vogel, 1971) with significant concentrations in grain boundaries together with caesium and molybdenum.

The effect of the oxygen/metal ratio on fuel-clad reactions in irradiated specimens does not directly compare with compatibility data obtained with unirradiated material (see section 2.2); it must therefore be concluded that additional factors are involved with irradiated fuels. In this respect it has been suggested (Keroulas, Le Bouze, Calais and Marcon, 1971; Keroulas et al., 1972) that the reactions may

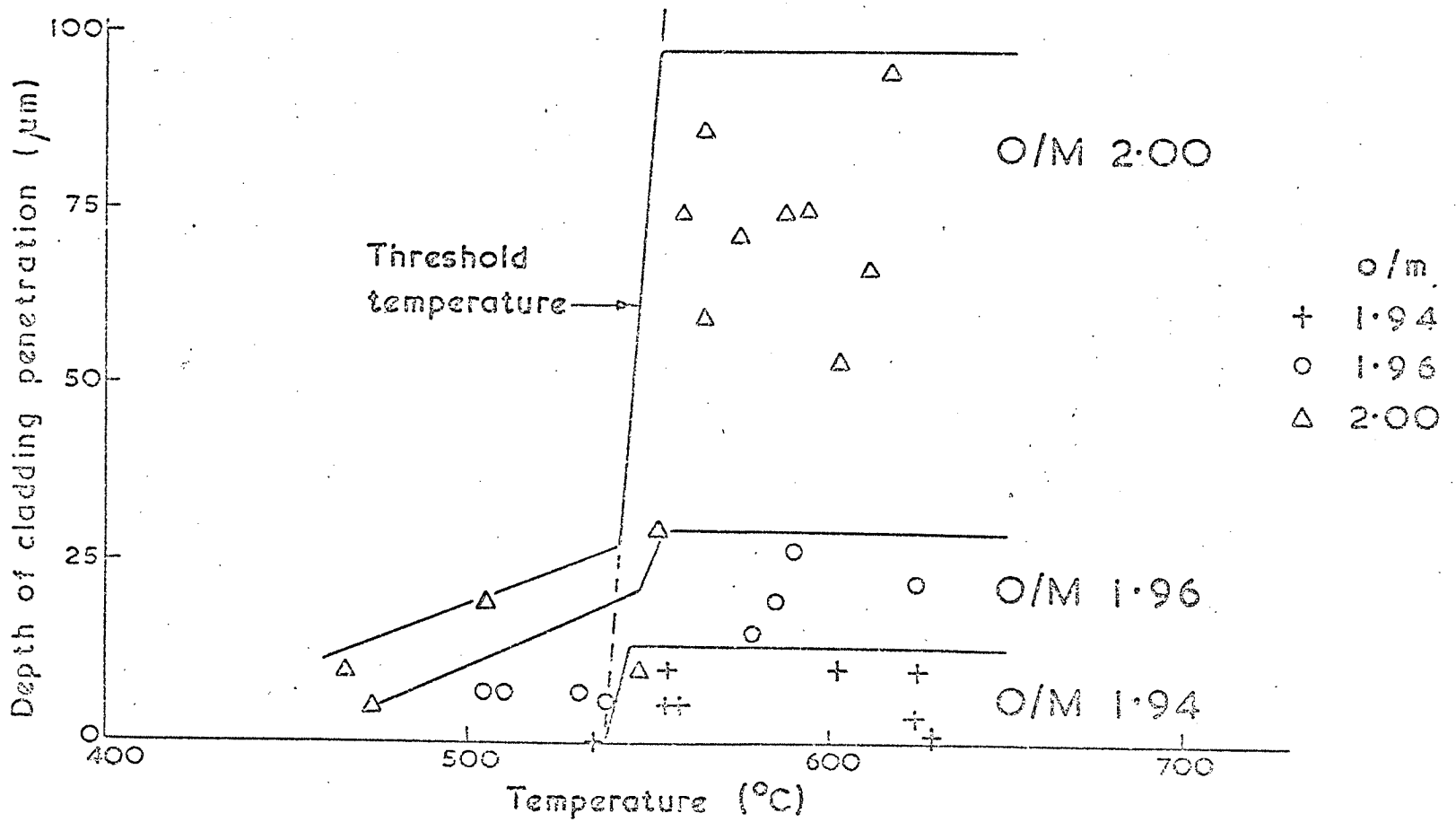

Figure 1. The effect of temperature on fuel-clad reactions (Weber and Jensen, 1971).

proceed via the intermediaries of volatile fission products and that certain operating conditions might cause cracking of any protective oxide on the cladding. This being so it would be expected that the rate of attack would not only increase with temperature but also with burn-up; thermal cycling might also enhance the reaction at various stages. From the data presently available the relative importance of each of these parameters has yet to be established.

2.4. Fundamental and Related Studies.

The reaction between the cladding materials and their oxides with certain fission product elements and their compounds has been studied to facilitate the interpretation of data obtained by post irradiation examination. Most of the work has been concerned with reactions involving those fission products which are volatile at reactor operating temperatures since they are likely to concentrate in the cooler regions of the fuel pin, i.e. at the fuel clad interface.

2.4.1. Caesium.

Caesium has been shown to be compatible with stainless steels below 1000°C and in the presence of both hypostoicheiometric and stoicheiometric uranium dioxide (Götzmann, Hofmann, and Thümmler, 1974). However other workers have shown that reaction products have been observed on steels in the presence of caesium at 1000°C after only 100 hours (Dulgeroff and Seele, 1960; Chandler, 1962; Gurinsky, Weeks, Klamut, Rosenblum and DeVan, 1965, Winslow, 1965). This may be attributed to oxygen impurity in the caesium and the subsequent

reduction of caesium oxide by the stainless steel to form a chromium oxide (Gurinsky, 1964).

Indeed recent studies indicate the important role that oxygen apparently plays in reactions involving caesium and stainless steels (Klueh and Jansen, 1967; Aitken, Evans, Rosenbaum and Rubin, 1971; Maiya and Busch, 1972; Batey and Bagley, 1974; Gotzmann et al., 1974). No reaction occurs with oxygen-free caesium but this element becomes aggressive towards stainless steels with the addition of approximately 500ppm oxygen. Reactions with oxygen-containing compounds of caesium (i.e. Cs_2CO_3; CsOH) also show considerable reaction (Hofmann, Thümmler and Wedemeyer, 1969; Götzmann et al., 1974).

In addition, caesium-enhanced oxidation of austenitic stainless steels (316, 316L and 20%Cr/25%Ni/Nb stabilised) has been observed by Antill, Peakall and Smart (1975). The effect did not require the formation of appreciable amounts of mixed compounds having caesium as a major constituent. Instead small amounts of caesium were taken up by the normal oxide scale.

Thus oxygen appears to be important in reactions involving caesium and stainless steel cladding and in this respect the studies of Aitken et al., (1971) using caesium oxide, type 316 stainless steel and mixed oxide fuel of varying oxygen/metal ratio are significant (Table 3). With fuels having an oxygen/metal ratio ≥ 2.00 intergranular attack was observed after 100 hours at 750° to 800°C whereas with fuel of oxygen/metal ratio ≤ 1.97 the attack was transgranular in form; this latter type which occurred after 100 hours at 550° to 700°C has not been observed in irradiated fuels of

TABLE 3.

Effect of Oxygen/Metal Ratio on Caesium Oxide (Cs_2O)-316 Stainless Steel (Aitken et al., 1971).

Oxygen-metal ratio	Type of attack	Temperature in region of attack
≥ 2.00	Intergranular	750°-800°C
≤ 1.97	Transgranular	550°-700°C

similar oxygen/metal ratio.

Stainless steels can also experience embrittlement in liquid caesium. Thus the low temperature studies (30°C) of Levinson (1964) suggested that exposure of stainless steel either to liquid or vapour caesium could lead to a reduction in ductility and yield stress.

2.4.2. Tellurium.

Tellurium is capable of causing chromium depletion of stainless steel (Calais et al., 1972). At 700°C a preferential chromium depletion of the steel occurs along the grain boundaries while at 800°C it is observed on each side of the grain boundaries. Both these temperatures showed the appearance of a ferritic zone. At higher temperatures (900° - 1000°C) the steel remained austenitic since the chromium depletion process is compensated by the thermal diffusion of chromium within the stainless steel cladding material.

Götzmann and Hofmann (1972) report attack by tellurium which is not dependent on the oxygen potential but is a function of the steel type. Liquid tellurium penetrates type 316 stainless steel to approximately 150μm depth after 4000 hours at 650°C provided there is an excess of tellurium (Lawson, 1969). In such conditions the product formed is iron telluride ($FeTe_{0.9}$) and the treated specimen is liable to disintegrate under a small strain.

In a comprehensive study of fission product attack of four stainless steels (Götzmann et al., 1974) it is observed that the first chemical reaction with tellurium is at 400°C. However it was observed that in the presence of hyperstoicheio-

metric fuel a chromium oxide (Cr_2O_3) protective layer was quickly formed on the surface of the cladding material which prevented subsequent reaction between the stainless steel and the tellurium. It was established that the reaction mechanism was a function of temperature and exposure time and that the thermodynamic stability of the respective tellurides was CrTe > NiTe > FeTe. When caesium was added to the system the two elements reacted preferentially thus reducing the cladding reaction, however, this is at variance with the experiments of Batey and Bagley (1974) and Maiya and Busch (1975). Small amounts of oxygen in these latter experiments may explain this variation. Thus if caesium oxide (Cs_2O) is more stable than caesium telluride then reaction with both caesium and tellurium would occur.

2.4.3. Iodine.

Type 316 stainless steel reacts rapidly with iodine and a liquid phase is observed at approximately 150µm depth after 150 hours at 650°C(Batey and Bagley, 1974). Indeed reaction exists at temperatures as low as 400°C irrespective of the oxygen/metal ratio of the fuel (Götzmann et al., 1974) but it increases with increasing oxygen potential.

The effect of iodine is nullified when it is combined as caesium iodide provided oxygen is absent (Batey and Bagley, 1974; Calais, Aubert, Le Beuze, Conte and Mikailoff, 1974). In the presence of oxygen intergranular attack occurs which compares with that obtained in reactions involving oxygen contaminated caesium.

Iodine- and tellurium-induced failures of stainless

steel specimens have been observed by Lobb and Jones (1973) when undertaking uniaxial creep tests at 750°C. It was deduced that iodine vapour embrittled the 20%Cr/25%Ni/Nb-stabilised stainless steel by chemical attack of the grain boundaries during deformation and the reduction of specimen ductility resulted from the nucleation of numerous surface intergranular cracks which subsequently grew to fracture under the applied stress. Similar results were obtained with tellurium and the rate of crack propagation appeared to be more rapid than with iodine.

2.5. Discussion.

A complicating feature in the post irradiation study of reaction products at the fuel-clad interface is that some of the effects may have been produced after the fuel has been removed from the reactor or during sample storage and preparation. This is illustrated by the report that samples of cladding for metallographic examination showed further corrosive attack and loss of cohesion between the grains after a storage period of three months (Neimark and Brown, 1969). Thus the interpretation of results can be inhibited by secondary reactions which can mask the effects of the primary reaction. However, when reactions occur at the inner surface of fuel cladding and when intergranular penetration is observed it has been established that:-

a) element relocation is invariably involved, either in the fuel or the cladding, or both,

b) certain properties of the fuel can be significant e.g. oxygen/metal ratio, porosity, density or composition;

and c) irradiation and temperature conditions can be important.

There is little direct evidence to show that fission products are involved in fuel-clad reactions in A.G.R. fuel. More positive evidence concerning this type of reaction at the clad inner surface comes from fast reactor fuel assessments where caesium, iodine and tellurium have been detected and where relocation of the cladding elements has been observed.

Of the fuel properties which have been considered variations in stoicheiometry appear to be reponsible initially for differences in cladding attack with the porosity or density being relatively less important. Thus in out of pile fission product reactions, caesium and caesium iodide react with the cladding steels only in the presence of some oxygen and the effects produced in the steels have identical features to those observed on irradiated fast reactor cladding.

The variation of oxygen potential in the fuel depends on the fissile nuclides present since due to differences in the fission yield curves of uranium-235 and plutonium-239 (Figure 2) a relatively higher oxygen potential will result from the plutonium bearing fuels. Rand and Markin (1967) have proposed that a constant CO_2/CO ratio will determine the oxygen potential at any time across a fuel pin assuming a given overall composition; the effect of burn-up on the oxygen/metal ratio has also been calculated by Adamson and Rand (1969). In these latter studies the possibility that the cladding would act as an oxygen sink was considered but it was concluded that with the formation of a thin protective oxide on the clad inner surface and the removal of excess

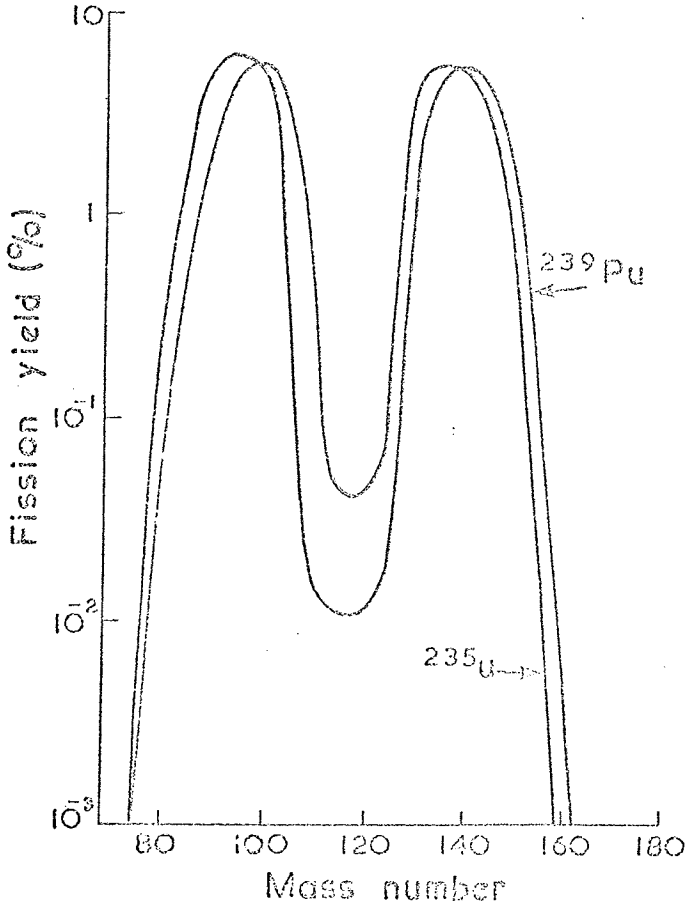

Figure 2. Thermal neutron fission product yield curve for uranium-235 and plutonium-239.

oxygen from the outer regions of the fuel with redistribution in the temperature gradient, there would not be a compatibility problem. Nevertheless, the important aspect of this work, from the fuel-clad compatibility viewpoint, was that austenitic steels should be oxidised at temperatures up to 1500°K and with a CO_2/CO ratio $\geq 10^{-3}$, relating to an overall oxygen/metal ratio ≥ 1.987.

Keroulas et al. (1972) and Calais et al. (1972) state that several sequential conditions must occur to achieve a fuel-steel reaction:-

a) the stoicheiometry of the fuel at the outer edge must deviate sufficiently to enable it, from a thermodynamic viewpoint, to react with the steel,

b) the mixed oxide $[(FeCr)_2O_3]$ formed prevents further oxidation of the steel,

and c) due to thermal transients the $(FeCr)_2O_3$ layer may crack thus enabling volatile fission products to react with the underlying chromium depleted layer. However after the initial stages of oxidation when a thermal transient may damage the Cr_2O_3 film the incorporation of iron oxides into the growing scale improves the oxide scale adhesion and thermal shock resistance (Francis, Curtis and Hilton, 1971).

The above mechanism is also discussed by Ohse and Schlechter (1972). They conclude that caesium oxide (Cs_2O) is stable in contact with mixed oxide fuel at 600°C when the oxygen/metal ratio of the fuel exceeds approximately 2.0005. Again, as above, general corrosion occurs by formation of mixed steel oxides which may subsequently crack or even become detached due to thermal cycling or volume changes during

the corrosion.

Thus the data suggest that the availability of oxygen at the fuel-clad interface, probably with the production of an oxide film, is the initiating factor in any reaction. The subsequent role of fission products in the continuation of the reaction is now considered.

As has been previously mentioned, the principal fission products which have been observed in association with fuel-clad reaction products are the volatile elements caesium, iodine and tellurium. They are transported down the temperature gradient in the vapour phase via interconnected porosity and cracks in the fuel (Bober and Schumacher, 1973). In an evaluation of their effects on the steel it is necessary to consider the precise chemical form in which the elements exist within the fuel environment.

Figure 3 shows the free energy data for the iodides and oxides of caesium and the major austenitic steel constituents (Glassner, 1965; Allen, 1973). In an ~~oxidising~~ iodine environment caesium iodide will be formed in preference to the iodides of the steel constituents, with chromous iodide being the next most stable iodide. However, in the presence of an oxidising environment chromous iodide will be the least stable of the steel iodides and would be expected to readily form chromium oxide. Although iodine may remain in an elemental state for some period after its formation in fission (Reed and Ramsdale, 1971; Johnson and Crouthamel, 1970) and out of pile studies show that a reaction between iodine and austenitic steels can occur (Robins, 1972; Whitlow and Hilton, 1972), the gross form of the attack is dissimilar

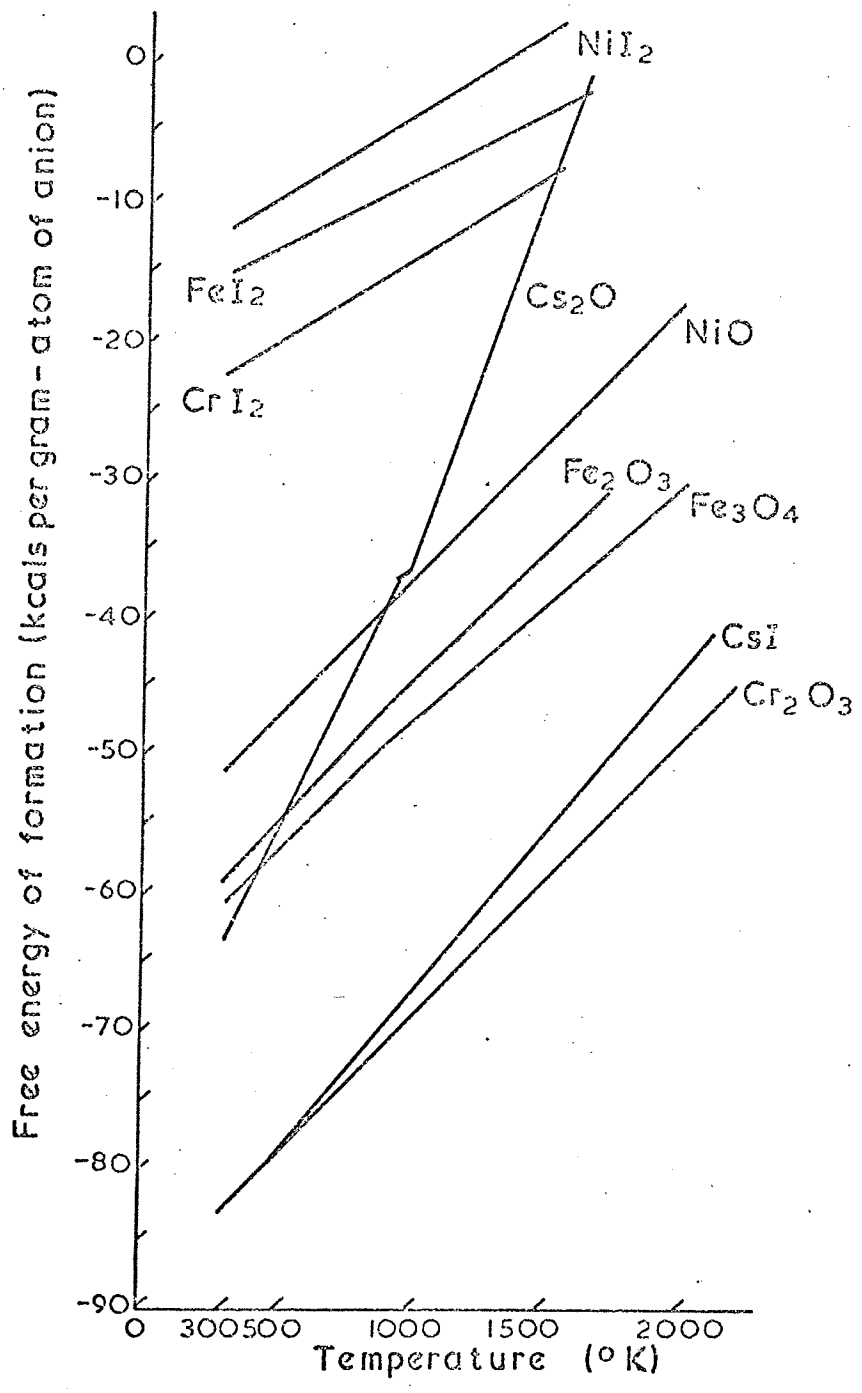

Figure 3. Free energy data for the iodides and oxides of caesium, iron, chromium and nickel.

to that observed during the post irradiation examination of A.G.R. fuel elements. It is therefore assumed that where iodine is involved it reacts in the form of caesium iodide; indeed the Cs/I atomic ratio is quoted as being $\sim$ 4:1 (Findlay, 1972) and therefore all the iodine would be expected to be present as caesium iodide.

Should this latter compound react with chromium oxide to form a chromate then not only would this result in the removal of the oxide protection but iodine would be released for reaction with the chromium depleted steel. Thus the roles of the iodides of the alkali metals may be governed by the following sequence of reactions:-

1) Fe,Cr,Ni (steel) + UO_2 $\rightarrow$ Cr_2O_3, the extent of reaction being dependent on the fuel stoicheiometry and temperature.

2) Cr_2O_3 + CsI $\rightarrow$ Cs_2CrO_4 + I_2

3) Fe,Cr,Ni (steel) + I_2 $\rightarrow$ FeI_2, CrI_2, NiI_2.

In a relatively oxidising environment any chromous iodide will be preferentially converted to chromic oxide so that the sequence of reactions 2 and 3 may be repeated. Additionally, depending on the precise conditions of temperature and oxygen potential some reaction of the iron and nickel would be anticipated. Thus a mechanism of this type would explain many of the effects which have been seen at the inner surface of reactor cladding even though iodine is not always observed and the presence of caesium is detected in a number of cases only by its radioactivity.

Apart from the reactions occurring at the fuel-clad interface, iron and nickel particles have been observed in segregated areas of the fuel. The observations of iodine in the area of intergranular attack has led to the hypothesis that iodine contributes significantly to the mechanism of the metal transport via a Van-Arkel-De-Boer (1925) type reaction. This involves the reaction of iodine with the cladding followed by vapourisation and transportation of the resulting iodides to the higher temperature zone in the fuel matrix where they decompose. Support for this view comes from the observation that the caesium-137/caesium-134 ratio is greater in the centre of uranium dioxide fuels than towards the outer edge (Morgan, Hart, Jones and Edwards, 1961; Reed and Ramsdale, 1971; Philips, Waterbury and Vanderbough, 1974).

The increased presence of caesium-134 (compared to caesium-137) at the outer edge may be because the longer lived iodine-133 ($t_{\frac{1}{2}}$ = 21 hours) travels further towards the outer edge than iodine-137 ($t_{\frac{1}{2}}$ = 24 seconds). Iodine-133 and iodine-137 are the precursers of caesium-134 and caesium-137 respectively (Figure 4). The importance of this mechanism could again depend on the oxygen potential within the fuel and under some conditions the ferrous iodide might be oxidised before iron transport can occur.

The validity of the Van-Arkel-De-Boer mechanism and that postulated above can be criticised when the thermodynamics of caesium iodide are considered. Examination of Figure 3 shows that caesium iodide is highly stable relative to the steel iodides and as the amount of caesium liberated during fission will be greater than the amount of iodine (Figure 2)

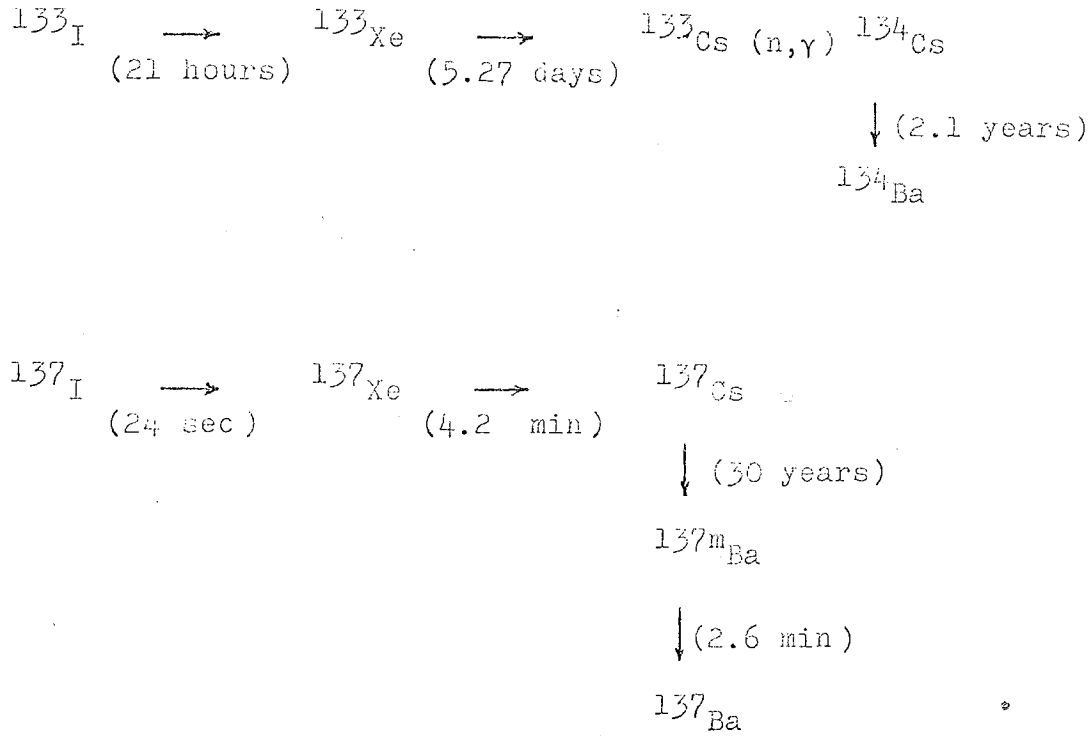

Figure 4. Decay chains for iodine-133 and iodine-137.

it must be expected that iodine will be present in the fuel as caesium iodide. Also any iodine liberated during the reaction between chromium oxide and caesium oxide should be quickly "gettered" by the excess caesium. Hence iodine may only be effective in any corrosion mechanism with the stainless steel clad if the caesium can be removed by reaction with either fuel or fission product where the resultant product is more stable than caesium iodide.

There is very little information on the role of tellurium in fuel-clad reactions. From out of pile tests tellurium can have a deleterious effect on steels and it can cause the introduction of a ferritic zone similar to those observed in some fast reactor studies. It is also unnecessary to invoke the requirement of an oxide film or a sufficient oxygen potential at the steel surface before attack occurs.

Available data have shown that the volatile fission products (Cs, I and Te) can all be present in the fuel-clad region of irradiated fuel pins. Indeed this would be expected purely from temperature gradient and volatility considerations and hence their presence is in no way indicative of any reaction involvement. From fast reactor data the observed reaction can be reproduced by the reaction between stainless steel and caesium given a sufficient oxygen potential. For thermal irradiation however, the amount of available data is very limited but because of the lower oxygen potential resulting from the uranium-235 fission (compared to plutonium-239) the caesium reaction may not be so important.

The extent of attack appears, in general terms, to be a function of the oxygen/metal ratio, the clad temperature,

the fuel burn-up, the fuel density, the availability of fission products and possibly impurities in the fuel. The uranium (and indeed the plutonium in mixed oxide fuels) which is shown as being compatible with stainless steel in out of pile studies (see section 2.2) is still compatible under irradiation.

To limit the effect that any fuel-clad reaction might have on clad endurance it is clear that future studies should concentrate on establishing the relative importance of these parameters.

Because of the limited amount of literature regarding the irradiated fuel-clad compatibility in the A.G.R. the initial experimental study described in this thesis has concentrated on an examination of the reaction products formed at fuel-clad interfaces on A.G.R. fuel. Subsequent to this post irradiation examination a more detailed specific study of the effect of one fission product, tellurium, on 20%Cr/25%Ni/niobium stabilised stainless steel was then undertaken. These are described in the following chapters.

CHAPTER THREE. EXPERIMENTAL TECHNIQUES.

3.1. Introduction.

The samples that are to be examined in the post irradiation study of the interior surface of reactor fuel elements (Chapter 4) are extremely radioactive and therefore the techniques chosen must not be affected by the emitted radiation. The selection of techniques to be used must also take into account the limits on the amounts of ionising radiation to which personnel can be exposed stipulated by the International Commission on Radiological Protection (Table 4). A classified worker, i.e. a person who is registered to work with ionising radiations, is limited to a maximum whole body radiation dose of 5 rems per year. The rem is a unit which refers to the absorbed radiation dose from any form of ionising radiation and is a product of the energy absorbed and the relative biological effectiveness (R.B.E.).

i.e. Rem = Rad x R.B.E.

where 1 rad is equivalent to 100 ergs of absorbed energy per gramme of tissue and the relative biological effectiveness is a function of the linear energy transfer, i.e. the energy transferred to the tissue per unit length.

In the experimental study of clad inner surfaces both beta and gamma activities will be encountered. Exposure to these radiations can be limited by:-

a) maintaining as large a distance as possible between the specimen and the operator (e.g. by the use of long forceps etc.). The radiation level from a point source decreases

TABLE 4.

Maximum Permissible Radiation Doses.

Exposed part of body	Classified worker	Individual member of the public
Whole body, blood forming organs, gonads.	5rems/year 3rems/13weeks	0.5rems/year
Skin, thyroid, bone.	30rems/year 15 rems/13weeks	3rems/year
Other single organs (including lens of eye).	15rems/year 8rems/13weeks	1.5rems/year
Hands, forearms, feet and ankles.	75rems/year 40rems/13weeks	7.5rems/year

with increasing distance and this can provide an effective way of reducing the radiation dose rate exposure. The dose rates for gamma emitters (1MeV) at various distances and size of source are shown in Figure 5.

b) the introduction of shielding (e.g. lead wall, remote controlled facility etc.). The penetration ability of beta and gamma radiations are shown in Figures 6 and 7. For materials emitting beta radiation a perspex screen or glove box may be sufficient but for highly radioactive gamma emitters a denser material (e.g. lead) may be required. This could slow the operation down and if a remote controlled handling facility is necessary make the experiment slow, expensive or extremely difficult.

c) reducing the operation time to a minimum. The quicker the experimental work is completed the lower the exposed radiation dose.

and d) reducing the size of the specimen. This reduces the total radioactivity of the system and therefore if it is feasible provides the best solution.

A combination of the above considerations was used in the post irradiation study. Initially the fuel pins were received and sectioned in remote controlled shielded facilities. Subsequent to the removal of the uranium dioxide fuel the clad was further sectioned until the activity was sufficiently reduced to enable handling with 10" forceps behind localised shielding.

The second section of the experimental work (Chapter 5) in this thesis does not involve the use of radioactive materials and therefore the considerations discussed above do not apply.

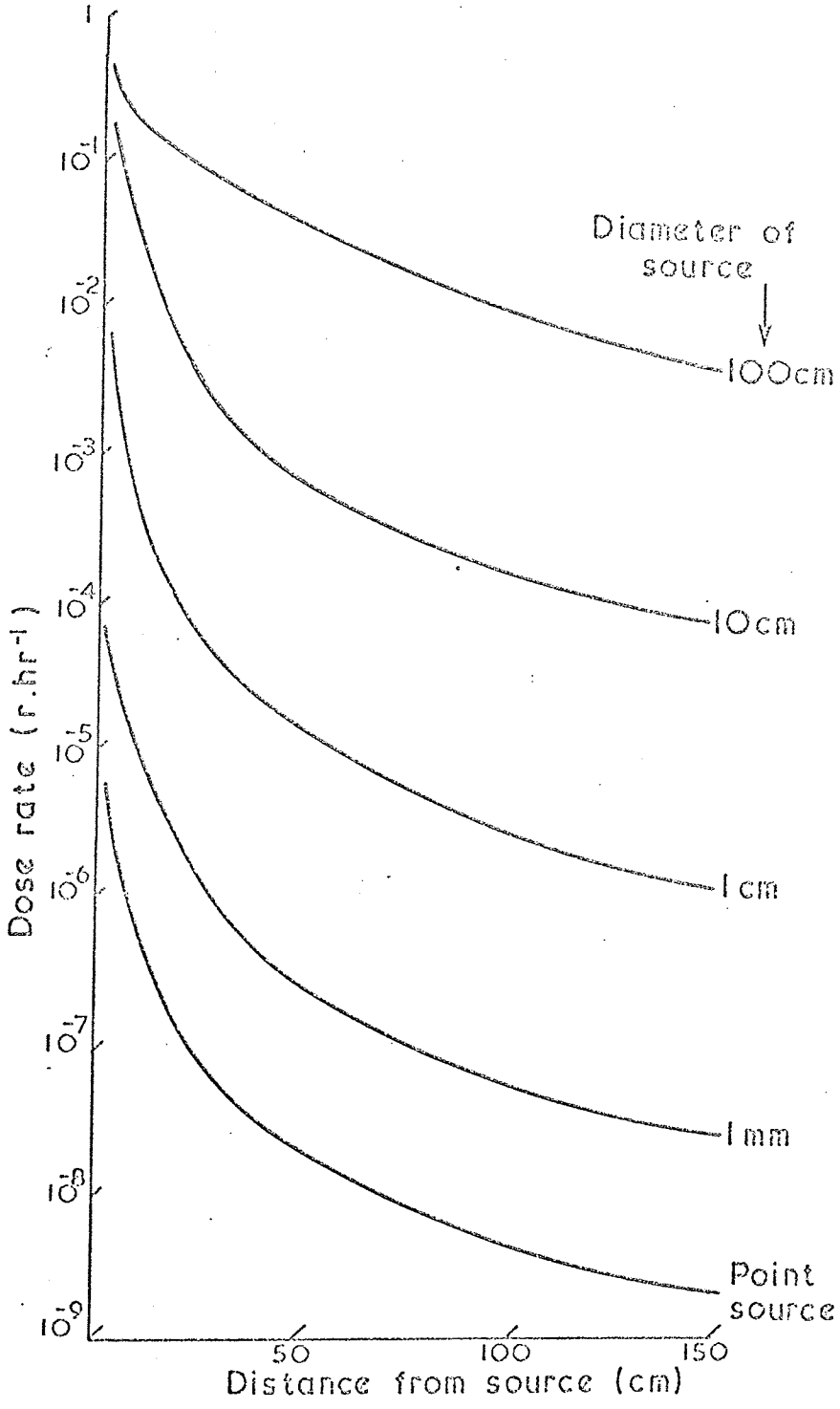

Figure 5. Dose rates from gamma source at varying distances.

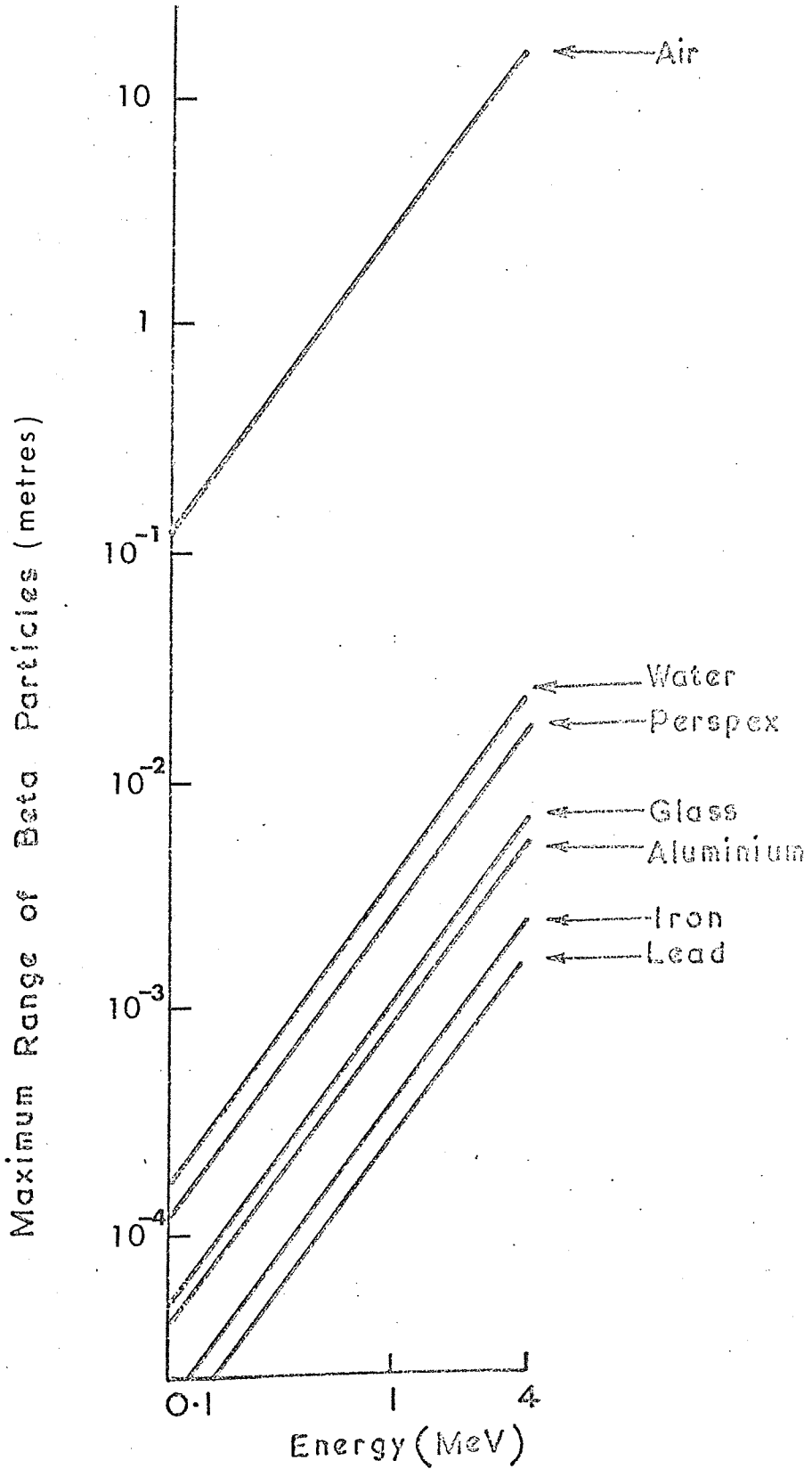

Figure 6. Penetration ability of beta radiation.

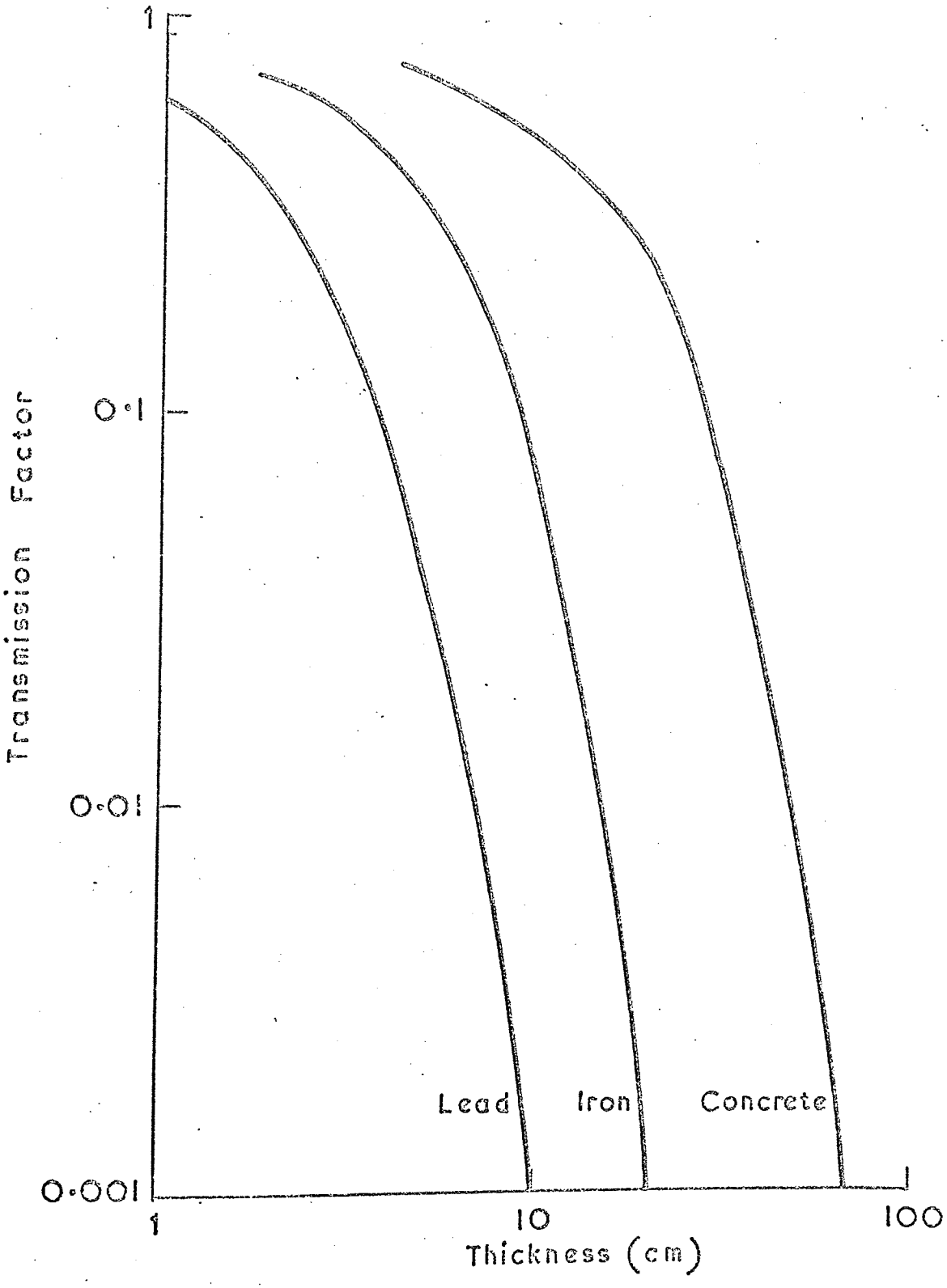

Figure 7. Attenuation of 1MeV gamma radiation.

However, in general, the same type of investigation is involved i.e. the characterisation of reaction products on surfaces, and so long as the chosen techniques are not affected by radiation they can be utilised in both parts of this study.

From experience obtained during similar studies involving oxidised stainless steels the main consideration in the evaluation of analytical techniques to be used in this study is that they should be able to analyse small areas of material. The ability to show the component distribution would also be advantageous. In fact the sensitivity and resolution are more important facets than accuracy and precision because of the considerable variations in composition that are likely to be encountered in this multi-component system. In this case it is more important, from a mechanistic viewpoint, to establish those areas where enhancement or depletion occur than to have accurate analyses over many regions of the surface. However precise analyses in selected areas are useful to check the possibility of any compound formation.

In addition the possibility of re-examination or study by a further technique may be desirable and therefore the ability to analyse non-destructively would be an advantage.

3.2. Preparative and Optical Procedures.

3.2.1. Micromanipulative and Optical Studies.

During the examination of reaction products on the inner clad surfaces certain examples were isolated for investigation. The removal of these products and their accurate mounting and positioning for further study was

achieved by using a Research Instruments TVC 500 double probe micromanipulator. The instrument, which features only one control for all three dimensional movements and a positioning accuracy of 0.25μm, was used with either 2 or 5μm tipped tungsten probes or with a pair of DeFonbrune remote controlled pneumatic forceps (manufactured by Beaudouin).

Viewing was accomplished through an Olympus Zoom binocular microscope with a magnification range of x20 - x180. The distance between the specimen and the microscope eyepiece was approximately 300mm thus considerably reducing the radiation level to the eyes by approximately a factor of one hundred. A 50mm lead shield was placed between the operating area and the operator and the whole instrument enclosed in a 12mm perspex box. This latter feature acted as a dust cover; in this way foreign material was not confused with the sample.

Samples of deposit were removed from the inner surface of the A.G.R. can sections by the above technique and examined microscopically after they had been mounted on copper electron microscope grids (149μm) with polybutene.

3.2.2. Metallography.

The extent and type of attack on prepared samples was determined by a metallographic study. The specimens were mounted in either clear or copper filled mounting plastic and polished to 0.25μm finish with diamond polishing compound. The polishing of the irradiated specimens was undertaken mechanically and non-aqueous solvents used throughout to avoid removal of soluble species from the reaction area (e.g. caesium compounds).

3.2.3. Etching.

In an attempt to show areas of varying composition or structure in the region of any reaction, selected specimens were electrolytically etched in 10% oxalic acid solution maintained at 60°C. This etchant has been developed to reveal grain boundary structure (Brown and Healey, 1969).

A development of this procedure was attempted by colour etching the stainless steel specimens in a metabisulphite-hydrochloric acid solution (Beraha, 1968). The etchant stock solution consisted of approximately 5% hydrochloric acid containing 2% ammonium bifluoride. Immediately before use 600mg of potassium metabisulphite ($K_2S_2O_5$) per 100ml of stock solution was added. The specimens were etched for 30 - 60 seconds at room temperature, washed in water and dried with alcohol.

The metabisulphite decomposes in acid media whilst in contact with a metallic area (Ephrain, 1949) to hydrogen sulphide, sulphur dioxide and sulphur. The colour obtained is due to the precipitation of a thin sulphide film (mostly nickel sulphide). This will precipitate on ferritic, marstenitic and austenitic matrices only. The variation of colours is caused by the difference of the thickness of the sulphide film which depends on the surface energy of the intersected crystallographic planes. Because the steel under observation contains 25% nickel it shows a good colour response.

3.2.4. Scanning Electron Microscopy.

Within recent years the scanning electron microscope (S.E.M.) has become increasingly used as a tool in a broad variety of scientific and technical fields. The reason for this increase in popularity is that it enables the user to observe the surface of specimens at higher magnifications (x10,000). Thus it has advantages compared with both the conventional light microscope, which has a very limited depth of field at high magnifications making it impossible to study rough specimens, and the transmission electron microscope which has the great depth of field and resolution associated with "electron optics" but cannot work directly with solid samples.

The S.E.M. uses a scanning focussed beam to strike the specimen. The secondary electron signal varies as the surface slope changes and a topographic image is displayed on a cathode ray tube. This effect can also be obtained in electron probe microanalysis but is not so effective due mainly to th higher beam intensities used to generate adequate X-ray count rates.

The instrument used for this study was a Cambridge Stereoscan. Specimen surfaces were examined and, in addition, sectioned specimens were studied for subsurface effects in regions of attack.

3.3 Analytical Techniques.

3.3.1. Considerations.

A summary of analytical techniques is shown in Table 5. Of the non-destructive techniques the electron probe micro-

TABLE 5: Analytical Techniques

Technique	Elements Detected	Simultaneous Detection	Precision (%)	Destructive	Lower Limit of Detection	Sample Size	Sensitivity (grams)
Chemical	Most	No	1-5	Yes	10-100ppm	>0.1g	
Atomic Absorption	∿ 50	Some	1-5	Yes	0.1-100ppm in solution	1 ml	10^{-10}
Flame Emission	Alkali and alkaline earth	No	1-5	Yes	0.1-10ppm in solution	1 ml	10^{-11}
Emission Spectrography	Metallic	Yes	3-10	Yes	1-10ppm	20mg	10^{-11}
Laser Microprobe	Metallic	Yes	10	Yes	1-10ppm	3-50μm	10^{-8}
X-ray Diffraction	Crystal Structure	Yes	5-10	No	1-5%	1-10mg	10^{-6}
X-ray Fluorescence	Z > 11	Yes	1-5	No	10-1000ppm	$4cm^2$	10^{-7}
Electron probe Microanalysis	Z > 4	Yes	1-5	No	100-1000ppm	$1-200\mu m^2$	10^{-14}-10^{-16}
Energy dispersive X-ray analysis coupled to scanning electron microscope	Z > 11	Yes	1-10	No	100-1000ppm	$10^{-2}\mu m^2$-cm^2	10^{-12}-10^{-16}
Auger Spectroscopy	Z > 3	Yes	10	No	10-800ppm	$1\mu m^2$-$1cm^2$	
ESCA	Z > 2	Yes	10	No	1-5%	$4mm^2$-$1cm^2$	
Activation Analysis	Most	Yes	1-10	Yes and No	0.001-100ppm	>1μg	10^{-11}

Z :- element mass number

analyser has the advantage that it can analyse several elements simultaneously and it can also analyse very small areas (approximately 1μm diameter). This latter feature of electron probe microanalysis is superior to X-ray fluorescence which usually requires a sample area of at least $1cm^2$ and a sampling depth of approximately 100μm depending on the energy distribution of the primary beam and the absorption characteristics of the sample. Microfocus X-ray tubes have been employed (Long and Cosslet, 1957; Zeitz and Baez, 1957) to reduce the diameter of the primary beam but the spatial resolution is improved only at the expense of large losses in X-ray intensity and detection sensitivity.

An additional technique that provides similar information to the electron probe microanalyser is energy dispersive X-ray analysis coupled to a scanning electron microscope. This technique has also been employed in this study and has the advantage that it provides the excellent electron "optics" of the scanning electron microscope; however it does not have such a good resolution as the electron probe microanalyser.

Both electron probe microanalysis and energy dispersive X-ray analysis can be considered to be surface analysis techniques since their depth of penetration is of the order of 1μm. However in instances where a thinner reaction layer or deposit has been produced a further technique has to be considered. Auger spectroscopy is a true surface technique that examines only the outer 1 - 4 atomic layers of the material and this has proved successful in analysing products deposited during the compatibility studies with tellurium.

The main disadvantage of electron probe microanalysis and energy dispersive X-ray analysis is their inability to give an indication of the chemical combination of the elements detected, although by quantitative analysis certain possible formations can be discussed. To confirm some of these findings X-ray diffraction has also been used. Although suffering from a lower limit of detection of approximately 5% the crystal structure of the material under investigation can be determined.

Additional information can also be supplied by utilising the radioactivity of the irradiated specimens. Samples from the post irradiation study were therefore counted by γ-ray spectrometry.

The various techniques used in this study are now considered in detail.

3.3.2. Electron Probe Microanalysis.

The electron probe microanalyser has made a great impact in the study of materials. Despite its high initial cost and the high degree of operational competence required, its ability to analyse chemically extremely small quantities of material has greatly influenced its choice as one of the analytical tools in this study.

The principle of electron probe microanalysis (E.P.M.A.) was revived by Castaing (1951) although the possible significance of the technique had been predicted earlier by Moseley (1913, 1914). It involves bombarding the specimen with electrons and analysing the emitted X-rays in a crystal spectrometer using a suitable X-ray detector (Figure 8).

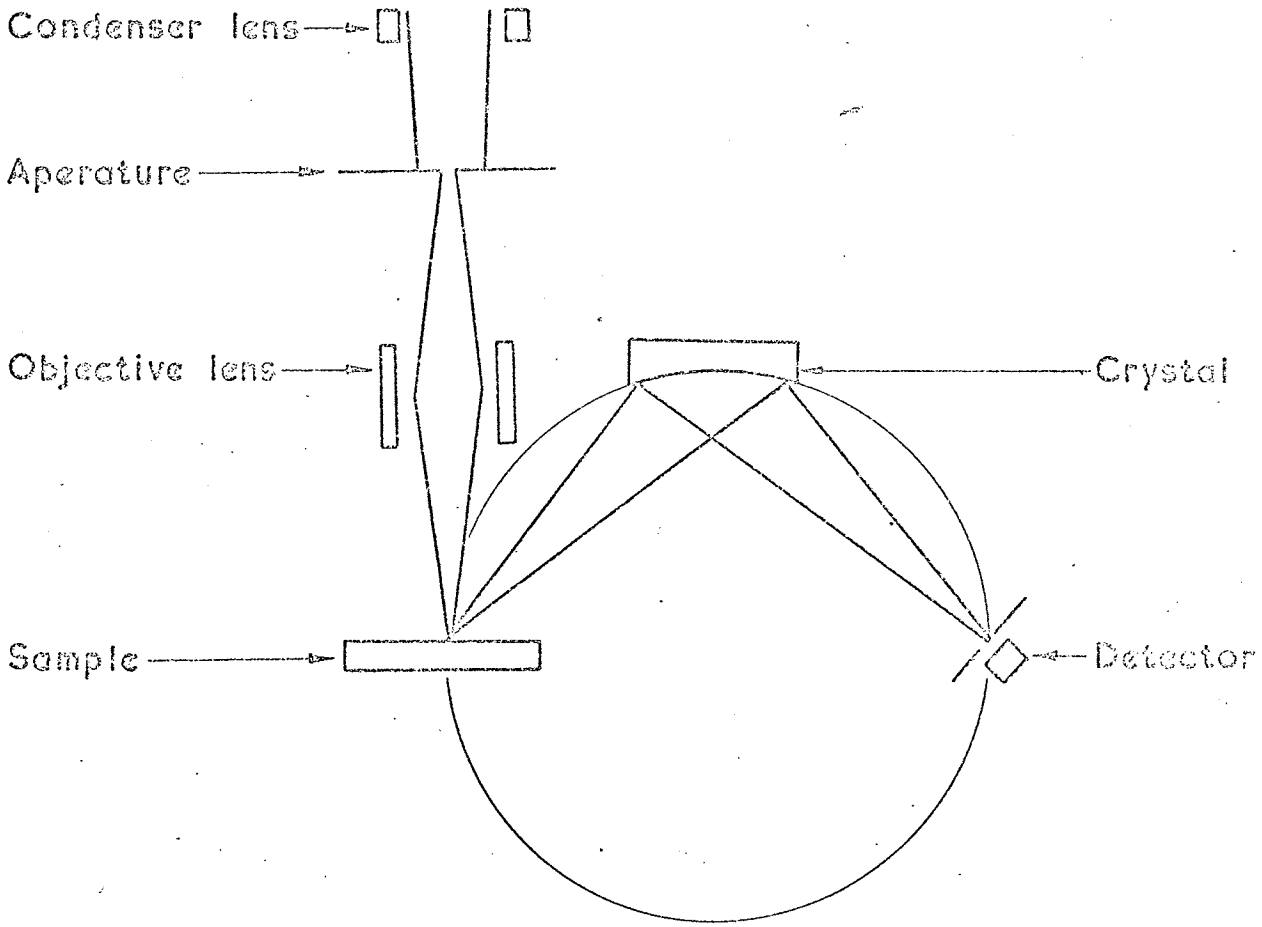

Figure 8. Schematic diagram for the principle of electron probe microanalysis.

The electron beam can be focussed on to a very small area of the sample (approximately 1μm diameter).

Qualitative analysis is achieved by rotating the crystal and scanning the detector to monitor the X-ray output. This is recorded as a function of Bragg angle ($n\lambda = 2d.\sin\theta$) (see section 3.3.5.) and the characteristic wavelengths identified by reference to standard tables. In addition the distribution of constituent elements can be obtained by scanning the electron beam and monitoring the selected element.

Once the qualitative composition of the sample has been ascertained a quantitative analysis may be obtained by measuring accurately the X-ray intensities for each element together with those of pure element standards*. In principle, the weight fraction of element A (C_a) is given by the ratio of the measured intensity of element A in the sample (I_a) to that measured under identical conditions from the pure element (I_s). Corrections have to be made for background radiation and dead-time of the counters.

$$\text{i.e.} \quad C_a = \frac{I_a}{I_s}$$

In practice, however, the calculated concentration varies from the true amount due to several effects for which

---

*Footnote:

In cases where it is unsuitable to use the pure element as the standard (either due to chemical instability or where the element is gaseous or liquid at room temperature) a compound containing a high concentration of the element may be used.

allowances have to be made. Except in cases where the specimen consists of two elements of adjacent atomic number these effects can lead to significant errors (sometimes > 10%).

Because the X-rays are generated below the surface they have to travel through the specimen before emerging and hence their intensity is reduced by absorption. There is also the possibility that the absorption of X-rays will vary between samples and standards.

The observed X-ray intensity can be enhanced due to fluorescence. This is achieved when the radiation of an associated element is of sufficient energy to excite the characteristic radiation of the element under study.

When elements of widely differing atomic number are present the intensity of the characteristic X-radiation is not proportional to the concentration due to retardation and backscatter. Retardation occurs because the energy of the electrons decreases as they travel into the specimen. They will only produce X-radiation whilst their energy exceeds a critical excitation potential. The distance travelled before this occurs varies according to the atomic number. Effects due to backscatter occur when electrons interacting with target atoms by elastic scattering are redirected such that they escape from the specimen with an energy greater than the critical excitation potential. Therefore any further X-radiation production is lost. The combination of retardation and backscatter are often termed as the "atomic number effect". A diagramatic representation of these features is shown in Figure 9.

The corrections needed to allow for these departures

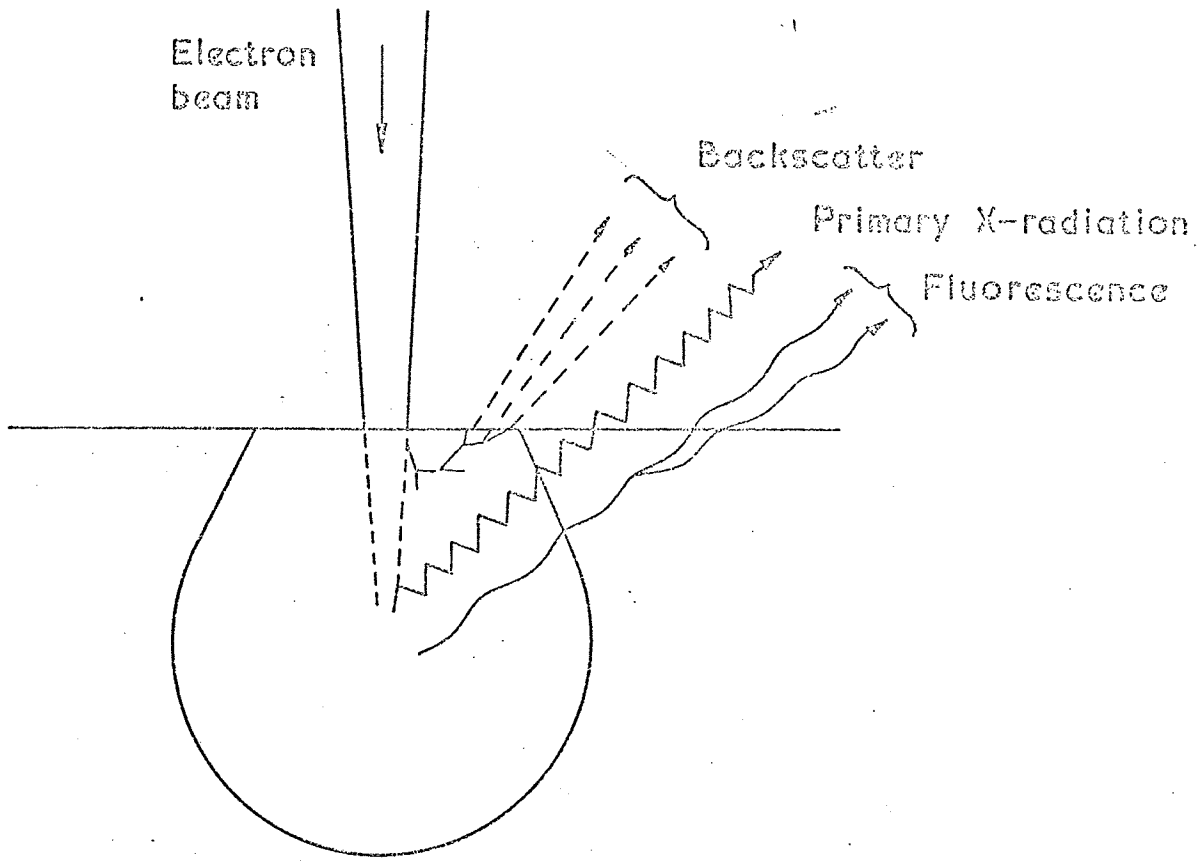

Figure 9. Diagramatic representation for corrections required in electron probe microanalysis.

from the ideal situation are complicated and have been the subject of several reviews (e.g. Martin and Poole, 1971). For analysing systems containing three of more constituents calculation by computer becomes attractive. Several programs have been presented and in this study that reported by Duncumb and Jones (1969) has been used. This program has been designed to reduce the required data to a minimum and is very convenient for the electron probe microanalyser operator. because the majority of the necessary information is stored in the computer.

The present study utilised a Cambridge Instrument Company Microscan 5. A schematic diagram is shown in Figure 10. This instrument is equipped with two linear spectrometers having an X-ray take-off angle of 75^{o}, each containing three interchangable crystals selected from lithium fluoride, rubidium acid phthallate, mica, quartz or barium stearate deposited on mica.

The instrument has been modified to enable the examination of radioactive specimens (Sparry and Pearce, 1972). The modification consists of 4cm thick tungsten-nickel-iron alloy (Heavy Alloy; density 18g cm^{-3}) shielding attached to the specimen chamber, thus reducing considerably the radiation level to the operator. Direct shielding of the counters is not employed although extra shielding at the rear of the specimen movement gear-box has reduced the background level to one of the spectrometers.

3.3.3. Energy Dispersive X-ray Analysis.

As stated in section 3.2.4. the scanning electron

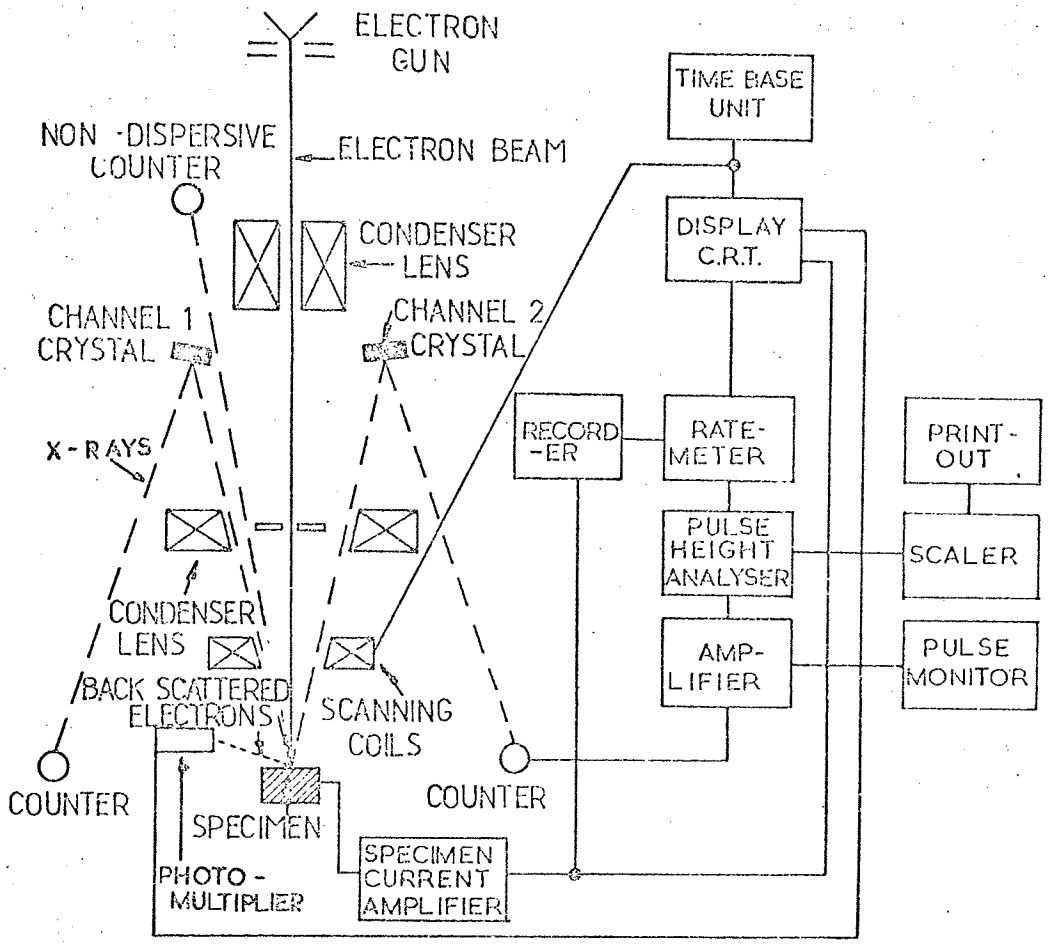

Figure 10. Schematic diagram of the Cambridge Microscan 5.

Note:- Channel 1 counter connections and signal data handling units are not shown.

microscope provides superior "optics" to the electron probe microanalyser. Indeed with some specimens in this study difficulty was experienced in locating a particular region of interest on the microanalyser even though the general area was marked by hardness indentation equipment. This was overcome by using an energy dispersive spectrometer attached to the S.E.M.; in this way the advantages of E.P.M.A. were coupled with the benefit of the excellent "optics" of the S.E.M. Its main limitation is the poorer ~~spatial~~ energy resolution compared with the normal wavelength spectrometer used in E.P.M.A. A particularly relevant example of this limitation is evident in the study of stainless steel where the main manganese ($K\alpha$) peak is masked by a chromium ($K\beta$) peak.

The spectrum obtained with energy dispersive X-ray analysis (E.D.X.) is simple in appearance because only the $K\alpha$, $K\beta$, $L\alpha$, $L\beta$, $L\gamma$ and M lines are present (Figure 11). This is a considerable reduction on the number of peaks observed by the wavelength spectrometer of E.P.M.A. where diffraction at any angle can occur for which the Bragg equation ($n\lambda = 2d.\sin\theta$) is satisfied and since "n" can have any integer value many "orders" of diffracted lines are possible.

3.3.4. Auger Spectroscopy.

Auger spectroscopy is a useful tool for the analysis of monolayer depths on the surface of specimens. This method of electron ejection was first discovered by Auger (1925a and b) and although Lander (1953) recognised the potential of the technique it was not until the work of Weber and Peria (1967) and Harris (1968a and b) that this mechanism became used more

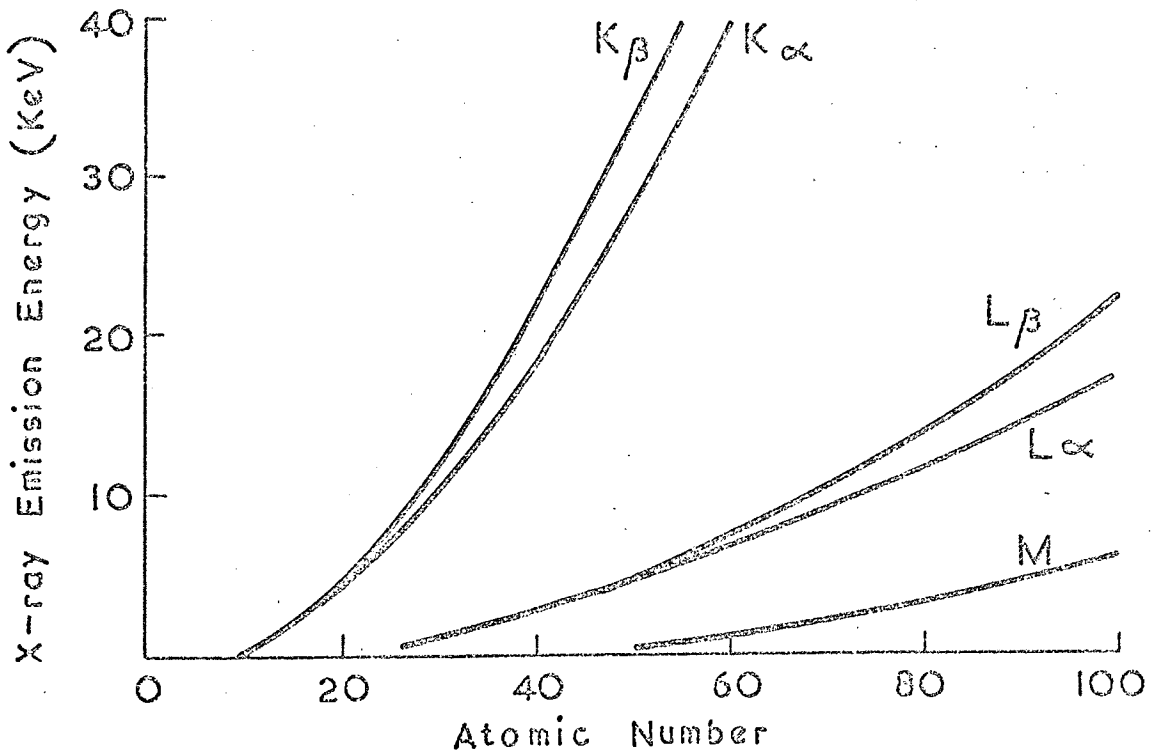

Figure 11. Energies of the principal X-ray emission lines.

widely.

The Auger process occurs when the atom is excited by an incident primary beam of electrons thus removing a tightly bound core electron. Although the primary electron beam will penetrate several atomic layers into the specimen, the Auger electrons have very much lower energies and as such only those generated very near the surface of the specimen can escape. The Auger electrons produced further into the specimen are lost due to inelastic scattering before they can escape from the surface. It is generally accepted that they will only escape from a maximum depth of four atomic layers, depending on their energy, and therefore the technique genuinely provides an analysis of the surface.

The instrument used in this study was a cylindrical mirror analyser manufactured by Vacuum Generators Ltd.

3.3.5. Powder X-ray Diffraction.

This method of X-ray diffraction was developed independently by Debye and Scherrer (1916, 1917) and Hull (1917a and b). It involves the diffraction of monochromatic X-radiation by a specimen. The specimen "reflects" the incident X-rays off all its crystal planes and when their wavelengths are in phase they reinforce each other to form a diffracted beam.

A simple method for the evaluation of this observation was developed by Bragg (1912). In Figure 12 BAC and EDF are X-rays being reflected at an angle θ from successive crystal planes of spacing "d". The incident X-rays are in phase along the wave front AX. Now if AD is perpendicular to the crystal planes then the extra path length travelled by the bottom

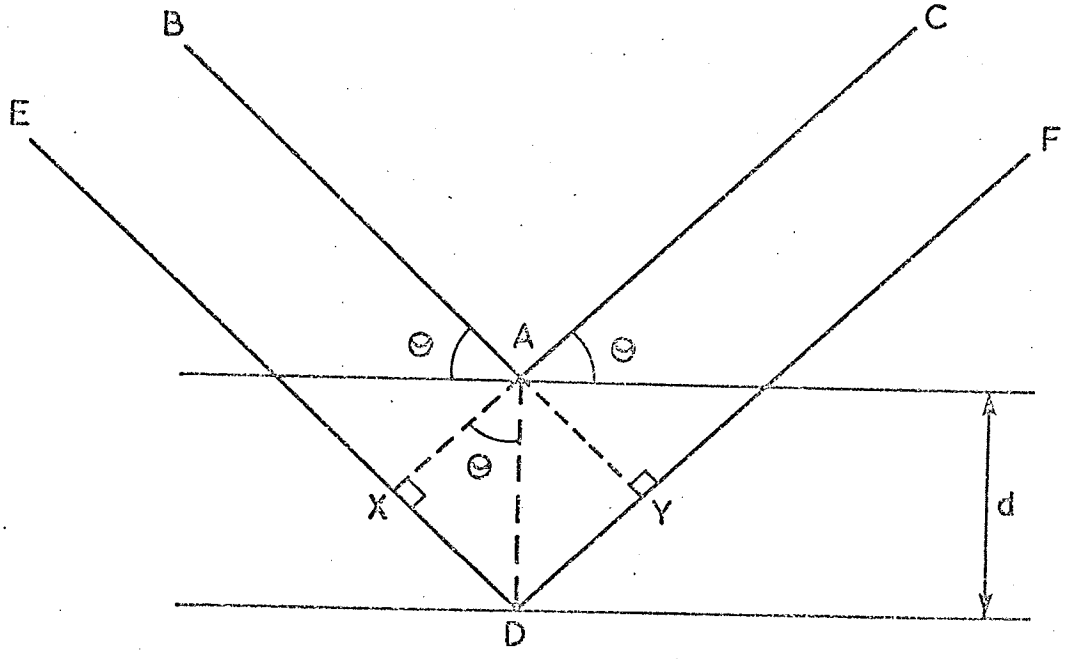

Figure 12. Evaluation of Bragg Angle.

wave is:-

$$XD + DY = 2d.\sin\theta.$$

For reinforcement to occur this must equal the integral multiple of the X-ray wavelength (λ) and hence:-

$$2d.\sin\theta = n\lambda.$$

This is known as the Bragg equation.

The use of the technique in this study was limited to the study of the reaction products by the powder method i.e. the material to be examined is reduced to a powder thus presenting many small crystals orientated at random in the primary X-ray beam. Therefore, by the law of averages, the X-rays will be diffracted off all possible crystal planes. The random approach is assisted by specimen rotation. Because of the random orientation of the crystals the diffracted beam is emitted as a cone and by placing a strip of photographic film around the specimen the position of these diffracted beams is recorded.

By measuring the position of the recorded lines and thence by reference to standard tables the specimen is identified. The main advantage of this technique is that it identifies the solid phase rather than providing an elemental composition.

3.3.6. γ-Ray Spectrometry.

This technique utilises the γ-activity of a specimen. γ-rays are emitted with discrete characteristic energies which when passing through matter are transferred to that medium. Detection and measurement of these energies can enable the non-destructive determination of a number of radionuclides by

direct measurement of an irradiated sample.

The present study used a high resolution Canberra lithium-drifted germanium [Ge(Li)] detector of approximately $40cm^3$ coupled to a 4000 channel multi-channel analyser. The energy imparted to the detector material raises electrons from lower to higher energy bands. An applied electric field sweeps these charges through the material so that an electrical pulse is obtained.

The reason for the attractiveness of these semi-conductor detectors lies in the improved energy resolution compared with scintillation detectors. The resolution of the system used in this study enabled the determinations to be undertaken without any peak overlap and thus complex spectrum stripping procedures were not required. Until recently the main disadvantage of this system was that the efficiency was much lower than the scintillation detectors. However, with the introduction of larger semi-conductors the efficiencies are now comparable.

CHAPTER FOUR. POST IRRADIATION EXAMINATION OF A.G.R. CLAD INNER SURFACES.

4.1. Introduction.

Irradiated fuel-clad chemical interactions have been observed on numerous occasions (see Chapter 2) but the majority of data relate to the fast breeder reactor system. However the environment existing in the fuel-clad region of an A.G.R. fuel element differs from the fast breeder reactor situation and so the importance of a species in relation to incompatibility may vary.

This chapter decribes a post irradiation examination of the inner clad surfaces of A.G.R. fuel pins of differing irradiation and thermal histories.

4.2. Experimental.

Samples of 20%Cr/25%Ni/niobium stabilised stainless steel clad removed from A.G.R. fuel pins which had attained a range of irradiation and thermal conditions were examined. Failures had occurred in two of the pins from which the samples had been taken. Details are given in Table 6. After initial examination by optical microscopy (x20 - 80) samples of reaction product on the inner surface of the can were removed by micromanipulation and counted by γ-ray spectrometry. The samples of clad were then mounted edgewise in copper filled mounting plastic and examined by optical microscopy ($\geq$x200) for evidence of attack. Features of specific interest were marked with a diamond microhardness

TABLE 6: Irradiation and Thermal Histories of Clad Samples

Burn-up (MWD te^{-1})	Can Temperature ^{o}C	Fuel Centre Temperature ^{o}C	Remarks	Depth of Attack
4400	∿ 730	∿ 1100	Unfailed	Showed Double-Layer max. 50 μm
5650	∿ 795	∿ 1300	Unfailed	max. 10 μm
7270	∿ 655	∿ 1110	Unfailed	max. 22 μm
7270	∿ 655	∿ 1110	Failed	-
∿ 10,000	∿ 660	∿ 1600	Unfailed	15 μm
∿ 10,000	∿ 660	∿ 1600	Failed	Reaction product 70 μm thick
21,900	∿ 595	∿ 1190	Unfailed	7 μm

indentation tool so that they could be identified quickly for detailed examination.

The samples of reaction product were vacuum coated with an aluminium conducting layer (0.2 - 0.5nm). All samples were examined by electron probe microanalysis. Constituent elements were identified by scanning the X-ray emission using the mica, lithium fluoride, quartz and rubidium acid phthalate crystals whilst their distribution was determined by the X-ray image technique. In addition line scans for the individual constituent elements were monitored across the reaction zones. Semi-quantitative point analyses were undertaken; where marked segregation occurred point analyses were carried out in each area.

In an attempt to highlight areas of varying structure in regions of attack, selected clad specimens were colour etched.

4.3. Results.

4.3.1. General Observations.

The inner surface of the unfailed specimens had remained either shiny in appearance or possessed a matt grey finish. The shiny areas, however, were covered in a yellow-brown deposit (Figure 13). Within these areas brown translucent spherical nodules were observed (Figure 14), the largest being approximately 25μm in diameter. Only one failed pin (7270 $MWD.te^{-1}$) was available for surface observation. This was black in colour and very heavily scaled; one brown nodule was noted.

Figure 13. Inside surface of an unfailed A.G.R. clad specimen. (x10)

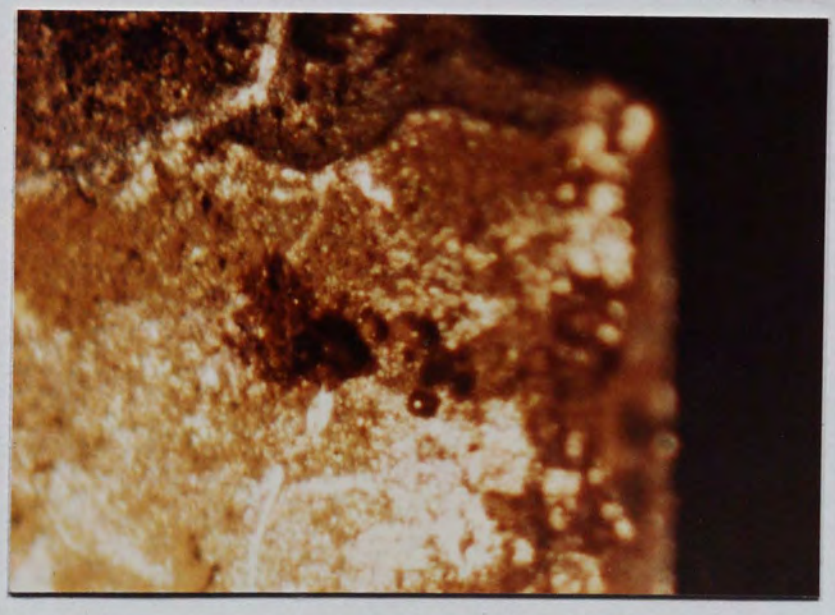

Figure 14. Area of inner surface of A.G.R. clad showing brown translucent spherical nodules. (x100)

4.3.2. Examination of Reaction Products removed from the Inner Surface of Irradiated 20%Cr/25%Ni/Nb-Stainless Steel Fuel Cladding.

The microscopic examination showed that the nodules had a very smooth glassy appearance (Figure 14), whilst scanning electron microscopy studies of a fractured sample indicated an outer crust of approximately 2.5μm in thickness.

The results of the electron probe microanalytical examination of the spherical products removed from both failed and unfailed 7270 MWD.te^{-1} pins are shown in Table 7. They were composed mainly of iron, chromium and nickel but small quantities of manganese and oxygen were also observed. The chromium constituent was either similar or slightly depleted compared with the basic 20%Cr/25%Ni/niobium- stabilised stainless steel but nickel was enhanced in most cases. There was no evidence of segregation over the area of the particles although from point analyses relatively more nickel was apparent towards the outer surface of the spheres.

The general product that had been removed from the unfailed clad specimens also showed the same constituents as the spherical product. However, in this case gross segregation of the constituents was observed, (for an example see Figure 15). The iron:nickel ratio varied from 1:0.1 to 1:1.5 while the iron:chromium ratio varied between 1:0.2 and 1:50 (see Table 8).

Uranium and oxygen were the main constituents of the scale removed from the failed pin together with segregated regions of the steel constituents. X-ray diffraction studies of the scale showed a uranium dioxide pattern that was identical with a sample of the original fuel. One specimen contained

TABLE 7.

Electron Probe Microanalytical Point Analyses

of Spherical Product.

Sample	Fe : Cr : Ni : Mn	Remarks
20/25/Nb steel	1 : 0.37 : 0.46 : 0.012	Calculated
1.	1 : 0.27 : 1.22 : 0.05	Analysed from outside of sphere.
1.	1 : 0.37 : 0.74 : trace 1 : 0.26 : 0.60 : trace	Analysed from inside of sphere.
2.	1 : 0.37 : 0.52 : trace 1 : 0.32 : 0.41 : trace	Analysed from inside of sphere.
3.	1 : 0.12 : 0.92 : 0.005 (from failed specimen.)	Analysed from outside of sphere.

TABLE 8.

Electron Probe Microanalytical Point Analyses of General Product removed from Unfailed 7,270 MWD.te^{-1} Clad Sample.

Sample	Fe	Cr	Ni	Mn
20/25/Nb steel	1	0.37	0.46	0.012
1.	1	0.28	0.20	trace
	1	0.30	0.62	trace
2.	1	1.19	0.31	0.03
	1	2.25	0.49	0.15
	1	0.78	0.15	0.03
	1	0.47	0.12	0.03
3.	1	0.18	0.34	trace
	1	15.35	0.63	trace
	1	2.07	0.64	trace
	1	0.38	0.26	trace
4.	1	0.57	0.40	0.02
	1	50.51	1.47	0.55
	1	1.34	0.32	0.02
	1	1.32	0.26	0.06

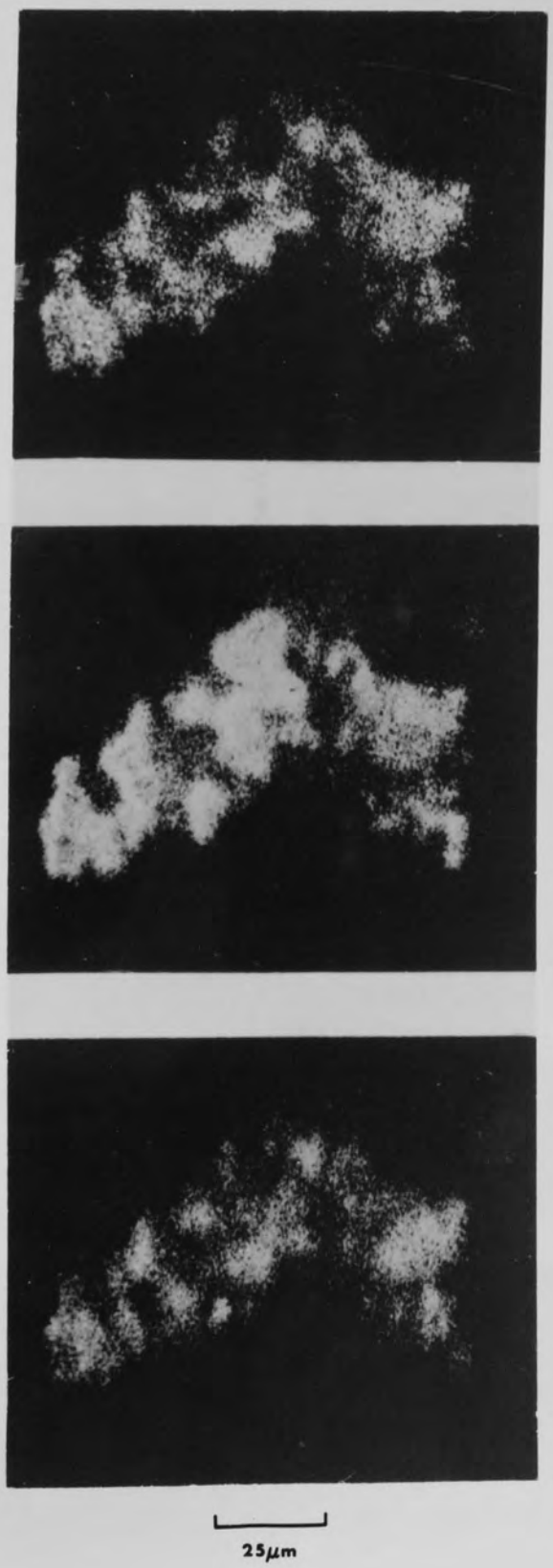

Figure 15. EPMA elemental distribution in general product from unfailed AGR fuel clad.

silicon segregated from the other constituents (Figure 16).

Each of the samples from both the failed and unfailed pins contained caesium-134 and caesium-137. Cerium-144 and ruthenium-106 were also present in material removed from the failed pin.

4.3.3. Cross Sectional Examination of Clad Samples.

When the specimens were examined in cross section two types of surface condition were noted. With the first type (Figure 17) the reaction zone had a maximum depth of 22μm (Table 6) and appeared as a roughening of the clad surface. In the second type (Figure 18) two regions were evident in the surface layer; the outer region being separated from the steel matrix by a dark phase. Colour etching of this "double-layer" showed that both the outer layer and the clad behaved in a similar manner, suggesting that both regions had a similar composition; the technique could not however provide any detail in grain structure within the dark phase.
The "double-layer" effect was observed in only one instance; this was with an unfailed specimen. The maximum distance between the outer strip and the parent matrix was approximately 50μm. The extent of the double-layer was also very limited because on further metallographic polishing it disappeared.

The reaction layer of the first type contained iron, chromium, nickel, silicon, caesium, uranium and oxygen (Figure 19). It was not of uniform thickness and the silicon, caesium and uranium were segregated from the iron, chromium and nickel. The oxygen appeared to be distributed throughout the reaction product. The position of caesium in relation to the major

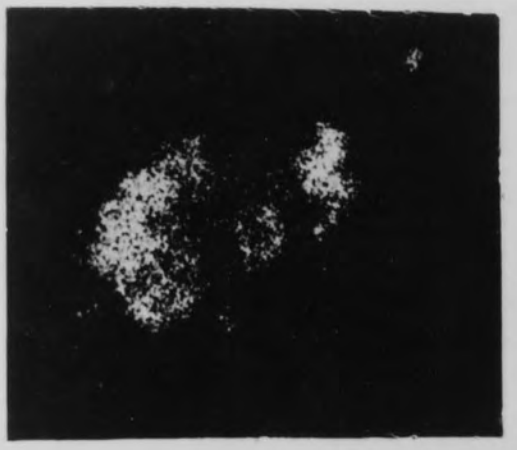

Uranium.

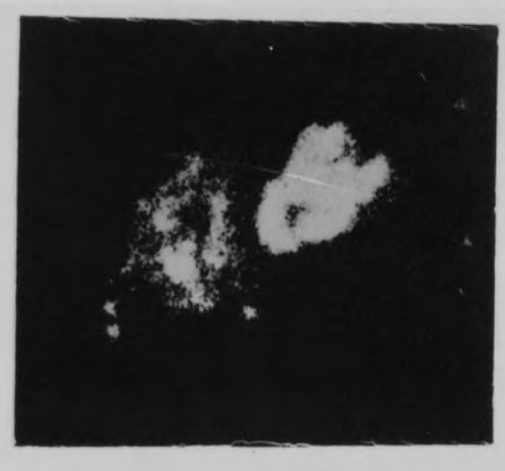

Iron.

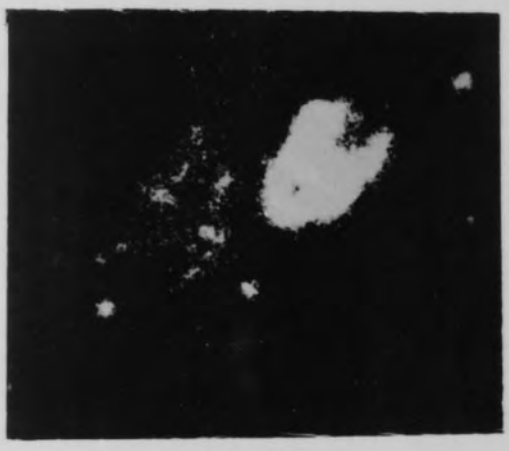

Chromium.

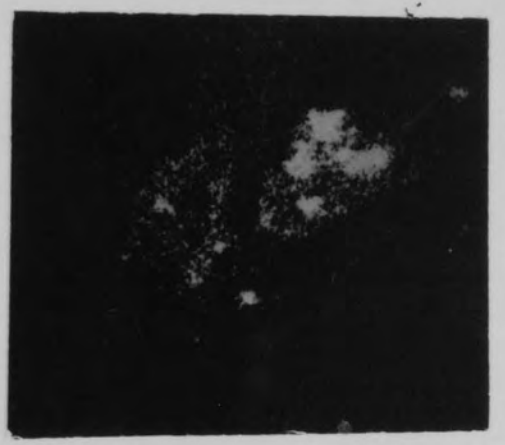

Nickel.

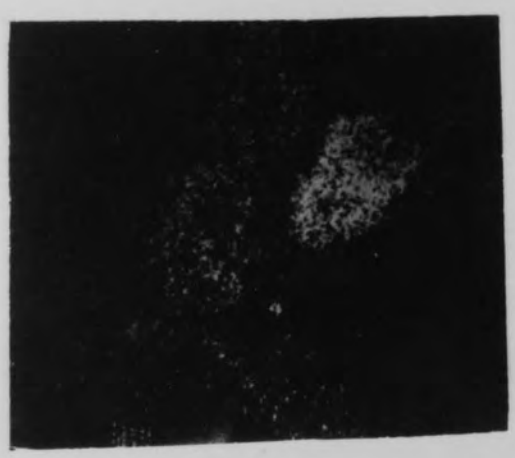

Manganese.

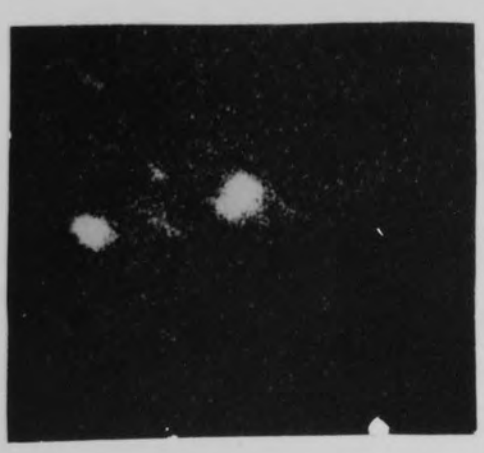

Silicon.

Figure 16. EPMA elemental distribution in sample from failed AGR fuel clad.

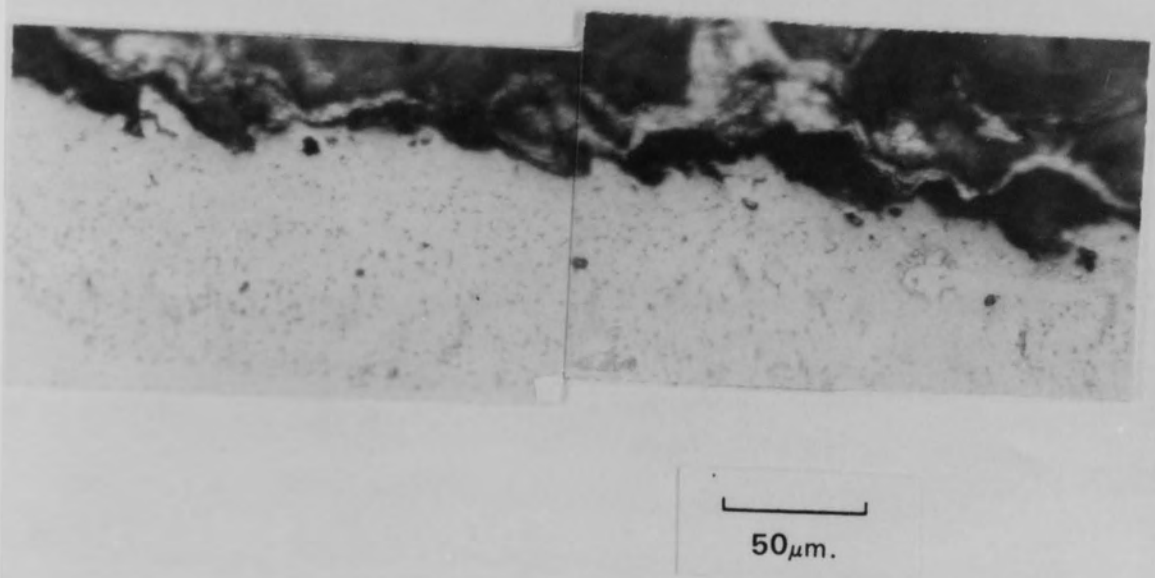

Figure 17. Example of inner surface reaction zone (type 1).

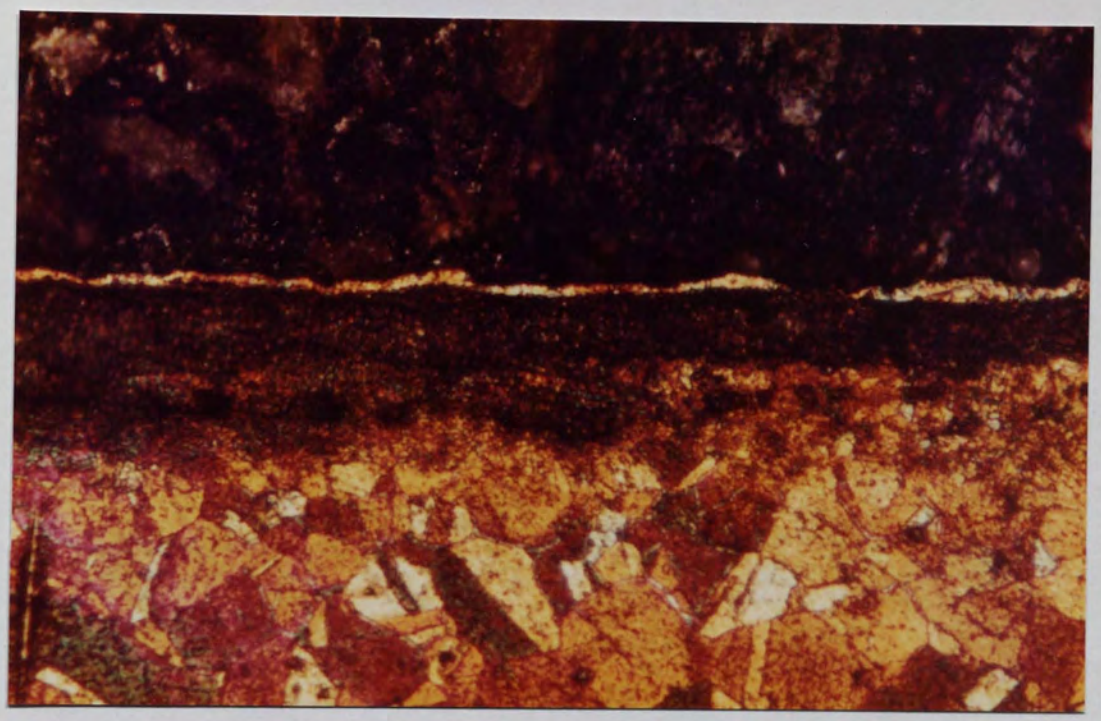

Figure 18. Reaction zone featuring "double-layer" effect.

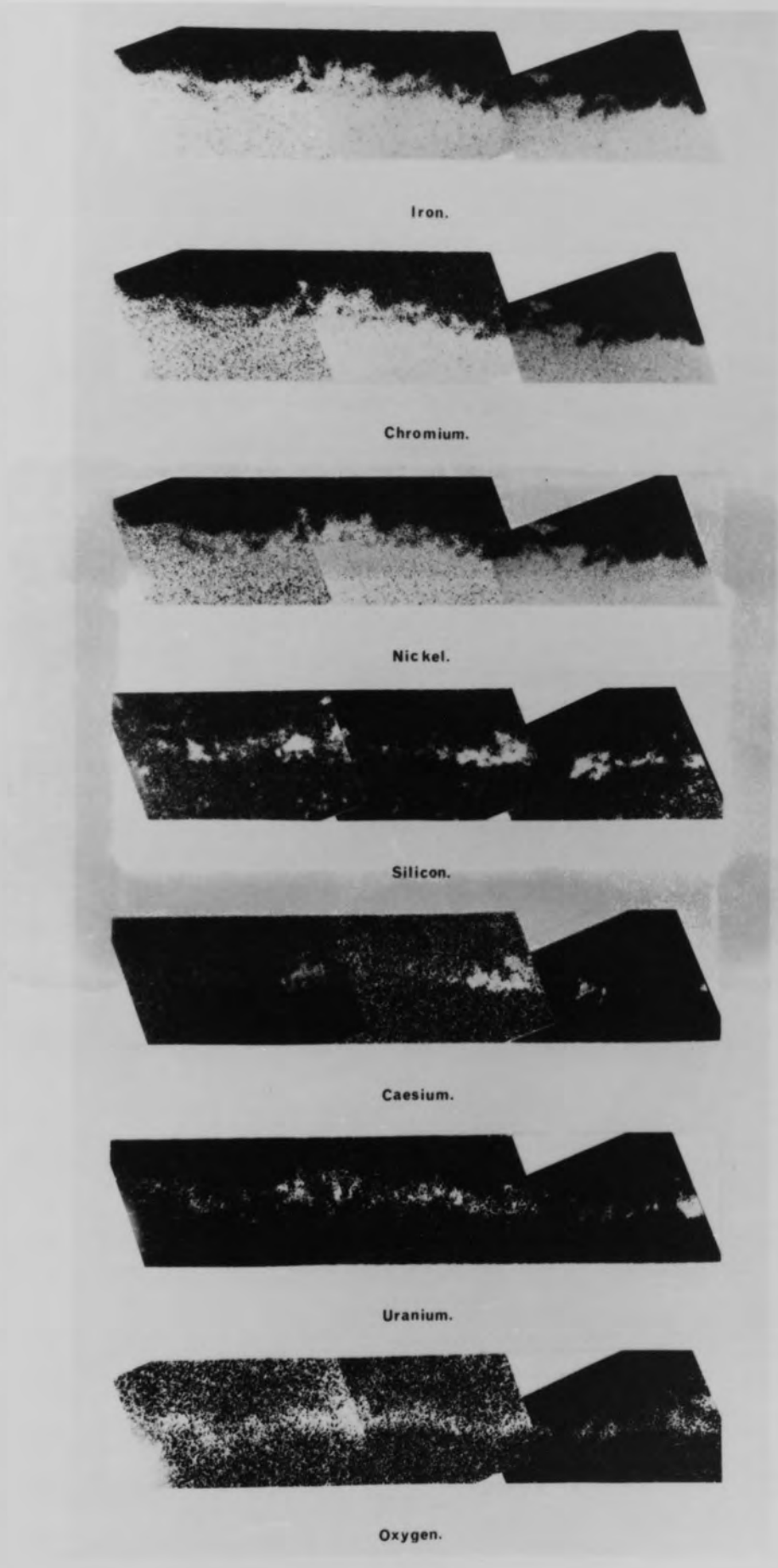

Figure 19. EPMA elemental distribution in reaction zone (type 1).

clad constituents is shown more clearly by an electron probe microanalytical line scan (Figure 20). Caesium was enhanced in the fuel-clad region.

This type of attack did not appear to show an enhancement with increasing burn-up; there was, however, some evidence of a temperature dependence. For example, an attack of 7μm was observed on a specimen from an unfailed pin having attained approximately 21,900 MWD.te^{-1} but with a clad temperature of only 595°C while approximately 20μm deep reaction was apparent on a similar specimen which had attained 655°C and a burn-up of about 7,270 MWD.te^{-1}.

The second type of reaction product also contained iron, chromium and nickel distributed throughout the reaction layer and up to the outer skin. Point analyses showed no significant differences between the relative amounts of each of these elements in the outer layer, the dark phase or the parent matrix. Bearing in mind the limited extent to which this feature was observed it is possible that the electron beam may have been penctrating through the "double-layer" and analysing steel underneath. The electron penetration is calculated to be approximately 1.2μm for the voltage used (Castaing, 1960) which is consistant with this view.

Oxygen, caesium and uranium were not detected in the dark phase but silicon and tellurium were present. Although the silicon was distributed as segregated areas it was not associated with carbon; these regions were therefore not silicon carbide particles which might have contaminated the surface during metallographic preparation. None of the other component elements appeared to be enhanced with the

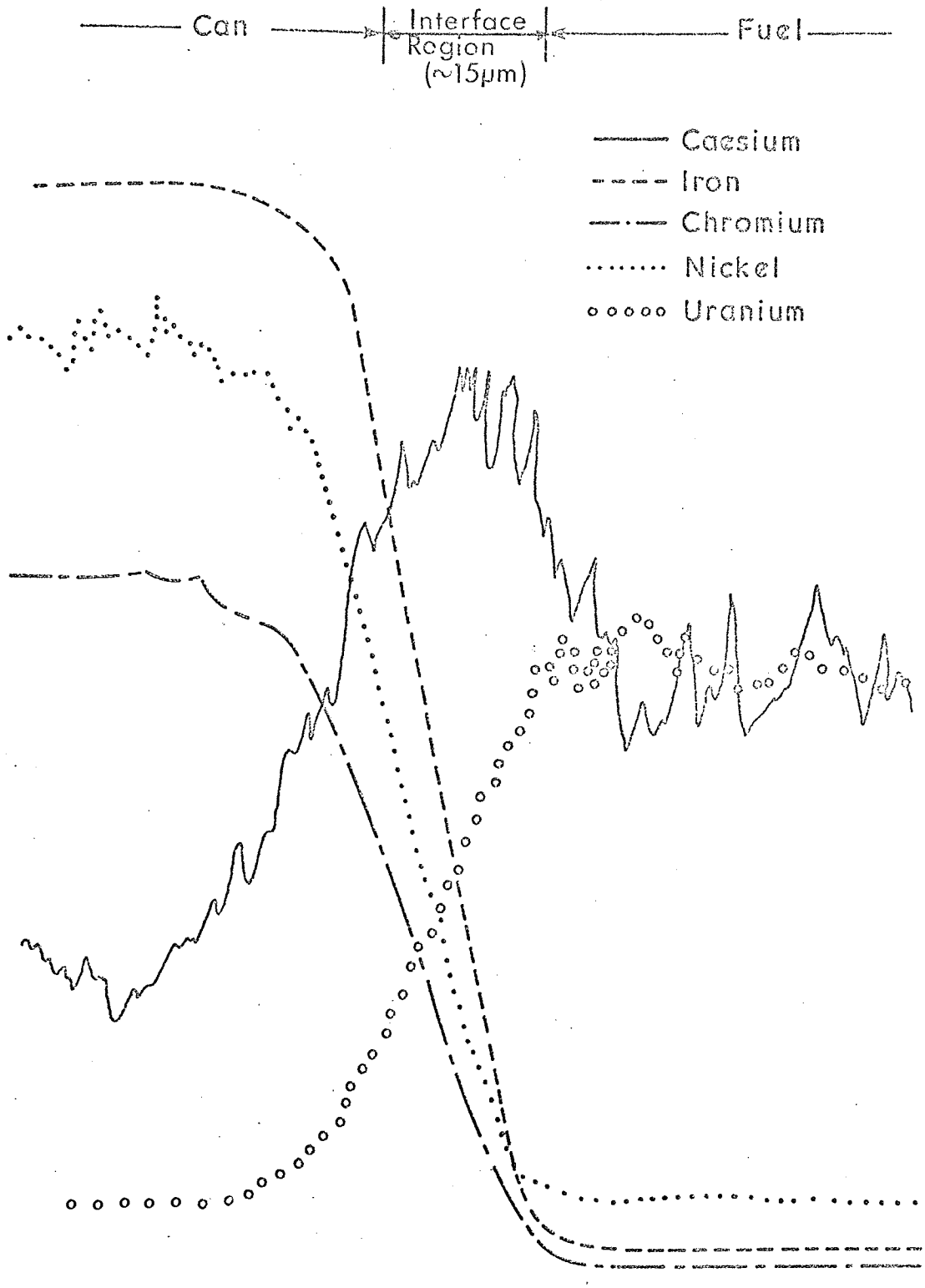

Figure 20. EPMA elemental line scan showing position of caesium.

silicon and in fact the electron probe microanalytical data showed that the iron, chromium and nickel contents decreased in the silicon rich areas.

Examination of the failed pin specimen revealed thicker reaction layers (up to 70μm) than those observed on the unfailed pins (Figure 21). Iron, chromium, nickel, manganese, caesium and oxygen were present in these layers and the distributions of the elements are shown in Figure 22. The product next to the metal surface was chromium rich, the intermediate layer was enriched with iron and nickel but depleted in chromium whilst the outer layer was enriched in chromium and iron but depleted in nickel. Oxygen was distributed fairly evenly throughout the reaction product but caesium appeared as segregated areas in the outer region only. Figure 22 includes a schematic diagram showing these relative distributions, whilst Figure 23 is an elemental line scan through an area where caesium was located in the outer chromium rich region.

4.4. Discussion.

4.4.1. General Discussion.

The observed attack on the inner surface of the cladding material can be accounted for in several ways:-

a) the interaction may have occurred before irradiation i.e. it would have occurred without being subjected to irradiation,

b) the cladding material may have been contaminated and the observed features developed during subsequent irradiation,

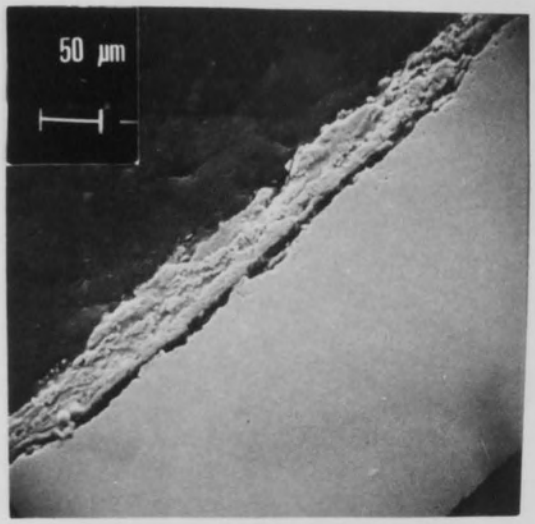

Figure 21. Reaction product on inner surface of a failed clad specimen.

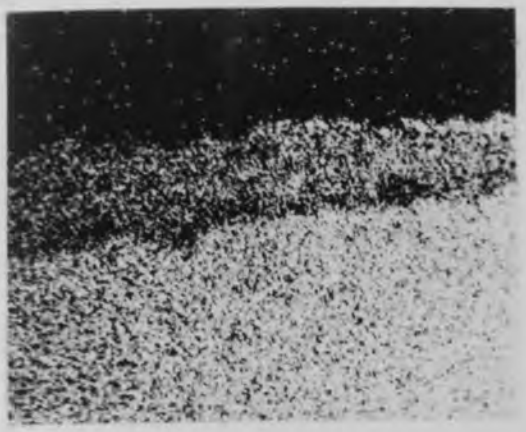

Iron.

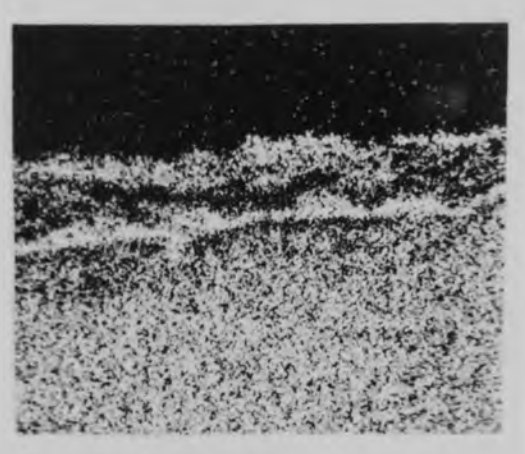

Chromium.

100μm

Nickel.

Oxygen.

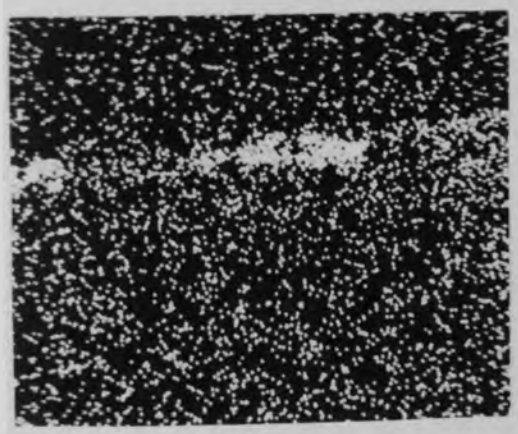

Cæsium.

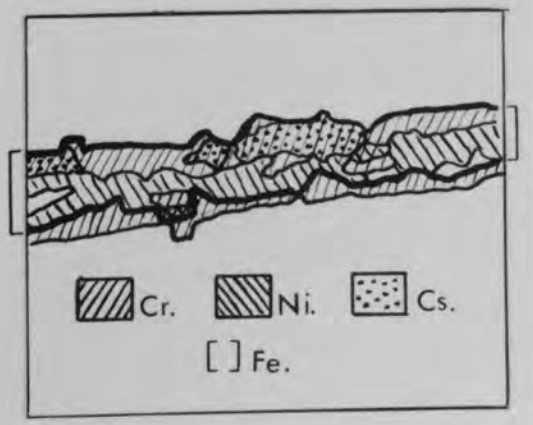

Schematic Diagram.

Figure 22. EPMA elemental distribution of reaction product on failed clad specimen.

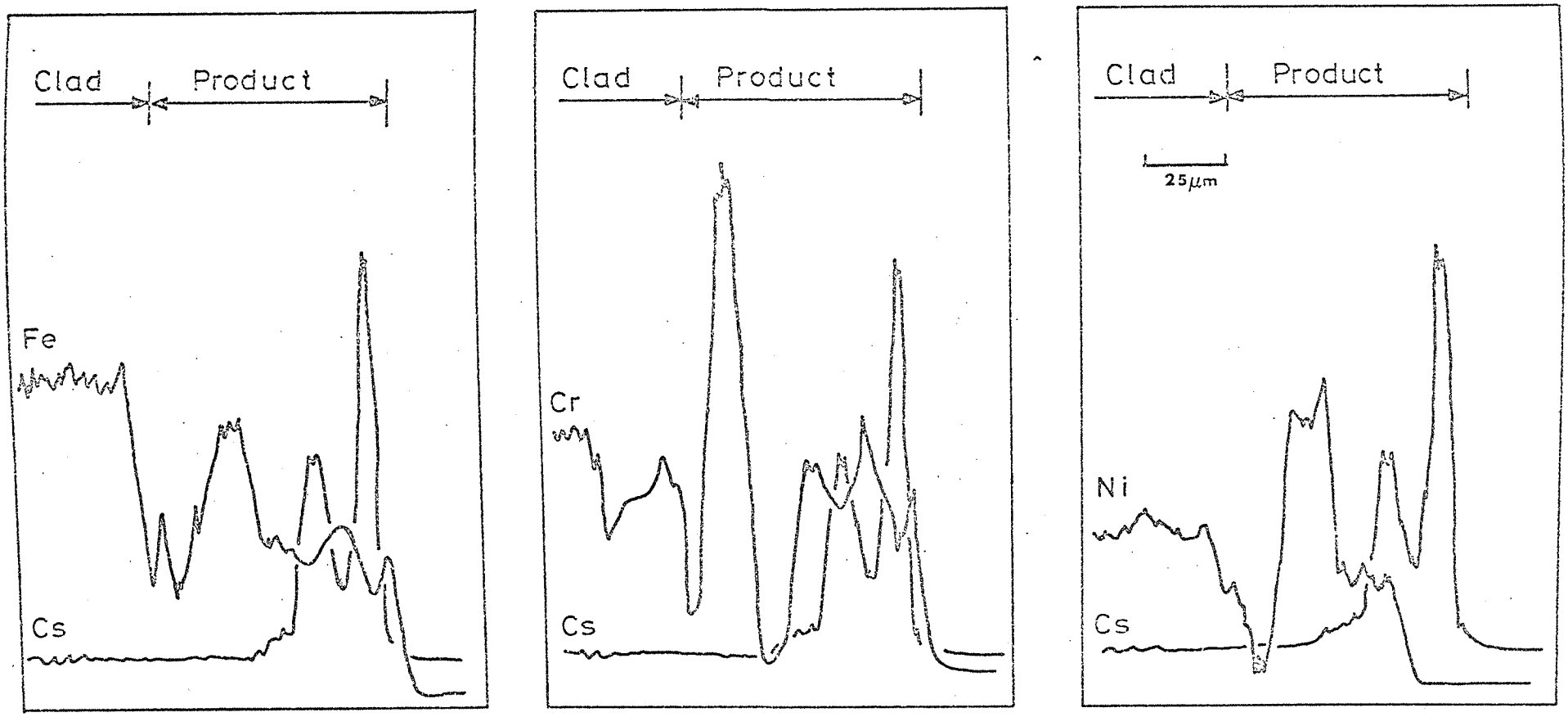

Figure 23. EPMA elemental line scans of reaction product on failed clad specimen taken through area where caesium was located in outer chromium rich region.

and c) the interaction may have occurred in the reactor as a consequence of the fuel pin environment.

When considering (a) and (b) above it must be noted that interactions before irradiation occur principally due to improper degreasing procedures, while studies into the compatibility of uranium dioxide and stainless steel indicate that corrosion effects are unlikely except perhaps when hyperstoicheiometric fuel is used (see Chapter 2). Since hyperstoicheiometric fuel is not used in the A.G.R. the following discusion is based on the premise that the interaction occurred as a result of the fuel pin environment during irradiation.

4.4.2. Reactions on Unfailed Clad Inner Surfaces.

From the data expressed in Chapter 2 it was evident that the volatile fission products can play a major role in the attack of the clad inner surface. The only fission product observed in the general areas of attack was caesium but it had not penetrated into the grain boundaries. This is at variance with the majority of the available fast reactor data that has shown caesium in areas of intergranular attack. The mechanisms invoked rely on an oxygen potential and this differs between fast and thermal fuels. However, although the caesium that was observed in the reaction layer was segregated from the steel constituents the presence of this element at the inner surface of the clad may still indicate that it contributes to a fuel-clad reaction.

Iodine was not observed on any of the specimens examined but this is not too surprising since the iodides of

iron, chromium and nickel are oxidised fairly rapidly in an air environment (Ramsdale and Hilton, 1972). The specimens in this study were examined approximately 3 years after the initial cutting procedure.

Therefore the observation of oxygen during the present electron probe microanalytical studies must be interpreted with caution because its presence may result from either the primary reaction with the clad constituents or a secondary effect; i.e. oxygen may have reacted with the steel clad during irradiation (in addition to oxygen made available during the fission process oxygen may also come from non-stoicheiometric fuel containing excess oxygen or by stoicheiometric uranium dioxide fuel with a high centre temperature leading to the formation of hypostoicheiometric uranium dioxide), or oxygen may have reacted with any reaction product on subsequent exposure to a carbon dioxide or an air environment during examination.

The reaction product on the surface did not resemble the type of product usually observed on an oxidised stainless steel surface and therefore straightforward oxidation of the clad inner surface is improbable. The involvement of oxygen, therefore, may be a secondary effect as mentioned above.

Silicon was observed in this reaction layer segregated from the steel components and associated with the caesium and uranium. No general depletion of the silicon content in the steel towards the inner surface was observed and the silicon was also segregated from the steel constituents. The formation of silicates or silicides produced either by combination of uranium and silicon from the steel or reaction between the

steel and silicon impurity in the fuel seems unlikely.

The maximum reaction depth observed for the general attack was approximately 22μm. However on the 21,000 MWD.te^{-1} example that had only attained a low temperature (approximately 595^{o}C) a low level of attack was observed. This may be explained by the threshold temperature dependence suggested by Fitts et al., (1971) who have shown in fast reactor studies that a temperature of approximately 600^{o}C may have to be attained before attack commences.

The main feature of the brown spherical nodules was that there was no segregation over their area and as such they differed from the general product. This suggests a gross attack of the stainless steel. However, the electron probe microanalytical examination did show that there was relatively more nickel in the outer crust of the spheres than in their core, whereas the iron:chromium ratio remained similar throughout the particles. The appearance of the nodules suggested that they may have been molten. Now in general the iodides have low melting points (e.g. FeI_2 at $\sim$550^{o}C (Allen, 1972)) and it is thus possible that this agrees with the postulated secondary involvement of oxygen mentioned earlier for the general areas of attack. However it has been shown in Chapter 2 that any iodine liberated during fission would be expected, from thermodynamic considerations, to be present as caesium iodide. Therefore if these nodules were the product of iodine involvement then reaction of the clad with caesium iodide would have had to occur followed by the subsequent oxidation of the steel iodides. Compatibility studies of the caesium iodide-stainless steel system show reaction only in the presence of

oxygen (Chapter 2) and that the results are similar to caesium-oxygen-stainless steel studies. Therefore preferential reaction of the caesium to form a product that is more stable than caesium iodide would be necessary.

However the internal chemistry of a fuel element is very complicated and it may be that elemental iodine can exist under certain conditions or that because of the large excess of steel constituents, compared to both caesium and iodine, steel iodides could be formed. In this case the involvement of iodine would account for the observation of both the nodular and general attack.

Of the types of attack noted on the unfailed clad specimens examined the "double-layer" effect was noted on only one occasion. However, studies at the United Kingdom Atomic Energy Authority (U.K.A.E.A.) by Skinner and Newbigging (1973) have shown that this type of effect is apparent on approximately 40% of specimens examined. The observation in the present study occurred on an unfailed clad specimen having attained a burn-up of approximately 4,400 $MWD.te^{-1}$ and a clad temperature of approximately 730°C. The specimen had achieved the lowest burn-up of those examined and although the clad temperature was in excess of 700°C it was not the maximum of the range examined. It would therefore appear unlikely that this type of effect is an extension of the more general attack observed.

The studies of Skinner and Newbigging (1973) show that the typical depth of attack of the "double-layer" reaction zone is 10μm compared to a maximum of 50μm reported earlier in this chapter. Their electron probe microanalytical studies

showed the presence of both caesium and tellurium in the dark region of this double layer together with manganese and silicon. They suggested that the latter two elements may have been present as manganese silicate. However, although silicon was observed in the dark phase of the double layer in the present study it would not appear to be present as a silicate since oxygen was not detected and where silicon was enhanced in the reaction layer there was a proportional depletion of the steel constituents.

The only fission product observed in this specimen was tellurium which was present in the dark phase of the double layer. This agrees with the observations of Skinner and Newbigging (1973), although they also report the presence of caesium. It is significant because the tellurium was detected in the reaction layer and not just on the surface of the steel. At present there is very little information on the effect of this element on stainless steel although it is known to have a deleterious effect (Hampel, 1961).

Skinner and Newbigging (1973) report no evidence of progressive attack with increasing burn-up or clad temperature; although a threshold clad temperature of 550°C could be compared with the condition reported by Fitts et al., (1971). Some dependence on the fuel temperature was apparent because the feature was only observed on fuel elements that had achieved a maximum fuel temperature of 1150°C. Above this temperature a decreasing incubation period with increasing fuel temperature was reported. The specimen that showed the "double-layer" phenomenon in the present study had only achieved a fuel centre temperature of 1100°C although the clad temperature

was well in excess of any possible reported threshold requirement. Other specimens of a higher fuel centre temperature however did not show this feature.

Because of the non-progressive nature of this attack, the presence of silicon in their reaction layer and the observed dependence on the fuel temperature, Skinner and Newbigging (1973) suggested that the minor constituents in the fuel may be responsible for this type of attack. However, because of the segregation of silicon observed in the present study it would appear that this element is incorporated in the reaction layer by some process other than by a chemical reaction between the silicon impurity in the fuel and a clad constituent.

From the above discussion it is apparent that only circumstantial evidence was forthcoming on the parameters responsible for this attack. Indeed, there was no direct evidence from the present study to show that the extent of reaction was detrimental to the life of an A.G.R. fuel element although it must be realised that this study was limited to a small number of specimens. A more comprehensive post irradiation study undertaken on C.A.G.R. fuel elements would provide a better statistical approach under realistic operating conditions. However, the possible involvement of fission products requires further investigation particularly since the temperatures of the C.A.G.R. fuel elements will be generally higher than for those specimens studied in this thesis.

4.4.3. Failed Clad Inner Surface.

The reaction product on the failed pin showed an elemental distribution somewhat similar to those obtained when 20%Cr/25%Ni/niobium-stabilised stainless steel is oxidised in carbon dioxide at 900°C for several thousand hours. However, since the fuel was discharged from the reactor only 5 days after clad perforation (Jones, 1972), the extent of attack at the inner surface of the clad is much greater than would be anticipated from a reaction involving carbon dioxide alone (possibly $>10^3$ times). It is believed that the oxidation rate is accelerated by fission products and the presence of caesium associated with the chromium-iron outer layer may be significant. The observations presented by Skinner and Newbiggin (1973) on the examination of failed fuel elements and the studies of Antill et al., (1975) (see section 2.4.1.) confirm the possibility of a fission product enhancement of the clad-coolant reaction following failure.

The precise role of caesium has not been established but point analyses taken in the caesium rich areas showed that there was a sufficient quantity of this element present to enable compound formation to occur with the chromic oxide to produce caesium chromates.

Additionally γ-ray spectrometry has shown that the ratio of caesium-134 to caesium-137 activities was considerably greater in the reaction product than in the adjacent fuel. It is therefore possible that fission product iodine may also have been involved in the acceleration of the reaction between the stainless steel and carbon dioxide by forming steel iodides as intermediates.

4.5 Summary.

Two types of reaction product have been observed on the inner surfaces of specimens removed from unfailed A.G.R. fuel pins. First, a yellow-brown general product and second, a brown translucent spherical product which occurred in small clusters. The constituent elements in both these types of product were iron, chromium and nickel together with small amounts of manganese and oxygen. It is not known whether the oxygen is present from a primary or secondary reaction. Gross segregation was evident in the general type of product whereas no segregation was observed in the spherical nodules. The brown spherical areas appear to have been molten and gross attack of the steel may have occurred. The presence of an enhanced caesium-134 contribution on the reaction products may indicate that iodine has reached the fuel-clad interface.

Cross sectional examination showed two types of attack of the inner surface of unfailed A.G.R. clad specimens. The first was a general attack to a maximum depth of approximately 22μm. The attack did not appear to be directly related to burn-up but the clad temperature may be significant. The second type of attack was characterised by a "double-layer" effect. The outer region of this feature was separated from the parent matrix by a dark phase (maximum thickness was approximately 50μm) but appeared to be physically and chemically similar to the clad.

Silicon was the only element common to both types of attack in the unfailed examples, other than the main stainless steel constituents. Tellurium was the only fission product observed below the surface of any reaction on the unfailed

clad surfaces and due to its corrosive nature requires further investigation. There is circumstantial evidence that iodine may also have been involved in the reaction.

The evidence did not show that the extent of attack on the inner surface of unfailed A.G.R. cladding was detrimental to the life of a fuel pin. However, this was a study limited to relatively few specimens and depth of attack measurements would need to be undertaken on a routine basis to provide more statistical information.

An accelerated oxidation rate has been observed on the inner surface of a failed clad specimen and it is believed that this could be induced by the presence of fission products.

CHAPTER FIVE. COMPATIBILITY OF TELLURIUM WITH 20%Cr/25%Ni/Nb-STABILISED STAINLESS STEEL.

5.1. Introduction.

Tellurium is volatile under the operating conditions of the A.G.R. and therefore will concentrate in the cooler outer regions of the fuel pins together with the other volatile fission products, caesium and iodine. In the post irradiation study of A.G.R. fuel clad inner surfaces (Chapter 4) tellurium was the only fission product that was observed in the reaction layer on unfailed clad specimens and not just on the surface of the steel.

Little data are available on the role of tellurium in fuel-steel clad reactions in either thermal or fast reactor systems but out of pile studies have shown that it can have a deleterious effect on steels which is not dependent on the oxygen potential but is a function of the steel type (Götzmann and Hofmann, 1972).

To study the effect of tellurium on 20%Cr/25%Ni/Nb-stabilised stainless steel at C.A.G.R. operating temperatures, specimens of both the as received and pre-oxidised steel were examined by metallography, energy dispersive X-ray analysis and electron probe microanalysis after their exposure to a tellurium environment for varying periods.

5.2. Toxicology of Tellurium.

Tellurium is reported as being less toxic than selenium (Cooper, 1971) with elemental tellurium being the least toxic

form. Tellurium may be absorbed into the body orally, by inhalation and by absorption through the skin. To date no serious industrial hazard has been reported. It is however more potent than selenium at generating the characteristic obnoxious breath (Stone and Carbon, 1961) which is also documented as "the garlic odour". This symptom is a good indication of absorption of tellurium into the system but the incidence cannot be quantitatively related to the level of tellurium intoxication due to the varying susceptibility among individuals (Cooper, 1971). This unpleasant odour is due to the excretion of organo-tellurium compounds (Bagnell, 1966) and can vanish in a few days (Elkins, 1950). However garlic odours of the breath lasting up to 237 days have been reported by Cooper (1971). In addition to excretion through the lungs tellurium can be found in perspiration, urine and faeces.

Table 9 taken from Bagnell (1966) compares the maximum permissible concentrations of tellurium with other toxic substances although the maximum permissible concentration of tellurium in air at which no garlic breath is apparent is reported to be 0.01 - 0.02 mg. m^{-3} of air (Cooper, 1971).

Besides garlic odour of the breath the following symptoms have also been noted:- transient headaches, somnolence, metallic taste and dryness of the mouth, loss of appetite and nausea. A more comprehensive list of the likely symptoms to occur following acute exposure has been derived from experiments on animals (Mead and Gies, 1900); these include:- restlessness, tremor, diminished reflexes, paralysis, convulsions, somnolence, unconsciousness, disintegration of the mucous membranes of the stomach, cessation of respiration and finally death.

TABLE 9.

Relative Toxicity of Tellurium.

Substance	Concentration ($mg.m^{-3}$)
Carbon Monoxide	100
Hydrocyanic Acid	10
Selenium	0.1
Tellurium	0.1

5.3. Chemical Properties of Tellurium.

Tellurium is a member of Group VIb of the Periodic Table (Z=52; A.W.=127.6); it melts at 450°C and boils at 1390°C although a value as low as 990°C has also been quoted (Brookes, 1952). Its properties lie between those of the non-metals, oxygen and sulphur, and metallic polonium and it is insoluble in all solvents that do not react with it.

It burns in air (or oxygen) forming the dioxide, is unattacked by hydrochloric acid but is oxidised by nitric acid to form tellurous acid (H_2TeO_3). It also dissolves in hot alkali solution forming either the telluride or tellurite. Tellurium forms halides and combines with most metals at high temperatures to form tellurides. Its compounds are nearly always colourless except for the polytellurides which are deep red.

5.4. Internal Environment of a C.A.G.R. Fuel Pin.

5.4.1. Amount of Tellurium available in the Fuel Pin.

The total amount of tellurium produced in a C.A.G.R. fuel pin having a burn-up of approximately 18,000 MWD.te^{-1} is approximately 5.7g (Appendix 2). However the quantity of this element that reaches the fuel-clad interface will depend not only on the burn-up of the fuel but also on factors affecting the retention of this fission product in the fuel matrix i.e. temperature gradient, physical condition of the fuel (e.g. cracks, porosity etc.). In addition the concentration of tellurium at the clad surface will depend on any movement of this element along the fuel pin from a higher to a lower temperature region.

If all the available tellurium is dispersed evenly over the clad inner surface then a concentration of approximately 0.12mg.mm^{-2} tellurium would be possible. However it is anticipated that < 10% will be released from the fuel hence reducing this tellurium concentration to <0.01 mg.mm^{-2}. If movement of the tellurium occurs along the fuel pin then localised concentration of the tellurium may be caused in the cooler end regions of the pin. In addition irradiation levels up to approximately 25,000 MWD.te^{-1} are expected for C.A.G.R. thus increasing the anticipated amount of tellurium.

The main part of the following investigation was undertaken using a tellurium concentration of 0,1mg.mm^{-2} of steel surface. This concentration was chosen to obtain a reaction product of reasonable thickness for examination and hence mechanism evaluation. Subsequent to this (i.e. section 5.7) the effect of varying the tellurium concentration has been studied.

5.4.2. Surface Condition.

During the lifetime of a C.A.G.R. fuel pin it is likely that an oxidising environment will be instigated at the fuel-clad interface. It has been discussed in section 2.5. that the oxygen potential inside a fuel pin depends on the fissile nuclides present. In the A.G.R. the majority of fission takes place in uranium-235 which results in relatively little oxygen being made available; however oxygen may also come from hyperstoicheiometric fuel or the formation of hypostoicheiometric fuel due to high centre temperatures. Therefore the corrosive effects of fission product tellurium on oxidised 20%Cr/25%Ni/Nb

stabilised stainless steel have also been examined.

5.5. Experimental.

The chemical composition of the 20%Cr/25%Ni/Nb-stabilised stainless steel used in these experiments is shown in Table 10. Specimens having a known surface area ($\sim$200mm^2) were cut from 0.38mm thick sheet containing approximately 50% cold work and heat treated in static vacuum for 1 hour at 930°C followed by air cooling. The specimens were weighed, resealed in silica ampoules with approximately 0.10mg.mm^{-2} of spectrographically standardised tellurium after evacuating to better than 0.01μbar (10^{-5} torr) pressure. The sealed ampoules were then annealed for various periods initially at 750° and 850°C, controlled to ±2°C, to represent the range of inner clad temperatures of C.A.G.R. fuel. Supplementary anneals at 350°, 450°, 550° and 650°C were performed to obtain additional data on the mechanism of the reaction.

After exposure to tellurium vapour, the specimens were removed from the ampoules, reweighed and mounted edgewise in copper filled mounting plastic. Each specimen was examined by optical and scanning electron microscopy after polishing to 1μm diamond finish; in some cases specimens were given a short electrolytic etch in 10% oxalic acid.

For some tests at 750° and 850°C, exposed specimens were resealed in evacuated silica ampoules without further addition of tellurium and re-annealed at the same temperature for a further period of either 70 or 115 hours. A temperature gradient experiment was also conducted where the reheating was undertaken in a long silica tube in which the temperature

TABLE 10.

Composition of 20%Cr/25%Ni/Nb Stainless Steel.

Constituent (wt%)						
Cr	Ni	Mn	Si	C	Nb	Fe
20.2	24.6	0.63	0.45	0.03	0.60	Bal.

varied from the specimen temperature to almost room temperature at the other end of the tube.

Polished sections were examined by electron probe microanalysis using the Cambridge Microscan 5 analyser. Constituent elements in the surface corrosion product were identified and their distributions within the product were established by the X-ray scanning image technique. The composition of the steel beneath the corrosion product was determined by line scans for the individual elements across this region. These studies were supplemented by energy dispersive X-ray analysis of the reaction product surface and of polished sections through the product.

5.6. Results.

The experimental data and observations for the studies using $0.1 mg.mm^{-2}$ of tellurium at each of the temperatures examined are summarised in Tables 11 - 15 and discussed in the following sections. The first two sections are concerned with the reaction kinetics and depth of attack measurements while later sections report on the chemical investigations of the reaction products and steel surface. The results are summarised in section 5.6.5.

5.6.1. Weight Gain Measurements.

After exposure to tellurium vapour all specimens had a dull matt grey/black appearance and at 750^{o} and $850^{o}C$ had gained in weight by the same amount as the weight of tellurium added to the ampoule. This even applied for the very short heat treatments in which the ampoule had been raised to the

TABLE 11

Experimental Data for 850°C Studies

Exposure time (hours)	Initial amount of tellurium used (mg mm^{-2})	Reaction product thickness (μm)	Number of reaction layers evident	Thickness of individual layers (μm)	Intergranular attack (μm)	Chromium depletion depth* (μm)
10 min	0.10	18	2	Outer 8-12 Inner 6-11	5	20
1	0.11	19	2	Outer 5-12 Inner 5-14	11	26
7.5	0.11	20	2	Outer - isolated Inner - remainder	25	30
50.5	0.12	25	1	-	36	45
1014	0.12	20	1	-	44	90

TABLE 12

Experimental Data for 750°C Studies

Exposure time (hours)	Initial amount of tellurium used (mg mm^{-2})	Reaction product thickness (μm)	Number of reaction layers evident	Thickness of individual layers (μm)	Intergranular attack (μm)	Chromium depletion depth* (μm)
< 160 sec	0.11	22	2	Outer 18 Inner 4	< 2	8
10 min	0.11	20	2	Outer 13 Inner 7	4	20
1	0.12	25	2	Outer 17 Inner 8	8	13
7	0.12	22	2	Outer 5-12 Inner 10-17	13	25
53	0.11	20	2	Outer- isolated Inner - remainder	25	83
1027	0.11	23	1	-	45	110

TABLE 13

Experimental Data for 550°C and 650°C Studies

Exposure time (hours)	Initial amount of tellurium used (mg mm^{-2})	Amount of tellurium used during experiment (mg mm^{-2})	Reaction product thickness (μm)	Number of reaction layers evident	Thickness of individual layers (μm)	Intergranular attack (μm)	Chromium depletion depth* (μm)
550°C							
< 160 sec	0.10	0.08	11	1	-	< 2-3	-
7	0.10	0.10	17	2	Outer 12 Inner 5	3-4	6
650°C							
< 160 sec	0.10	0.09	11	1	-	< 2-3	-
7	0.11	0.11	17	2	Outer 14 Inner 3	7	8

*Measured from the reaction product/metal interface.

TABLE 14

Experimental Data for 450°C Studies

Exposure time (hours)	Initial amount of tellurium used ($mg\ mm^{-2}$)	Amount of tellurium used during experiment ($mg\ mm^{-2}$)	Reaction product thickness (μm)	Number of layers evident	Intergranular attack (μm)	Chromium depletion depth (μm)
< 120 sec	0.104	0.0005	< 3	1	None	None
10 min	0.100	0.016	3	1	"	"
20 min	0.102	0.035	NOT EXAMINED		"	"
30 min	0.102	∿ 0.047	9	2	"	"
45 min	0.101	0.066	NOT EXAMINED		"	"
1	0.095	0.076	12	2	"	"
1.25	0.106	0.101	NOT EXAMINED		"	"
3	0.097	0.097	21	2	"	"
7	0.096	0.096	19	2	< 2-3	< 5

Table 15.

Experimental Data for 350°C Studies.

Exposure time (hours)	Initial amount of tellurium used ($mg.mm^{-2}$)	Amount of tellurium used during experiment ($mg.mm^{-2}$)	Reaction product thickness (μm)
7.5	0.098	0.015	2
16	0.098	0.031	5
32	0.104	0.055	10
45	0.095	0.087	15
64.5	0.098	0.096	17

annealing temperature and then air cooled immediately, giving a total exposure time to tellurium vapour of <160 seconds. The only exception to this (at 750° and 850°C) was provided by the specimen annealed for 1014 hours at 850°C, where the weight gain was approximately 75% of the total amount of tellurium added. At the lower exposure temperatures of 550° and 650°C, the short term anneals of < 160 seconds also produced a weight gain less than the total weight of tellurium added. Brown fumes were visible in these ampoules upon withdrawal from the furnace and the condensation of a thin layer of tellurium in small patches on the wall of the ampoule on cooling was taken as evidence of incomplete reaction with the stainless steel. Incomplete reaction was also evident in the 350° and 450°C series of experiments. The results listed in Tables 14 and 15 show that complete reaction occurred only after approximately 1.25 hours exposure at 450°C and approximately 60 hours at 350°C.

Specimens annealed for 10 minutes and 1 hour in tellurium vapour at 750° and 850°C were reheated in vacuum. Only a slight weight loss (< 0.1mg) was detected on each sample after this treatment. In contrast, the specimen in the temperature gradient experiment showed a weight loss of 34mg during the subsequent heat treatment at 750°C for 115 hours. In this case sublimation of tellurium had occurred on the walls of the ampoule in a temperature range of 200° - 300°C and a narrow brown/purple band, which deposited on the ampoule at a temperature of approximately 520° ± 50°C (Figure 24), was shown to contain manganese and tellurium by Auger spectroscopy (Wild, 1974).

Figure 24. Deposit on temperature gradient ampoule.

5.6.2. Measurement of Reaction Product Thickness and Intergranular Penetration.

Optical and scanning electron microscopy showed a continuous reaction product on the surface of all specimens after exposure to tellurium vapour. Apart from the tests at 350° and the short term exposures at 450°, 550° and 650°C, where some tellurium remained unreacted, the thickness of reaction product was between 17 - 25μm and varied within this range according to slight differences in the amount of tellurium used.

Scanning electron microscopy showed that the reaction product consisted of two distinct layers (after polishing and lightly etching) for anneals <50 hours at 750°C and <7 hours at 850°C. Figure 25(a) shows an example of this duplex reaction product after 1 hour at 750°C and illustrates the more porous nature of the inner layer. Longer term tests at both temperatures produced a single layer reaction product (Figure 25(b)). Short term anneals (<160 seconds) at 650°C and below produced only a single layer reaction product; the morphology of the product at 350°, 450° and 550°C differed to that observed at 650°C (cf. Figures 25(c) and (d)). However, for longer exposures at these lower temperatures the duplex layer became progressively more evident until a product similar to that depicted in Figure 25(a) was apparent.

When specimens exhibiting a double layer product were re-heated in vacuum at their previous exposure temperature without further addition of tellurium, a single layer product of similar thickness resulted.

The depth of intergranular attack increased with

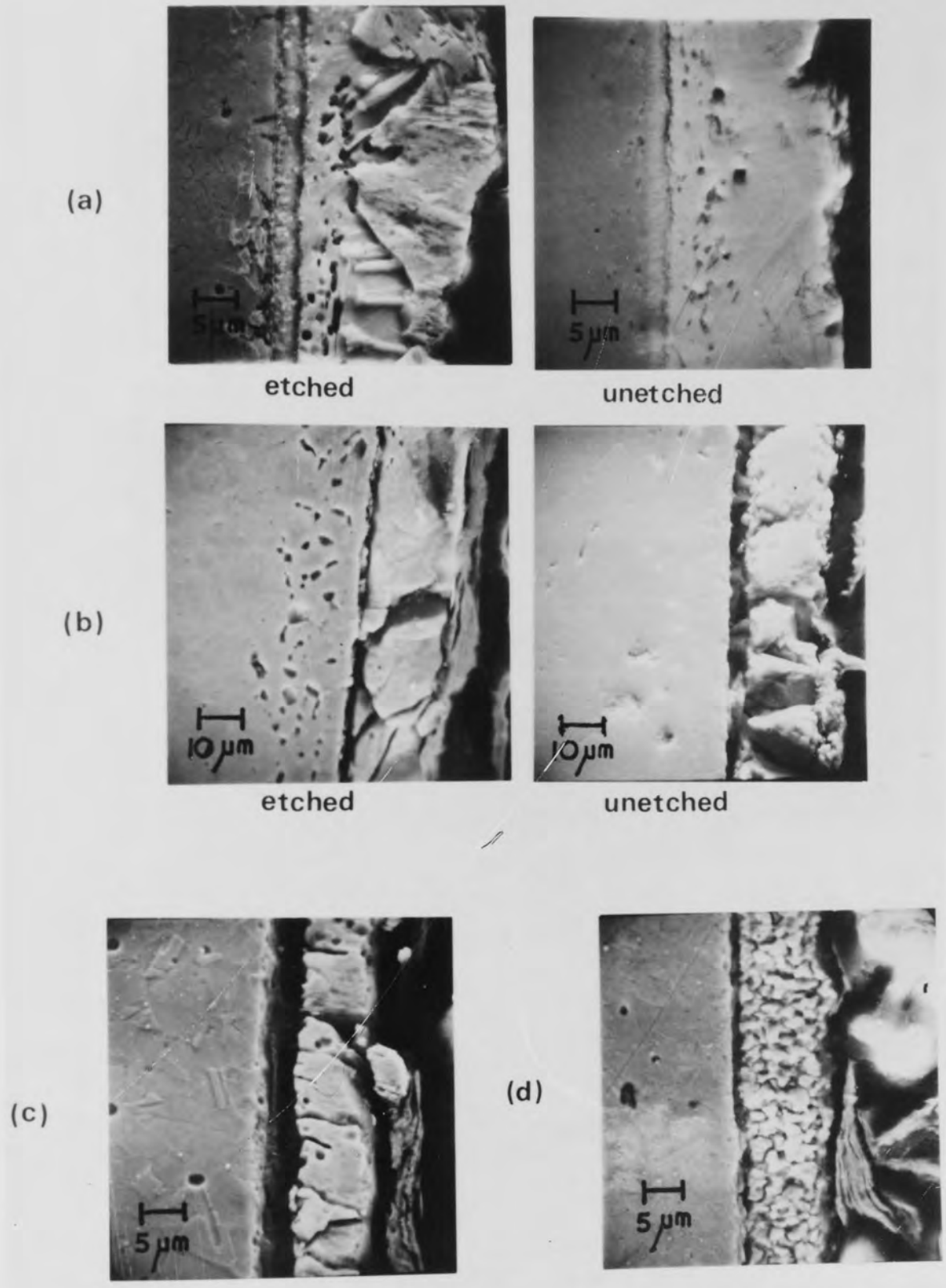

Figure 25. Scanning electron micrographs showing morphology of the reaction product and underlying metal after (a) 1 hour at 750°C, (b) 1000 hours at 750°C, (c) < 160 secs at 650°C and (d) < 160 secs at 550°C.

increasing exposure time to a maximum of approximately 45μm. A logarithmic plot of the depth of attack versus time (Figure 26) produced a straight line relationship of slope 0.3 - 0.4 for the results at 750° and 850°C until the maximum depth is achieved. The depths of attack were measured from the final metal-product interface. Attempts to obtain true depth of attack measurements using gold and platinum films as markers were unsuccessful because these metals also reacted with the tellurium vapour.

Subsurface intergranular voids (see e.g. Figure 25(b)) were found in specimens after >50 hours at 750°C and between 7 - 50 hours at 850°C. Specimens which had not developed subsurface voids during direct exposure to tellurium vapour formed them during the subsequent reheating in vacuum undertaken at 750° and 850°C.

5.6.3. Identification of Reaction products.

The duplex product consisted of a homogeneous iron-nickel-tellurium rich outer layer and a chromium-tellurium rich inner layer (see e.g. Figure 27). Traces of iron and nickel were also detected in the chromium rich layer after short exposure periods. Although CrFe (50-54$^{a}/_{o}$Fe) was identified the duplex layer could not be characterised fully by X-ray diffraction due to the presence of some additional unidentified lines and the apparent amorphous nature of part of the product.

As the tellurium exposure periods were increased the outer layer became discontinuous and islands of iron-nickel-tellurium rich product at the outer edge were formed (Figure 28). Extended exposures (≥50 hours at 750°C and ≥ 7 hours at 850°C)

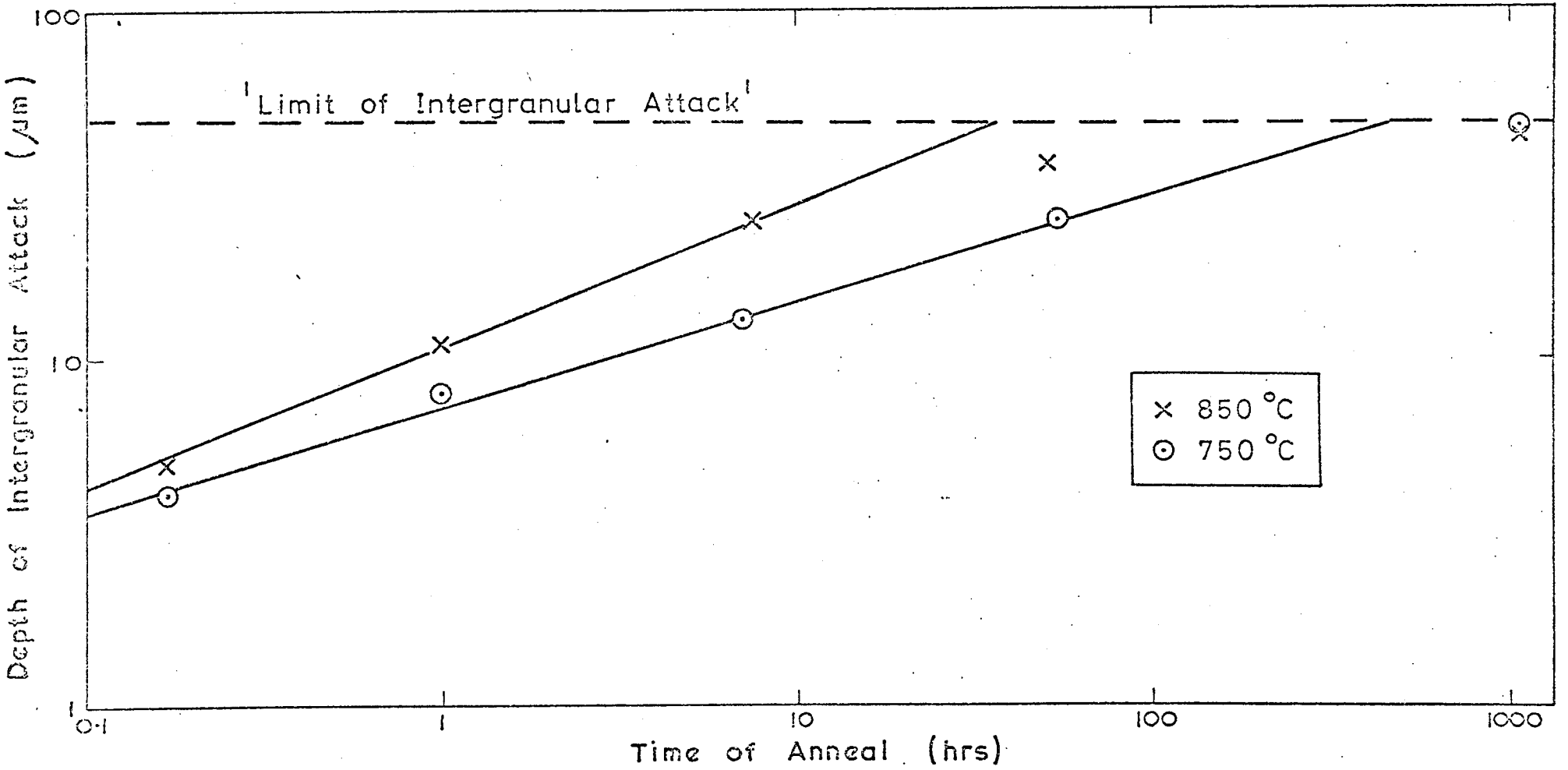

Figure 26. Depth of intergranular attack as a function of time for exposures at 750° and 850°C.

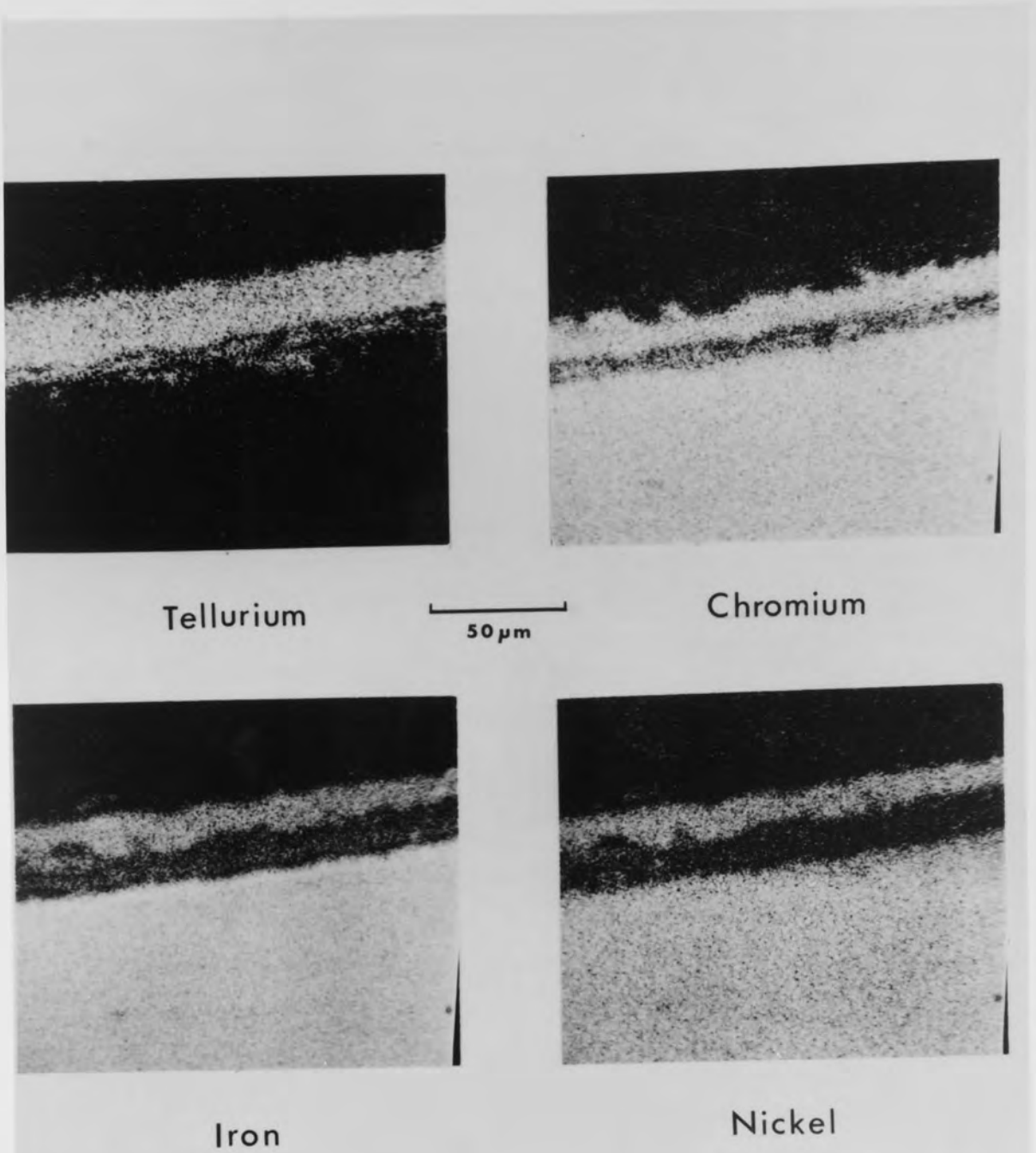

Figure 27. EPMA elemental distribution in duplex reaction product after 1 hour at 850°C.

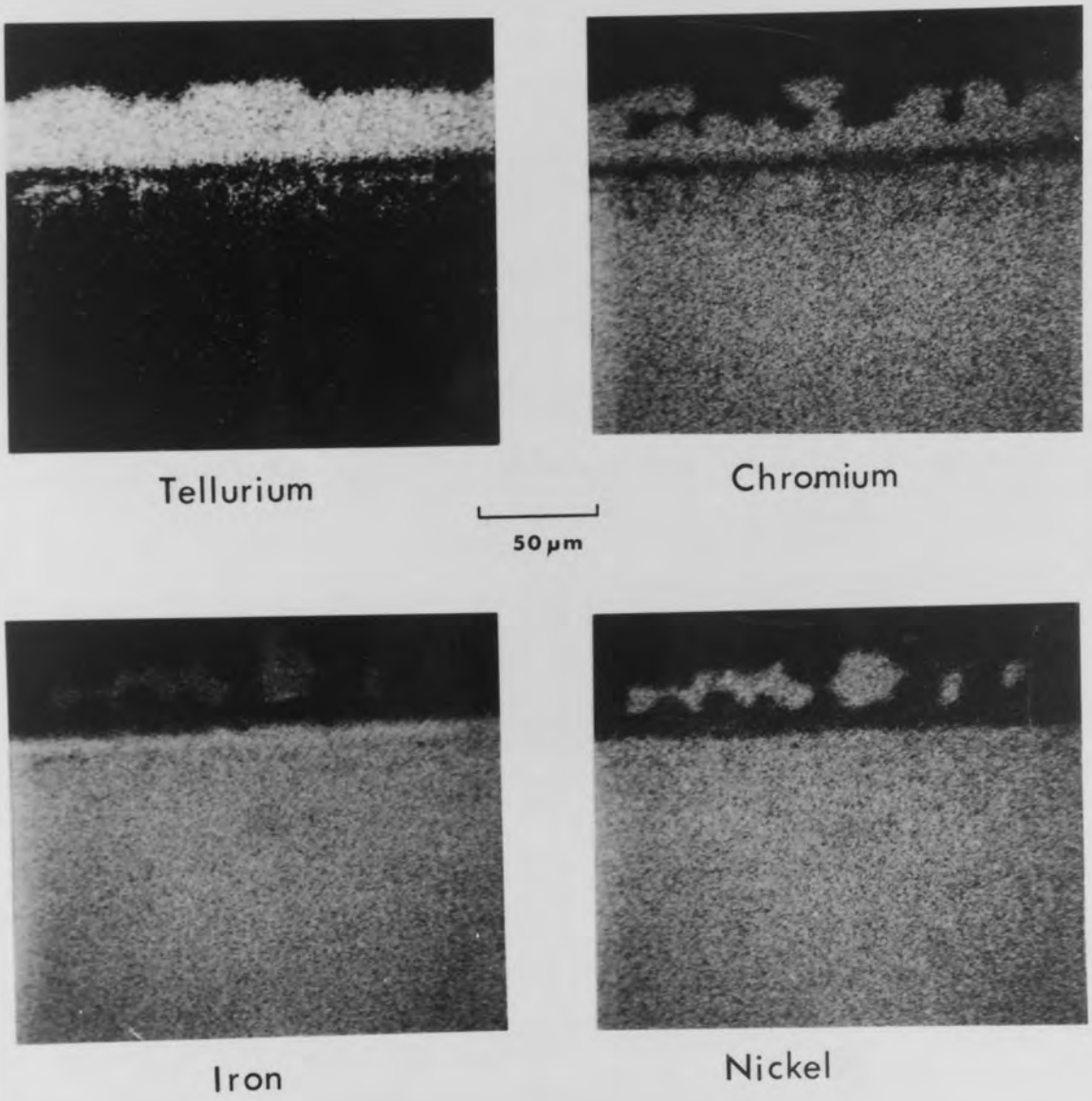

Figure 28. EPMA elemental distribution in reaction product after 50 hours at 750°C, showing discontinuous outer layer.

produced a single reaction layer containing mainly chromium and tellurium (Figure 29); any iron or nickel that was observed was confined to the extreme outer edge of the product. A small amount of manganese was also found distributed throughout this chromium rich product together with traces of silicon and niobium. X-ray diffraction studies confirmed that this product was CrTe (50 - 54$^{a}/_{o}$ Te); it was also shown to be magnetic.

Upon subsequent re-heating (at 750° and 850°C) of specimens exhibiting a duplex product, without further addition of tellurium, the product again contained only chromium and tellurium present as CrTe. However, in the temperature gradient experiment, tellurium was lost from the iron-nickel rich regions of the product and this resulted in a reduction of reaction product thickness. The product remaining was chromium telluride with pockets of iron and nickel in the outer regions of the scale.

At 550° and 650°C the short term heat treatments also produced a single layer product, but this was rich in iron, nickel and tellurium and contained only traces of chromium towards the product-metal interface. However, in short exposures at 350° and 450°C segregation between the iron and nickel constituents of the product became apparent. This is illustrated in Figure 30, which shows the elemental distribution of iron, chromium, nickel and tellurium through the product after an exposure of 10 minutes at 450°C. The tellurium peak on the surface shows very little penetration into the matrix of the stainless steel and nickel is the only element associated with it in the product. After a 30 minutes exposure an iron-nickel-tellurium reaction layer had formed but there was still

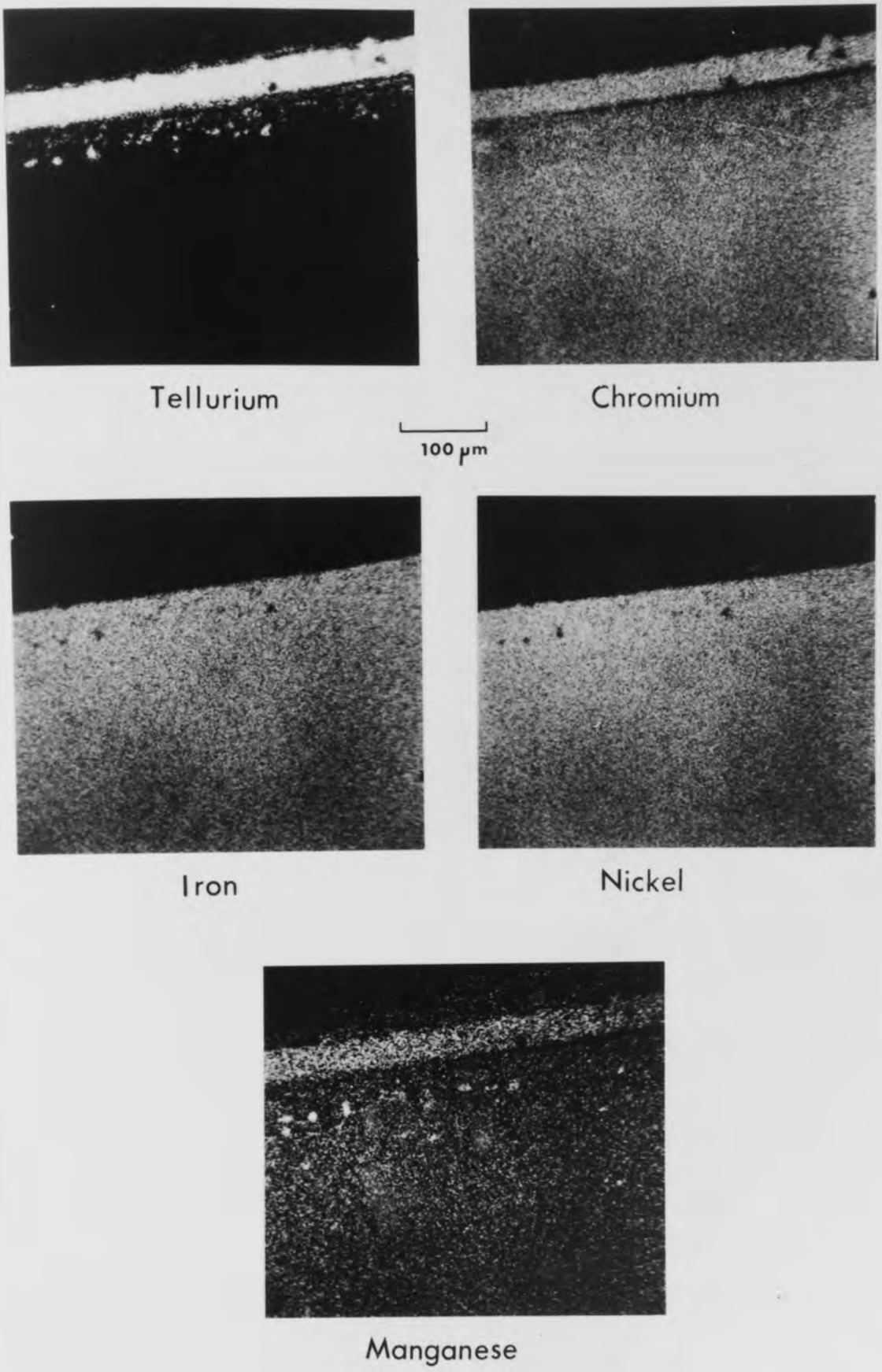

Figure 29. EPMA elemental distribution in single layer reaction product after 1000 hours at 750°C.

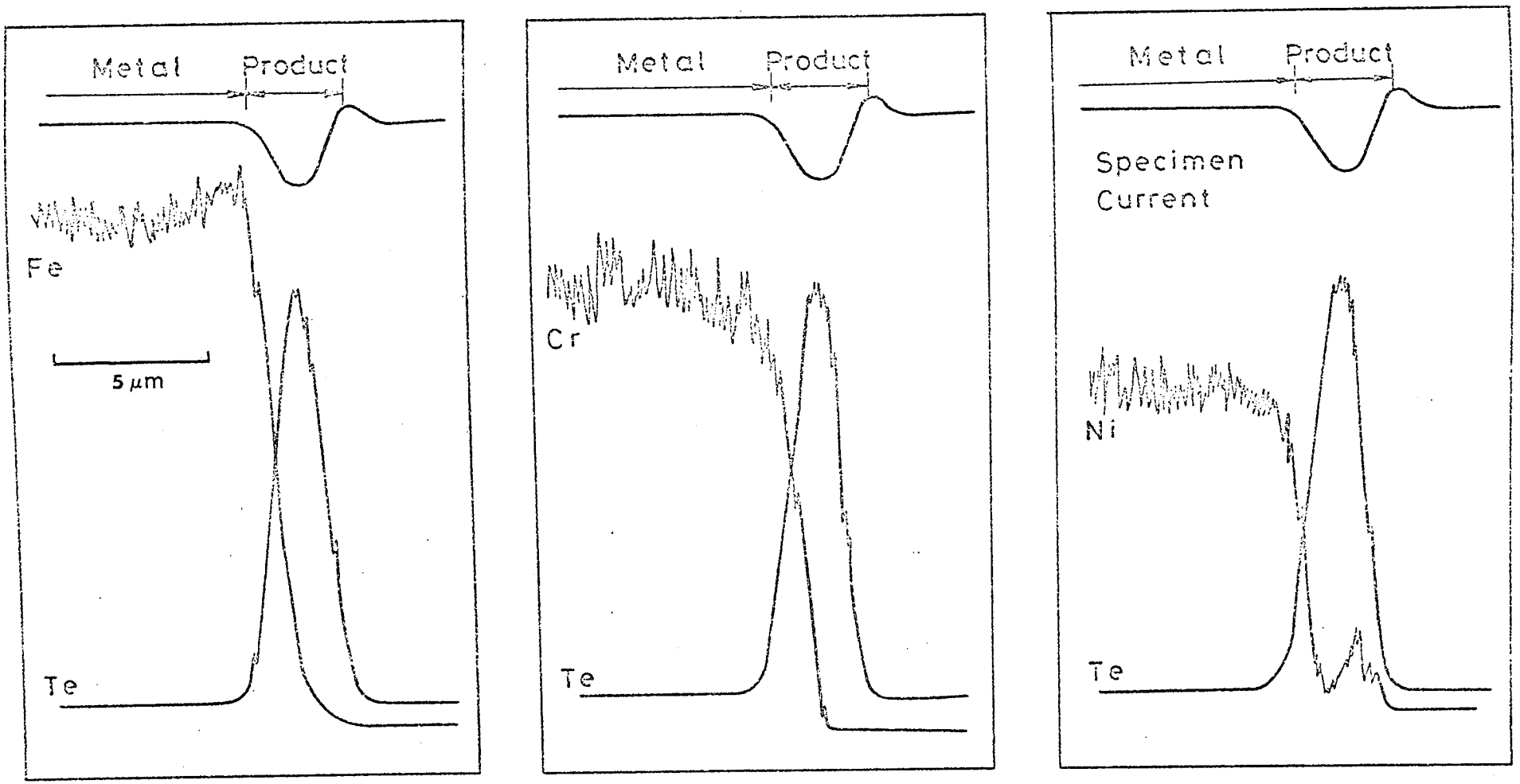

Figure 30. EPMA elemental line scans through reaction product after 10 mins. at 450°C.

an enhancement of nickel towards the outer edge (Figure 31). The initial stage in the formation of a duplex scale is also apparent, due to the appearance of a thin chromium peak in the product adjacent to the product-metal interface.

Surface studies of the reaction products showed the presence of iron-nickel-tellurium rich facets following short exposure periods (Figure 32). The facets became less pronounced as the exposure times were extended and the chromium Kα peak became evident especially in the non-faceted areas (Figure 33). Eventually the facets disappeared completely and the general spectra of an area of the surface showed high chromium and tellurium peaks and only small iron and nickel contributions (Figure 34). The presence of iron and nickel was associated with small nodules that were distributed over the surface (Figure 34). The chromium contribution which is apparent in the EDX spectra for these nodules is most probably due to the penetration of the areas by the incident electron beam thus exciting X-rays from the substrate material. (The electron beam penetration at 20Kv is calculated as approximately 1.5μm in stainless steel (Castaing, 1960).

5.6.4. Compositional Changes within the Steel.

Tellurium penetrated the steel at all temperatures and was always associated with intergranular penetration and subsurface voids mentioned in section 5.6.2. The tellurium peaks in these areas were invariably accompanied by chromium and manganese (Figure 29).

In the metal adjacent to the metal-product interface,

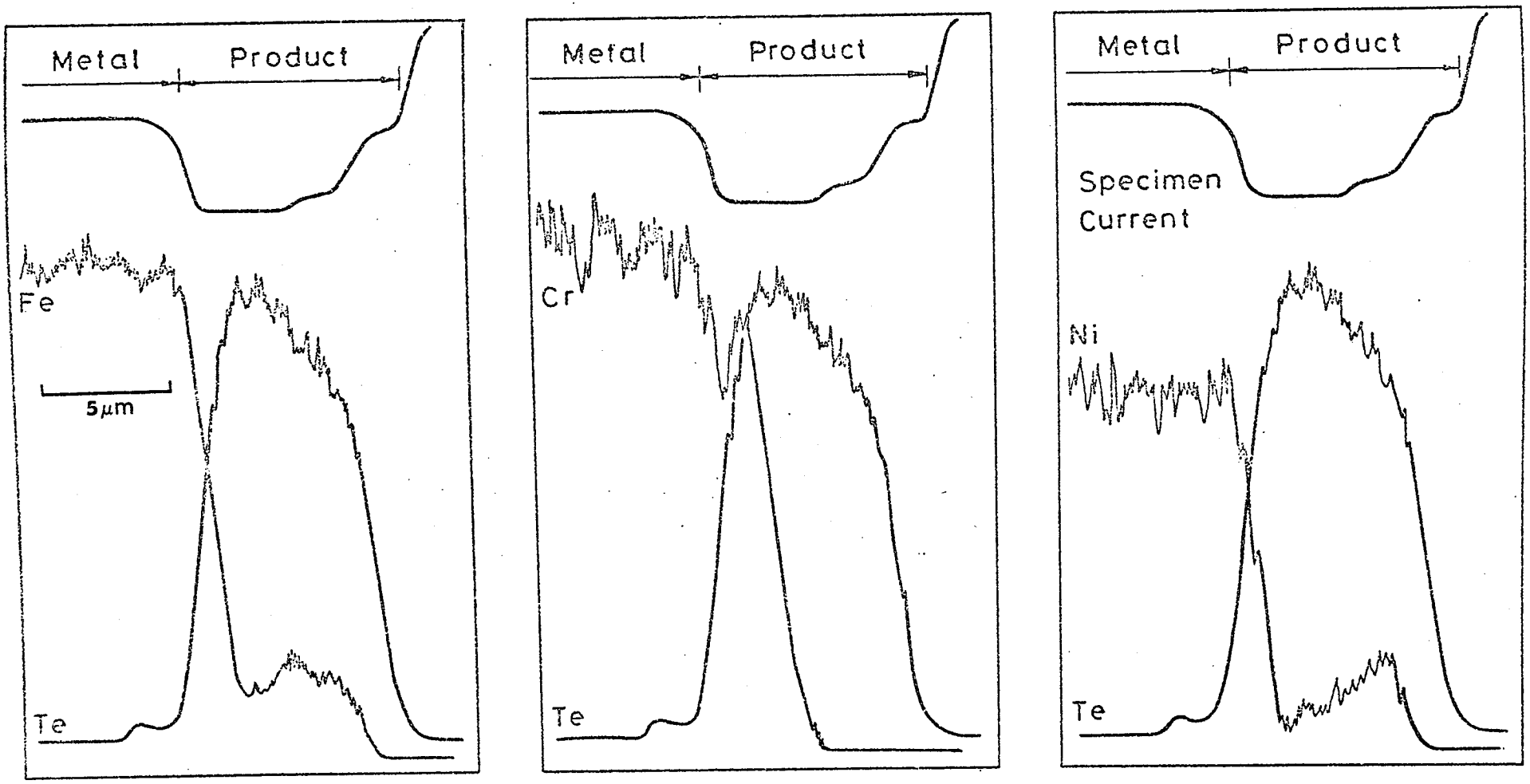

Figure 31. EPMA elemental line scans through reaction product after 30 mins. at 450°C.

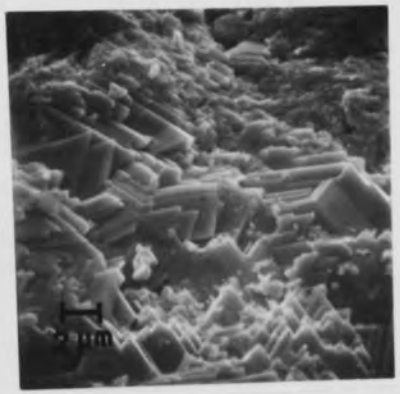

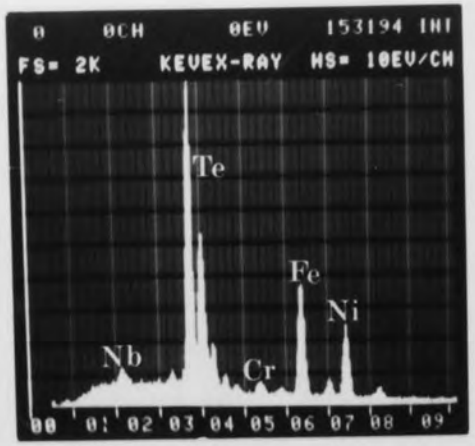

EDX spectrum of area

ENERGY (in KeV) OF MAJOR PEAKS

Nb	L_{α_1}	2·17	Cr	K_{α_1}	5·41
				K_{β_1}	5 95
Te	L_{α_1}	3·77	Fe	K_{α_1}	6·40
	L_{β_1}	4·03		K_{β_1}	7·06
	L_{β_2}	4·30	Ni	K_{α_1}	7·48
	L_{γ_1}	4·57		K_{β_1}	8·26

Figure 32. Scanning electron micrograph and EDX spectra of the reaction product after 1 hour at 850°C.

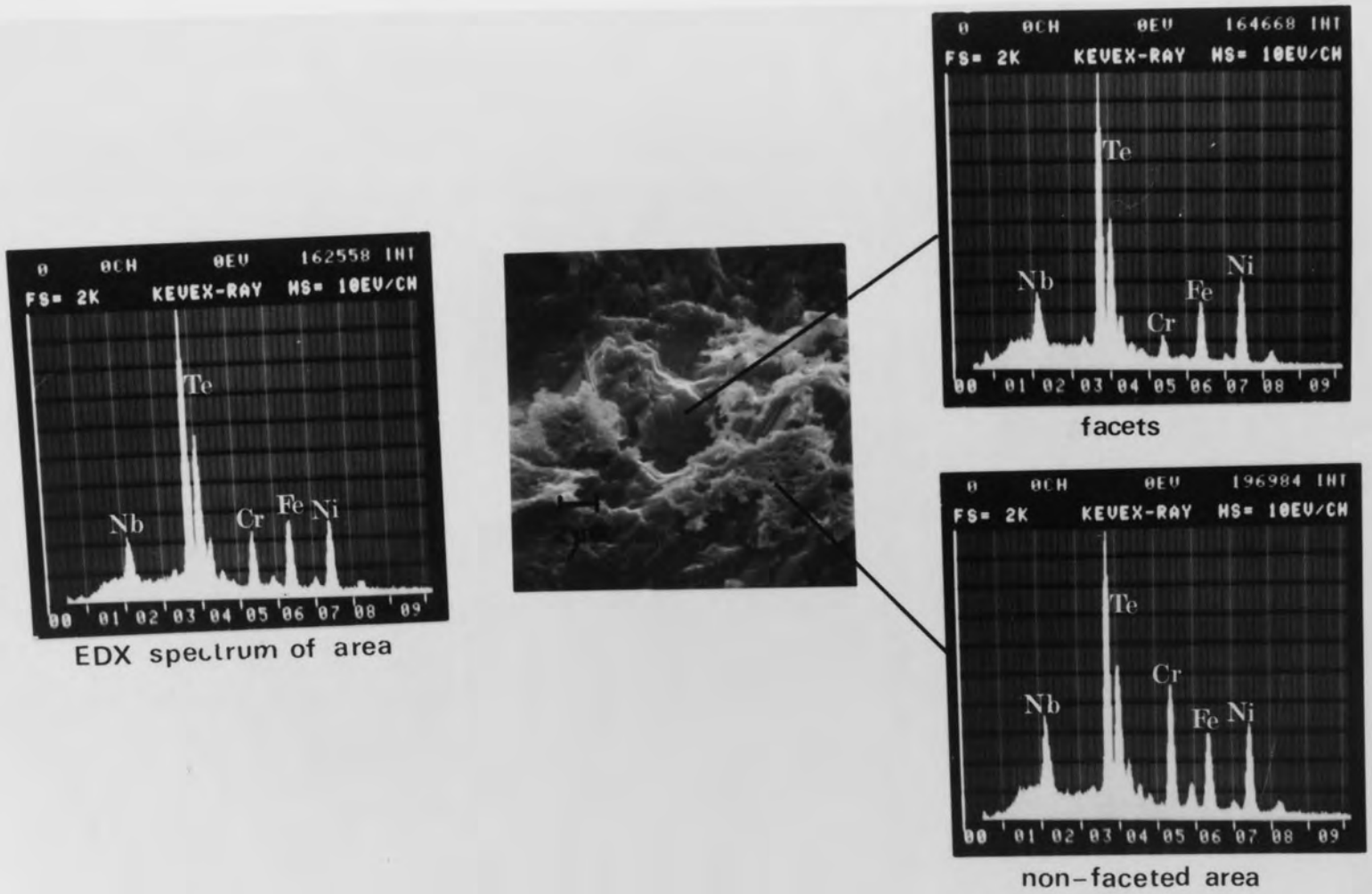

Figure 33. Scanning electron micrograph and EDX spectra of the reaction product surface after 7.5 hours at 850°C.

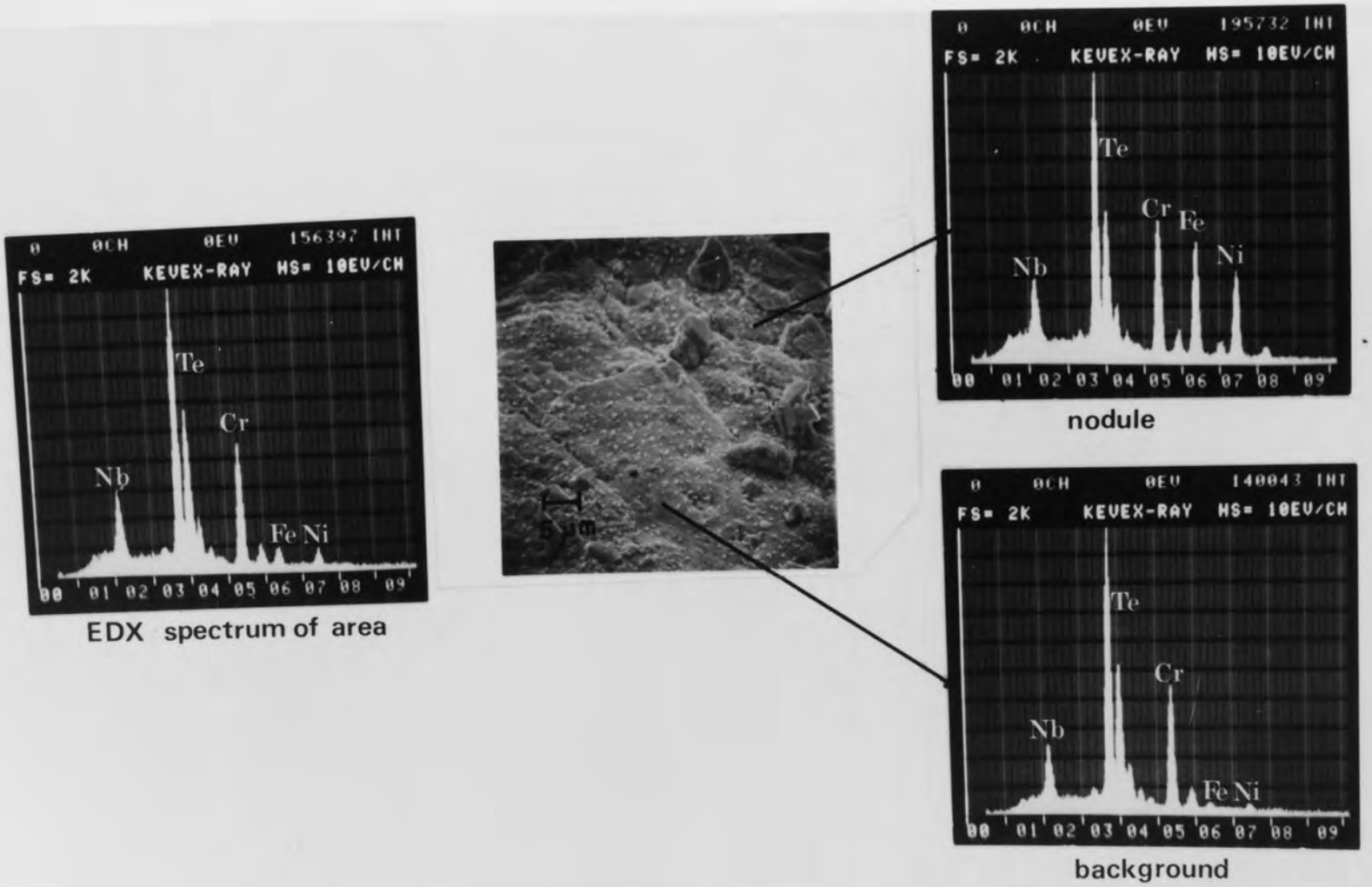

Figure 34. Scanning electron micrograph and EDX spectra of the reaction product surface after 1000 hours at 850°C.

tellurium and iron were the main constituents although traces of chromium and nickel were still evident. The response of this region upon etching was different to that of the remainder of the metal and a distinct layer was seen when viewed in the scanning electron microscope (see Figure 25(a)); the thickness of this layer remained constant at approximately 3μm. Electron probe microanalysis showed that further tellurium penetration of the steel occurred with the depth of penetration increasing with exposure time to a maximum of approximately 45μm after 1000 hours. The rate of penetration depended upon the annealing temperature but the maximum depth was independent of this temperature.

Line scans across the region of the metal beneath the corrosion layer showed significant chromium depletion to a depth of approximately 100μm after 1000 hours at 850°C (see Table 11). Re-heating in vacuum without further addition of tellurium also increased the extent of chromium depletion.

5.6.5. Summary of Results.

Rapid attack of the 20%Cr/25%Ni/niobium stabilised stainless steel by the tellurium vapour was found at all temperatures studied and only in the short term exposures at the lower temperatures (<650°C) was an incomplete reaction observed. At 550° - 650°C the initial reaction product consisted of a single layer rich in iron, nickel and tellurium. Only at the lower temperatures (≤450°C) was it possible to distinguish that the reaction with nickel occurred more rapidly than with iron. On further exposure this product became duplex due to the formation of an inner

chromium-tellurium layer at the metal-product interface. At temperatures >650°C the reaction rate was such that even short exposure resulted in the formation of this duplex product. As the exposure times were increased the duplex layer transformed to a single chromium-tellurium layer (CrTe: 50-54 a/o Te). The order of reaction between the main steel constituents and the tellurium was therefore nickel > iron > chromium.

The reaction between the stainless steel and the tellurium occurred very rapidly (<160 secs at 750°C) and the extent of the reaction was limited only by the supply of tellurium. Bearing this in mind the reaction product thickness ranged between 17 - 25μm after complete reaction had occurred and was independent of the reaction temperature.

The maximum depth of intergranular attack was limited to approximately 45μm from the metal-product interface. Compositional and microstructural changes were however observed in the subsurface of the metal in the form of voids (at the higher temperatures) and chromium depletion. For example, chromium depletion to a depth of approximately 100μm was achieved after approximately 1000 hours at 750° - 850°C.

5.7. Variation of Tellurium Concentration.

The experiments conducted above used an amount of tellurium based on the overall concentration derived in Appendix 2. In addition it provided a reaction product of suitable dimension for mechanistic evaluation. Based on the data in section 5.6. the studies have been extended to

observe the effects of both lower and higher tellurium concentrations.

The lower concentration studies were undertaken at 850°C with an initial tellurium concentration of approximately 0.01mg.mm^{-2} of stainless steel. The experimental conditions were as described in section 5.5. with exposure times of 8, 200, 860, 1125, 1992 and 5000 hours.

In the 8 hour anneals complete reaction occurred with the weight gain of the specimens corresponding to the amount of tellurium added to the ampoule. A single layer reaction product approximately 2μm thick was observed on the surface of the steel with which both chromium and tellurium were associated (Figure 35). There was little evidence of iron and nickel in the product. Chromium depletion was evident at the metal-product interface.

Chromium depletion extending up to approximately 50μm into the metal matrix was also observed in some but not all exposures ≥200 hours. However in all instances a reaction product was not observed and a varying weight loss was apparent subsequent to the anneal. This weight loss corresponded to integral multiples (x1, 2 or 3) of the stoicheiometric quantity of steel constituent required for the formation of a metal telluride (MeTe: where Me is iron, chromium or nickel). No tellurium was evident on the surface of any of these specimens although in isolated instances small tellurium-rich pockets were observed in the steel matrix usually associated with manganese. In some instances where weight loss had occurred it was possible to identify α-iron at the end of the ampoule by X-ray diffraction.

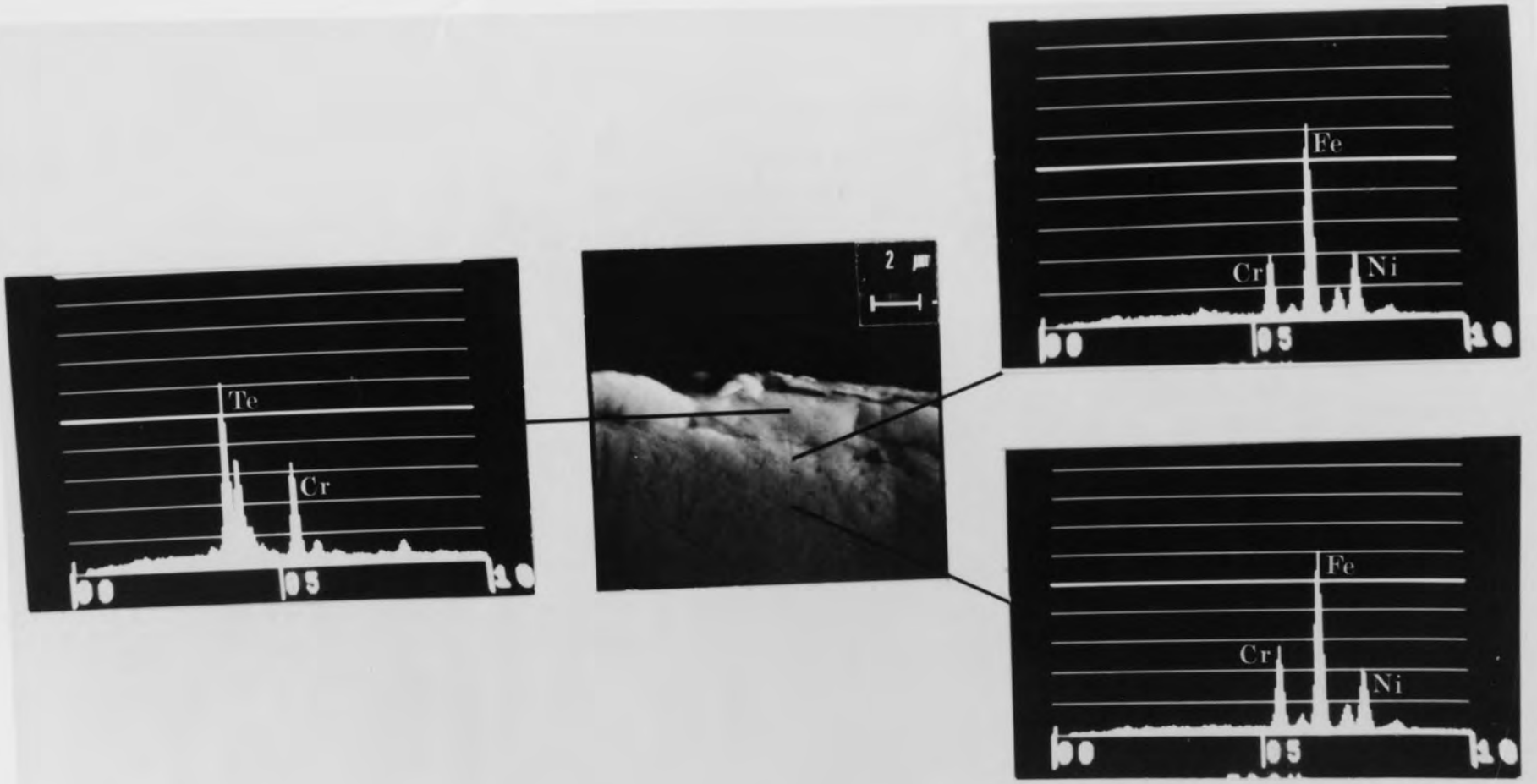

Figure 35. Scanning electron micrograph and EDX spectra of a cross section of the reaction product and underlying metal after 8 hours at 850°C using a tellurium concentration of 0.01 mg.mm^{-2}.

The higher concentration studies were also undertaken at 850°C with an initial tellurium concentration of approximately $1mg.mm^{-2}$ of steel. The experimental conditions were as above with exposure times of 1, 8 and 190 hours.

The specimens for all three exposure times had gained in weight by the same amount as the tellurium initially added. Reaction products ranging from 185 - 250μm were observed. Specimens heated for 1 hour formed a double layered product consisting of a chromium-tellurium inner zone and an outer iron-nickel-tellurium region (Figure 36). Small chromium-tellurium areas were also observed in the outer region.

After 8 hours exposure the product still consisted of the same components but the outer iron-nickel-tellurium layer had become discontinuous and the inner chromium-tellurium zone had increased in thickness. The products formed after the 190 hours anneal were consistent with those discussed above but in addition segregated iron rich areas were becoming evident in the outer regions (Figure 37).

In the metal adjacent to the metal-product interface a region similar to that discussed in section 5.6.4. was observed (Figure 37). In this case it was approximately 35μm thick and the elemental distributions were similar to the duplex product. However, the outer portion of this layer was rich in iron and nickel only, whilst chromium and tellurium were observed together in the inner zone. Intergranular attack was observed to an additional depth of approximately 50μm after 190 hours.

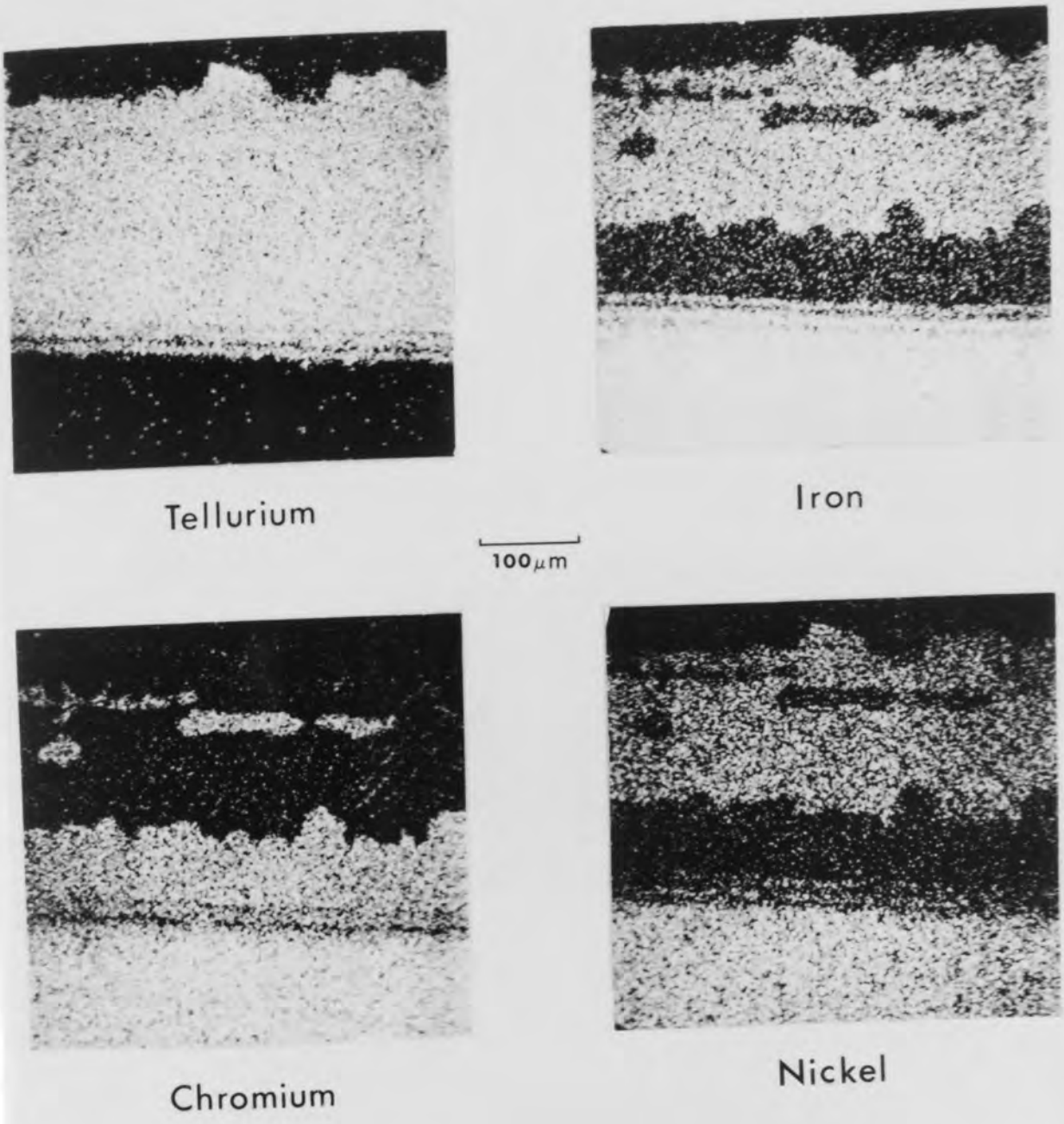

Figure 36. EPMA elemental distribution of reaction product after 1 hour at 850°C using a tellurium concentration of 1 $mg.mm^{-2}$.

Tellurium

Iron

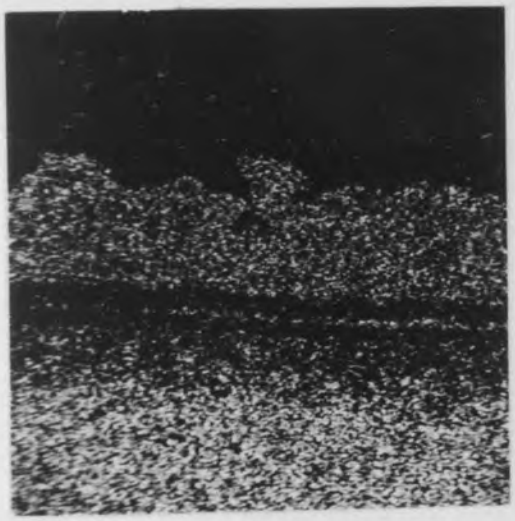

Chromium

Nickel

Figure 37. EPMA elemental distribution of reaction product after 190 hours at 850°C using a tellurium concentration of 1 $mg.mm^{-2}$.

5.8. Effect of Surface Oxidation.

In addition to the above experiments using virgin stainless steel surfaces the effect of surface oxidation was then considered. Stainless steel coupons (as in section 5.5) were oxidised in carbon dioxide at 850°C for either 8 or 100 hours. These were considered appropriate to possible inner clad conditions. The studies used an initial tellurium concentration of 0.1mg.mm^{-2} and the experiments were undertaken at 750°C.

Complete reaction was observed for each oxidation treatment and exposure period. In contrast to the studies with virgin steel surfaces a discontinuous product was observed on the specimen surface (see e.g. Figure 38). The reaction product thickness was approximately 35µm in each case.

In regions where the product gave greater cover the elemental distributions were as found earlier with the development of a duplex layer (see section 5.6.3.). There was no evidence of the original oxide layer in these areas.

However in other areas where more isolated regions of telluride product occurred the chromium oxide layer was still evident. Reaction with the tellurium had occurred only in cracks in the oxide layer (Figure 38a) and the product had "mushroomed" through this outer skin. Confirmation of the chromium oxide layer was evident from the X-ray scanning images shown in Figure 39. Chromium was enhanced on the surface of the steel while tellurium was only present in the reaction product in the vicinity of the break in the

(a)

50μm

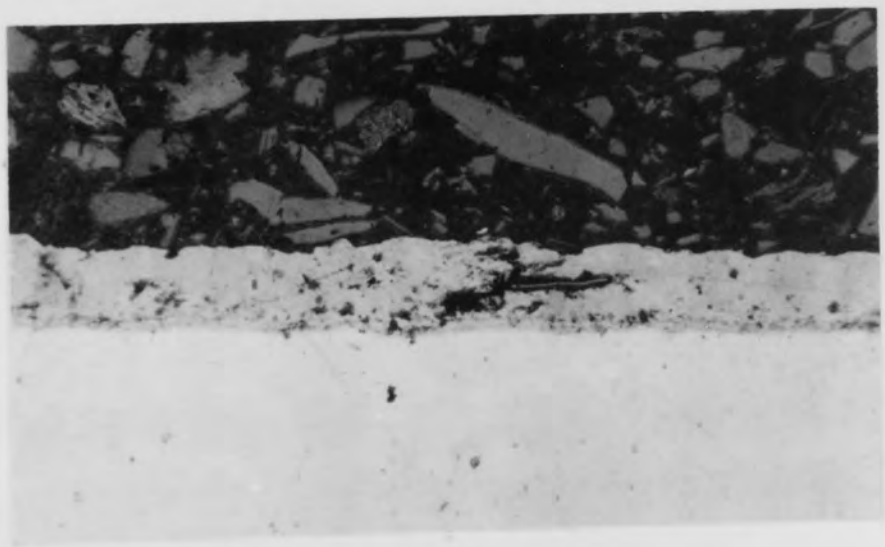

(b)

Figure 38. Optical micrographs of pre-oxidised stainless steel specimens showing (a) discontinuous reaction product and (b) continuous reaction product in spalled area.

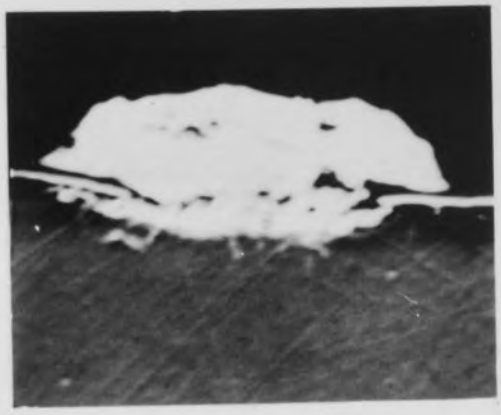

Electron

25μm

Tellurium

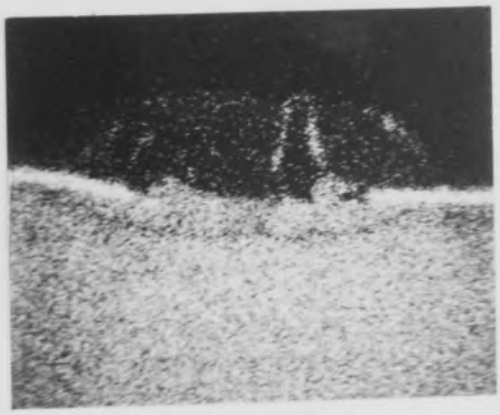

Chromium

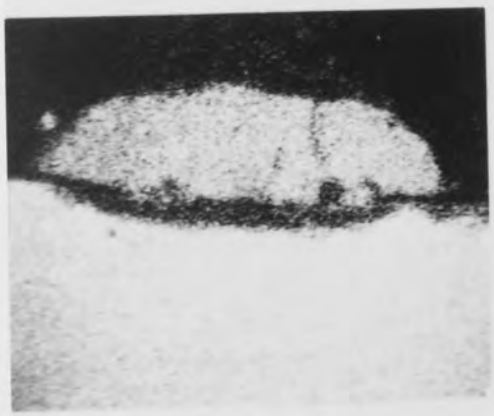

Iron

Nickel

Figure 39. EPMA elemental distribution in discontinuous reaction product on pre-oxidised specimen.

oxide layer. Iron, chromium and nickel were again associated with the tellurium. The iron-nickel-tellurium region was positioned outside the initial chromium oxide layer whilst the chromium-tellurium product grew beneath the original metal surface.

5.9. Thermodynamic Stability of Tellurides.

The results of the temperature gradient experiment (see section 5.6.3.) indicated that chromium telluride remained stable at 750°C. In contrast the iron and nickel tellurides dissociated allowing tellurium to condense on the cooler parts of the system; iron and nickel remained in the product.

To substantiate this result and to help explain the transition via a duplex reaction product to a chromium telluride layer the relative stabilities of iron, chromium and nickel tellurides were studied at 850°C. Stoicheiometric amounts of chromium metal foil and iron telluride, chromium metal and nickel telluride, and nickel metal and iron telluride were annealed separately in evacuated ampoules for periods up to 20 hours. The resultant products were weighed, tested for magnetic properties and studied by X-ray diffraction.

Observations of the chromium + iron telluride mixture during the heating period showed evidence of a surface reaction on the chromium after about 2 hours. The specimens were removed after 20 hours and the weight changes of the components indicated complete reaction. The products were magnetic and were identified as chromium telluride and α-iron by X-ray diffraction.

Similar results were obtained with the chromium + nickel telluride mixture but the products were nickel and chromium telluride.

After 20 hours the nickel + iron telluride mixture did not show complete reaction although weight gain measurements indicated an increase in weight of the nickel and a corresponding decrease in weight of the iron telluride. Some small magnetic particles were found but X-ray diffraction patterns did not agree with any available data for iron tellurides, nickel tellurides, iron or nickel.

The tellurides of the three main components of the steel were therefore placed in the order of their thermodynamic stabilities:- CrTe > NiTe > FeTe.

In addition the stability of the chromium telluride-chromium oxide system was examined at 850°C. Chromium telluride reaction product removed from a tellurium exposed specimen was characterised initially by X-ray diffraction and then heated in flowing carbon dioxide on a thermobalance. The weight loss was monitored with time and the products examined by X-ray diffraction.

A weight loss of 26% was observed after 9 hours. X-ray diffraction of the resultant product indicated a mixture of chromium oxide, iron oxides (mainly α-Fe_2O_3) and some nickel oxide. Tellurium compounds of chromium, nickel or iron were not detected.

It was apparent therefore that in an oxidising environment chromium oxide is more stable than the telluride.

5.10. Discussion.

It has been suggested (Batey and Bagley, 1974) that significant attack of austenitic stainless steel (Types M316

and FV 548) occurs only when tellurium is in the liquid phase (i.e. above 452°C). However, the present work shows the strong affinity of tellurium vapour for 20%Cr/25%Ni/niobium stabilised stainless steel at temperatures of 350°C and above. At the higher temperatures examined (750° and 850°C) complete reaction of the available tellurium and the steel was almost instantaneous (<<160sec.) and it is not until the temperature is ≤650°C that incomplete reaction occurs over short periods.

An estimate of the reaction rate could be determined from weight gain measurements but the speed of the reaction allowed sufficient measurements to be made only at the lower temperatures examined. The data (from Tables 13-15), plotted in Figure 40, show that the weight per unit area (x) of tellurium used in the reaction is approximately linear with time (t), i.e. $x = k(T)t$. The rate constants (k) at 350°, 450° and 650°C are determined as 5.5×10^{-7}, 2.3×10^{-5} and 5.9×10^{-4} $mg.mm^{-2}sec^{-1}$ respectively.

The corrosion product thickness after the reaction of tellurium vapour with the stainless steel was dependent on the quantity of tellurium consumed but was independent of the temperature (see Figure 41). The temperature did, however, influence the rate at which the ultimate product thickness was achieved since this depended upon the rate of reaction between the tellurium and the steel.

5.10.1. Subsurface Effects.

5.10.1.1. Intergranular Penetration and Subsurface Voids.

Beneath the chromium rich product there was a reaction zone of constant thickness (approximately 3μm and 35μm for

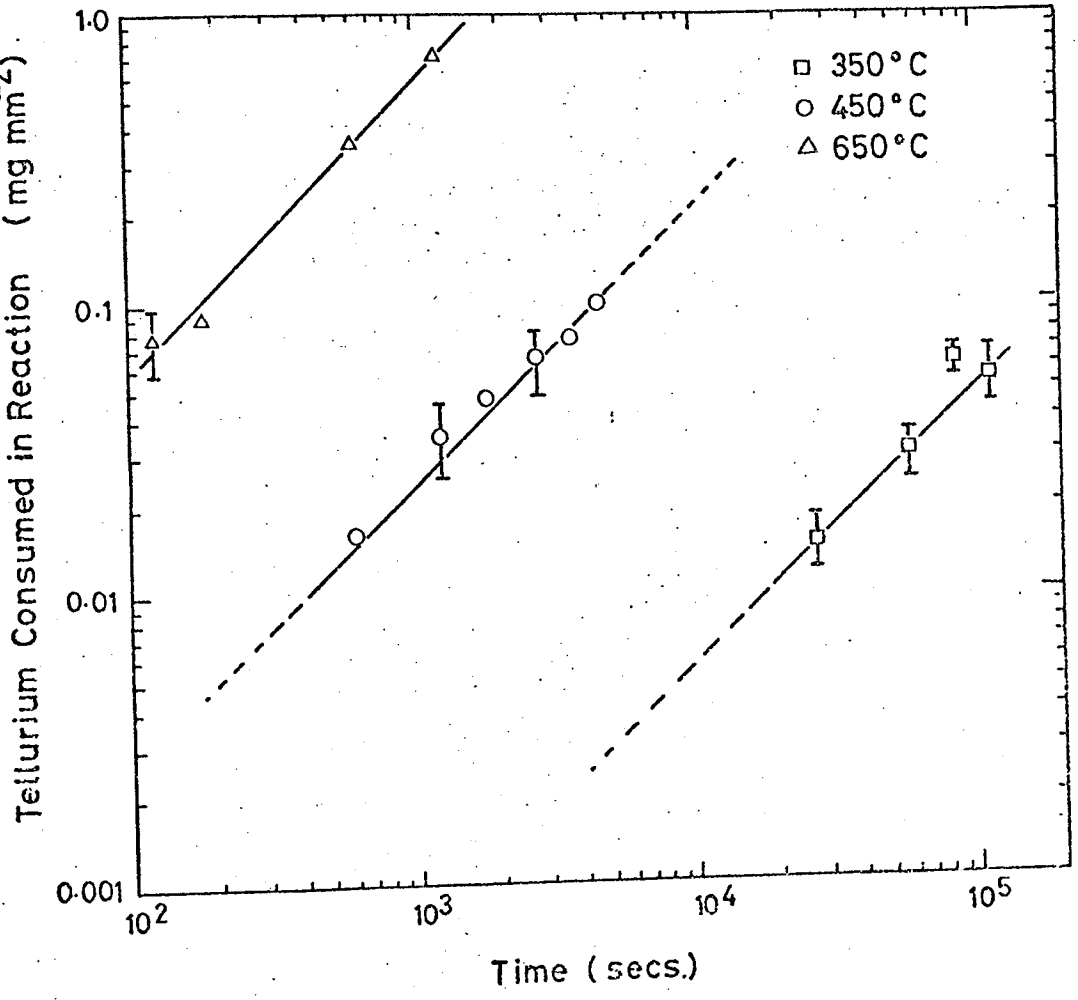

Figure 40. Weight gain per unit area of specimen as a function of time during exposures at 350°, 450° and 650°C.

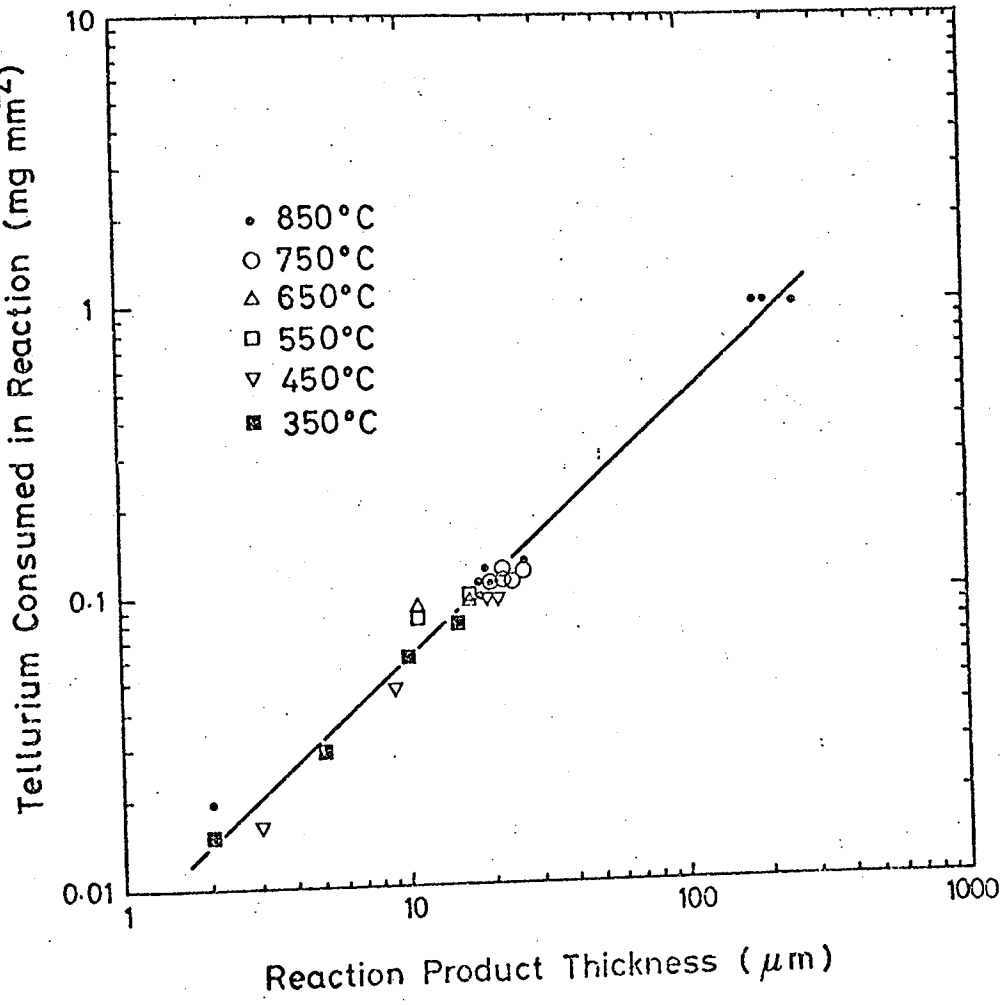

Figure 41. Variation of reaction product thickness with amount of tellurium used in reaction during anneals at temperatures between 350° and 850°C.

the 0.1mg.mm^{-2} and 1mg.mm^{-2} studies respectively) (see e.g. Figure 25a) which showed penetration of tellurium along a broad front. Intergranular penetration of tellurium occurred to a greater depth. The depth of attack (y) can be represented by a function $y = at^n + c$, where "a" and "c" are constants. Similar expressions have been obtained for the growth of reaction zones at temperatures >700°C (Götzmann et al., 1974) and for the depth of penetration of liquid tellurium at 650°C (Batey and Bagley, 1974) in austenitic stainless steels, where it has been assumed that c = 0 or << y. The values of "n" are quoted as 0.2 -0.5 and 0.25 for each of those studies respectively. If the same assumption is made in this study, "n" has a value of 0.3 - 0.4 for the 750° and 850°C anneals (Figure 26). However the value of "c" is dependent upon the amount of steel removed during the reaction, which is calculated to be approximately 3μm for the 0.1mg.mm^{-2} studies (assuming the density of the reaction product to be 4 x 10^{3}kg.m^{-3} and the thickness of the reaction product as 20μm). Given a similar value for "c", then "n" is reduced to ~0.25. The depth of attack is limited by the amount of tellurium available for reaction and the effect of temperature is solely upon the speed at which this limiting depth is achieved (Figure 26).

Batey and Bagley (1974) observed that liquid tellurium attack in M316 stainless steel at 650°C was marked by the formation of an intermetallic compound at the grain boundaries. In the present work, evidence of this is less conclusive and only the lighter, tellurium-manganese-chromium rich areas observed in Figure 25b could be

regarded as an indication of compound formation. Upon lightly etching, these areas opened out and appeared as grain boundary voids. Presumably this was caused by the dissolution of the reaction product during the etching process.

However, genuine subsurface voids were found (in unetched sections) from the early stages of anneals above 650°C. Subsurface voids have been found previously in 20%Cr/25%Ni/Nb stainless steel at 750°C during oxidation in carbon dioxide (McCoy, 1965) and during long term exposure (>1000 hours) to iodine vapour (Lobb and Jones, 1973). This phenomenon is usually ascribed to an excess vacancy concentration produced by movement (as cations) of one or more of the steel constituents outwards and concurrent injection of vacancies (see e.g. Gibbs and Hales, 1973). However it may be that, in this instance, either dissociation of chromium telluride particles under the influence of the chromium depletion gradient similar to that discussed by Evans, Hilton and Holm (1976) in their oxidation studies or volatilisation of tellurides are contributing to the formation of these voids.

5.10.1.2. Chromium Depletion.

The reaction between chromium from the stainless steel and iron and nickel tellurides in the reaction product results in a marked chromium depletion immediately beneath the product. In some stainless steels, depletion is sufficient to cause the formation of a ferritic layer (Keroulas et al., 1972), but the presence of such a layer has not been established in the reaction of 20%Cr/25%Ni/Nb

stainless steel and tellurium. The depth of depletion continued to increase with time after the tellurium-steel reaction was complete. This continued depletion was due to the diffusion of chromium from the bulk of the metal in an attempt to even out the concentration profile. Estimates of the diffusion coefficient of chromium in 20%Cr/25%Ni/Nb steel can be obtained from the shape of this profile (Smith, Killeen and Wild, 1974). The calculated diffusion coefficient necessary to account for a 110μm depletion depth after 1027 hours at 750°C is approximately $1.5 \times 10^{-16} m^2 sec^{-1}$. The tracer value of the lattice diffusion coefficient of chromium in 20%Cr/25%Ni/Nb stainless steel at 750°C is $5.2 \times 10^{-18} m^2 sec^{-1}$ (Smith, 1969a). The larger diffusion coefficient can only be accounted for by either (or both) a lattice coefficient enhanced by the injection of vacancies or a significant contribution of the grain boundaries to chromium depletion. This phenomenon appears to be characteristic of other fission product attack on stainless steel since long term exposure to iodine vapour at 750°C also produced enhanced chromium depletion (Lobb, 1976).

The extent of chromium depletion that would be expected, using this calculated diffusion rate, at a time when chromium is just becoming incorporated into the reaction layer is now considered. For example, after 1 hour at 750°C it would be expected that a chromium depleted region approximately 1μm deep would be observed. However, the experimental data shows a depletion depth of approximately 13μm (Table 12), whereas tellurium is observed to a depth of approximately 8μm. Hence based on this tenuous evidence

it would appear unlikely that chromium could be solely responsible for controlling the rate of reaction but it may be argued that tellurium plays a major role in the rate controlling process.

5.10.2. Reaction Stages.

The results obtained have shown that the reaction between tellurium vapour and stainless steel progressed in three stages, each of which will now be considered.

5.10.2.1. Initial Stage.

This step consisted of the formation of an iron-nickel-tellurium rich layer (see Figures 25(c) and (d)) and it was only observed at the lower temperatures examined ($<650^{o}C$) because of the speed of the reaction. At 550^{o} and $650^{o}C$, no separation of iron and nickel was found but at $450^{o}C$ nickel telluride started to form before iron telluride (see Figure 30). At first sight this appears to be surprising since the studies reported in section 5.9. and those of Götzmann et al. (1974) have shown chromium telluride to be more stable than either iron or nickel telluride and, from a thermodynamic viewpoint, chromium telluride should form preferentially in the reaction of steel and tellurium. Therefore this stage of the reaction must be governed by other factors such as the speed of the various chemical reactions between tellurium and the main steel constituents or the diffusion rates of the respective elements.

5.10.2.2. Intermediate Stage.

This stage started with the formation of chromium telluride and ended with the development of a double layer product. Chromium telluride first formed as a thin layer adjacent to the product-metal interface (see Figures 31(a) to (c)). The inner chromium rich layer grew as the reaction proceeded until all the corroding species was exhausted. At this point the product was duplex with scales of approximately equal thickness (see Figure 27).

5.10.2.3. Final Stage.

The chromium rich layer continued to increase in thickness at the expense of the iron-nickel rich layer, leading eventually to pockets of iron and nickel tellurides towards the outer edge of the product (Figure 28) and ultimately to the formation of a single layer product which was mainly chromium telluride (50-5[illegible] a/o Fe). As the reaction proceeded the remaining iron and nickel became incorporated in the outer regions of the product (Figure 37) until they eventually appeared as small nodules on the surface of the corrosion product (Figure 34). If the density of these nodules was assumed as $8.5 \times 10^3 kg.m^{-3}$ (i.e. the average for iron and nickel) and the density of the outer iron-nickel-tellurium layer as $4 \times 10^3 kg.m^{-3}$, the calculated weight of the nodules accounted (within a factor ~ 3) for the mass of iron and nickel in the iron-nickel-tellurium layer originally.

The transition from a duplex to a single scale occurred without weight loss and can be explained in terms

of the relative thermodynamic stabilities of the steel tellurides, i.e. upon exhaustion of the tellurium supply chromium reacts with iron and nickel telluride to form the more stable chromium telluride (see section 5.9.). Examination of Table 14 and Figure 31 shows that the inner chromium layer starts forming before the tellurium supply is exhausted. So although the studies of Batey and Bagley (1974) were undertaken in a large excess of tellurium the substrate chromium telluride product should still have been evident. No mention is made in their paper of such a layer and this is at variance with the present study. However, the formation of a final chromium telluride reaction product agrees with the results of Götzmann et al. (1974).

The above mechanism is appropriate for all the concentrations studied. However, in the longer exposure (≥200 hours), low concentration studies at 850°C an additional effect of weight loss was apparent. The weight loss was consistent with a reaction occurring between the tellurium and the steel followed by the subsequent removal of a telluride containing one, two or three stoicheiometric quantities of steel constituent.

This could be explained by the formation of a telluride with a metal/tellurium ratio > 1:1. The observation of α-iron in the ampoule subsequent to some of these anneals would substantiate such a mechanism with the formation of FeTe, Fe_2Te and/or Fe_3Te followed by their decomposition. However the participation of chromium in the reaction, shown by the depletion occurring when three equivalents of the metal were lost would favour a mechanism involving a sequential

removal of nickel, iron and chromium tellurides.

Further evidence supporting this mechanism is obtained from the temperature gradient experiment where decomposition of both iron and nickel tellurides occurred at 750°C. It may be expected that if a non-uniform temperature profile existed in these studies then over extended periods at 850°C a similar phenomenon may have occurred. This may also explain the apparent incomplete reaction in the 1014 hour, 0.1mg.mm^{-2} study at 850°C.

5.10.3. Effect of Surface Oxidation on the reaction.

A reaction between tellurium and the stainless steel was observed on the pre-oxidised specimens but it only occurred where either the original chromium oxide layer was missing or where a break in this layer existed. Thus the presence of this pre-oxidised layer afforded some degree of protection to subsequent tellurium attack. Within the areas of attack the reaction proceeded in a similar manner to that discussed in section 5.10.2.

As stated in section 5.6.2. attempts to undertake gold and platinum marker experiments were unsuccessful due to the reaction of these materials in the tellurium environment. However, the pre-oxidised surface studies have shown the chromium oxide to be more stable than the telluride product. Indeed, this was confirmed by the thermodynamic studies which showed chromium oxide to be more stable than the steel tellurides. Therefore, in areas where this oxide remained intact the approximate position of the original stainless steel surface could be located. Thus an electron probe

microanalytical examination of a region where the oxide had cracked but not spalled could be used as a marker experiment.

Such an area is featured in Figures 38a and 39 which show clearly the presence of the pre-oxidised layer. The iron-nickel layer was seen to grow outside the original steel surface whilst the chromium rich product was observed below the surface. This would indicate that the formation of the initial iron-nickel product involves the outward diffusion of these two stainless steel constituents whilst the latter stage in which chromium telluride is formed is dependent on the diffusion of tellurium inwards through the outer product. This could be accomplished either by movement down cracks in the product, by diffusion of tellurium through the iron-nickel rich layer or via the intermediate dissociation of the iron-nickel-tellurium product. The inward diffusion of tellurium is substantiated by the observation of intergranular penetration of this element shown in Figures 27 - 29.

The cracking and spalling of the pre-oxidised layer was brought about by the thermal shock that the specimens received when the temperature was lowered subsequent to the oxidation treatment. However, this effect may not be too far removed from the situation at the internal surface of an A.G.R. fuel pin. Although the inner surface of the fuel clad may be oxidised the thermal cycling of the fuel during normal reactor operation could cause cracking of this layer and thus aid any subsequent attack by fission product tellurium.

5.10.4. Overall Mechanism.

The results obtained from the studies using $1 mg.mm^{-2}$ of tellurium and those using pre-oxidised materials have provided additional mechanistic data. It is now possible to incorporate this evidence to establish the overall mechanism of the reaction between tellurium and 20%Cr/25%Ni/niobium stabilised stainless steel. This is now defined in the following series of steps.

a) Adsorption of tellurium on to the metal surface and thence gross reaction to form a thin surface layer. Evidence for this is detailed in section 5.7. where small amounts of chromium in the outer iron-nickel rich product were observed.

b) Diffusion of nickel and iron through this layer to form tellurides. This is substantiated by two observations. First there is no evidence of tellurium penetration in the early stages of attack (Table 14) and secondly the positioning of the iron-nickel-tellurium product outside the original steel surface.

c) Formation of chromium telluride beneath the original stainless steel surface and intergranular attack of the steel by tellurium. This is achieved either by the direct elemental penetration of tellurium or via dissociation of the iron-nickel tellurides. This step is substantiated by the positioning of the chromium telluride layer beneath the pre-oxidised layer.

d) Growth of the chromium telluride product at the expense of the iron-nickel rich outer layer. This continues after the exhaustion of the external tellurium supply and

occurs because of the greater thermodynamic stability of the chromium product.

Growth cannot take place at the outer surface of the chromium telluride layer because the residual iron and nickel are not observed dispersed in the outer regions of the final product. Instead they are generally present on the surface of the chromium product. Similarly at the inner surface, chromium depletion of the steel is observed showing that it has diffused into the product and also iron and nickel are not observed in the inner layers of the product. Therefore it would appear that the chromium telluride layer is growing within the existing chromium product where the outward diffusion of chromium meets the inward diffusion of tellurium.

Also at this stage there was evidence that a reaction occurred below the general reaction product with segregation of the iron-nickel and the chromium. It was apparent that this reaction was proceeding according to a similar mechanism as that being discussed and was supplied with tellurium either by the cracking of the main product or diffusion of tellurium through that product.

e) Formation of sub-surface voids. These occur possibly by the migration of vacancies, the dissociation of chromium telluride particles in a chromium depletion gradient or volatilisation of the telluride product in the grain boundaries.

and f) Continued chromium depletion in the bulk metal in an attempt to even out the concentration profile.

5.11. Summary.

The study of the reaction between tellurium and 20%Cr/25%Ni/niobium stabilised stainless steel undertaken in this chapter has shown that the reaction occurred with increasing rapidity at temperatures 350°C and above. Long term exposure at 750°C and above resulted in subsurface, intergranular voidage and significant chromium depletion of the underlying matrix.

The reaction between the tellurium vapour and the stainless steel progressed in several stages:-

(i) The early stages involved the outward diffusion of the nickel and iron constituents of the steel. The order of reaction was determined as nickel > iron > chromium and resulted in the formation of a single layer product of nickel and iron tellurides; segregation of the nickel and iron tellurides was only observed after short exposures at 350° and 450°C.

(ii) The intermediate stage was the development of a duplex reaction product as a chromium telluride layer formed beneath the iron-nickel rich layer. The rate controlling parameter for this stage of the reaction was determined as the diffusion of tellurium through the outer product.

(iii) The final stage of the reaction was determined by the thermodynamic stabilities of the tellurides. The order of thermodynamic stability was found to be chromium telluride > nickel telluride > iron telluride. Consequently the resultant product was a single layer of chromium telluride (CrTe).

Subequently, void formation occurred in the stainless

steel and continued chromium depletion was apparent.

It has been shown experimentally that chromium oxide is more stable than chromium telluride and it is for this reason that pre-oxidation of the steel surface afforded protection in regions where the oxide layer remained intact. However, reaction occurred as above in areas where spalling had taken place. Cracking of the oxide allowed localised tellurium reaction to take place.

CHAPTER SIX. TECHNOLOGICAL IMPLICATIONS.

6.1. Introduction.

The only entirely new feature in the A.G.R. is the fuel, and the much higher ratings and temperatures involved increase the problem of selecting reactor materials. In order to establish a safe, as well as an efficient, range of operating temperatures it has been necessary to determine the properties of uranium dioxide fuels in a variety of conditions. The studies presented in this thesis assist the appraisal of the continued integrity of the nuclear fuel in the A.G.R.

6.2. Fission Product Compatibility.

Earlier considerations (Chapter 2) have shown that unirradiated stoicheiometric and hypostoicheiometric uranium dioxide are compatible with stainless steel at temperatures suitable for A.G.R. operation. However reactions can occur at the inner surface of the fuel cladding during irradiation due to the release of fission products from the fuel during this period. This study has shown that the three volatile fission products, caesium, iodine and tellurium can have an influence on the inner surface of the steel.

It is apparent from the available literature that for caesium attack to be paramount then a significant oxygen potential should exist. In thermal irradiation the low oxygen potential should therefore limit the corrosive effects of this element. Similarly the attack of the steel clad by iodine should be restricted due to the greater thermodynamic

stability of caesium iodide compared to the steel iodides (Figure 3). Furthermore reaction between caesium iodide and stainless steel has been shown to occur only in the presence of oxygen and the reaction has been similar to that observed for caesium. However the post irradiation studies discussed in Chapter 4 show that factors other than the thermodynamic considerations may be relevent and circumstantial evidence suggests that iodine could well have been involved in the formation of the reaction products observed.

The involvement of caesium in the post-failure oxidation of the inner surface of the clad is more significant and has implications with respect to reactor operation. Thus, the data showed that following can failure the presence of fission products in association with an oxidising environment was sufficient to enhance the oxidation rate by $>10^3$ times. Enough caesium was detected in the reaction product to alter the composition of the protective chromium oxide layer to a presumably less protective caesium chromate. The operational implication of this work was that any failed fuel should be removed from the reactor as soon as possible after failure to limit fission product release.

The examination of the reaction between tellurium and 20%Cr/25%Ni/niobium stabilised stainless steel represents the first detailed study of the stainless steel-tellurium system. Such reactions could conceivably occur at a number of sites. Thus in high temperature regions ($\geq 650^{\circ}C$) localised attack may be expected in the immediate vicinity of fuel cracks where fission product "streaming" to the inner clad

surface occurs. However only low concentrations of tellurium will be present and thus attack would be expected to be limited to similar levels as shown in the low concentration studies described in section 5.7.

Reaction might also be expected at lower temperatures due either to movement of tellurium from high to low temperature regions or to the decomposition of tellurides formed in the higher temperature areas. This latter mechanism could be achieved by the conditions shown in the temperature gradient experiment. Movement of tellurium by either mechanism could result in the end cap region of the fuel pin being susceptible to this form of attack where possibly 0.5 grams of tellurium could be expected to accumulate assuming that 10% is released from the fuel.

It should be noted however that under reactor conditions tellurium could react with the excess caesium present in a fuel pin. Conflicting evidence is presently available on the outcome of such an association. Götzmann et al. (1974) state that it reduces the effectiveness of the tellurium because the caesium compound is thermodynamically more stable than the corresponding chromium compound but Batey and Bagley (1974) and Maiya and Busch (1975) have shown that the addition of caesium to tellurium, either to form a caesium-tellurium mixture or caesium telluride(Cs_2Te) compound, did not effect the corrosive nature of tellurium.

It may be expected that an oxidising environment will exist within the fuel pin during operation. Thus the internal surface of the stainless steel may become oxidised forming a chromium oxide layer. It was shown in section 5.10.3. that

the presence of such a pre-formed film inhibits the corrosive effects of tellurium. However, this film may be broken down either by mechanical cracking during operational thermal cycling or chemically by reaction with caesium iodide. In either case the protection afforded against tellurium attack will be diminished.

Finally, in the event of a fuel pin failure, it has been shown that steel tellurides are less stable than their respective oxides in a carbon dioxide environment. Also it is established (see Figure 3) that chromium possesses the most stable oxide and nickel the least stable oxide in an oxidising environment. Thus although chromium telluride is the most stable in a tellurium atmosphere it will become the least stable in an oxidising situation. This is analogous to the iodide-oxide system discussed by Ramsdale and Hilton (1972).

Therefore it may be expected that during a failure process resulting in ingress of carbon dioxide, subsequent to a stainless steel-tellurium reaction, the chromium telluride product which would normally be present will be oxidised by the carbon dioxide. Thus in any subsequent post irradiation examination the tellurium would either be observed in the elemental state or possibly combined with nickel (i.e. the least stable of the oxides).

6.3. Summary.

The uranium dioxide fuel used in the A.G.R. is compatible with the 20%Cr/25%Ni/niobium stabilised stainless steel cladding material but the presence of fission products could have an influence in two ways:-

(a) Subsequent to fuel pin failure enhanced-clad oxidation can be caused by the involvement of caesium. Corrosion rates, possibly $> 10^3$ times that normally observed may be expected due to the possible formation of caesium chromate. It would be necessary to discharge such fuel as soon as possible to avoid excessive release of fission products.

and (b) Although the study of irradiated clad inner surfaces did not show that the extent of attack was detrimental to the life of an A.G.R. fuel pin, reaction between fission product tellurium (and possibly iodine) and the stainless clad will occur. The cooler end cap regions are the most likely areas for this type of attack to cause concern.

CHAPTER SEVEN. CONCLUSIONS.

The evidence obtained in the post irradiation examination did not show that the extent of attack on the inner surface of unfailed A.G.R. cladding was detrimental to the life of a fuel pin. However, two types of reaction product were observed and cross sectional examination revealed both a general attack (maximum depth approximately 22μm) and an attack characterised by a "double-layer" effect. Tellurium was the only fission product observed below the surface of any reaction on the unfailed clad surfaces although there was circumstantial evidence that iodine may have been involved.

An enhanced oxidation rate ($>10^3$ times) was observed on the failed A.G.R. clad specimen. It is believed that this was caused by fission product caesium modifying the protective chromium oxide layer to less protective caesium chromate.

The study of the reaction between tellurium and 20%Cr/25%Ni/niobium stabilised stainless steel showed that the reaction occurred with increasing rapidity at temperatures 350°C and above. The order of reaction was determined as nickel > iron > chromium and resulted initially in the formation of a single layer product of iron and nickel tellurides, followed by the development of a duplex product and finally a single chromium telluride reaction layer. The stabilities of the steel tellurides were determined as chromium telluride > nickel telluride > iron telluride.

The mechanism of tellurium attack has been evolved and is detailed in section 5.10.4. The early stage of the reaction is concerned with the outward diffusion of iron and nickel whilst the latter stages are determined by the inward movement of tellurium through the outer reaction layer and the outward diffusion of chromium.

It has been shown that chromium oxide is more stable than chromium telluride and therefore pre-oxidation of the stainless steel surface inhibits the attack by tellurium except in regions where this protective layer is either damaged or removed.

APPENDIX I

Alloy Compositions

Alloy	Constituents [%]									Others
	Cr	Ni	Fe	Mo	Mn	Si	C	P	S	
304	18-20	8-12	Bal		≯2.00	≯1.00	≯0.08	≯0.045	≯0.030	
304L	18-20	8-12	Bal		≯2.00	≯1.00	≯0.03	≯0.045	≯0.030	
316	16-18	10-14	Bal		≯2.00	≯1.00	≯0.08	≯0.045	≯0.030	
316L	16-18	10-14	Bal		≯2.00	≯1.00	≯0.03	≯0.045	≯0.030	
321	17-19	9-12	Bal		≯2.00	≯1.00	≯0.08	≯0.045	≯0.030	≮5xC Nb
347	17-19	9-13	Bal		≯2.00	≯1.00	≯0.08	≯0.045	≯0.030	≮10xC Ta
20/25/Nb	19-21	24-26	Bal		0.55-0.85	0.45-0.75	0.01-0.07	≯0.02	≯0.02	≮10xC Nb
FV548	16-17	11-12	Bal	1.0-1.75			0.06-0.09			1.00 Nb
M316	17.0	13.5	Bal	2.5			0.03-0.06			
Hastelloy X	22	47	18.5	9	0.5	0.5	0.1			0.6W 1.5 Co
Incoloy 800	22.5	32	46		0.75	0.35	0.04			0.30 Cu
Inconel 600	15.8	76	7.2		0.20	0.20	0.04			0.10 Cu

APPENDIX TWO

An Estimation of the Amount of Fission Product Tellurium in a C.A.G.R. Fuel Pin.

It is evident from the data shown in Table A.2.1. that each tellurium isotope, apart possibly from ^{135}Te, exists for sufficient time, especially at the higher temperatures, to contribute towards the attack of the stainless steel cladding material. The relevent fission product densities, expressed as the number of atoms per tonne of uranium dioxide, are displayed in Table A.2.2. for an A.G.R. fuel element irradiated to 18,000 MWD.te^{-1} at 13 MW.te^{-1}. However this presents the amount of each fission product at the end of the irradiation; therefore to determine the total amount of tellurium generated an allowance must be made for the tellurium that has decayed during this period.

Table A.2.3. shows the fractional independent fission yield for each of the relevent decay chains (Tobias, 1973) and thence the amount of each nuclide that will have originated via a tellurium isotope. Thus, by combining these data with that expressed in Table A.2.2. the total amount of tellurium generated during an 18,000 MWD.te^{-1} irradiation (over a 1385 day period) is calculated as 1.80×10^{25} atoms per tonne of uranium dioxide or 5.7 grams per pin. This represents an overall concentration at the clad inner surface of 0.12 mg.mm^{-1} assuming that all of the generated tellurium is released evenly to the outer regions of the fuel.

TABLE A.2.1.

Half-lives of Tellurium Isotopes.

Isotope	Half-life
^{124}Te	stable
^{125}Te	stable
^{125m}Te	58 days
^{126}Te	stable
^{127}Te	9.3 hours
^{127m}Te	109 days
^{128}Te	stable
^{129}Te	69 minutes
^{129m}Te	34 days
^{130}Te	stable
^{131}Te	25 minutes
^{131m}Te	30 hours
^{132}Te	78 hours
^{133}Te	125 minutes
^{133m}Te	53 minutes
^{134}Te	43 minutes
^{135}Te	11 seconds

Table A.2.2. Fission Product Densities for an A.G.R. Fuel Element Irradiated to 18,000 MWD.te^{-1} over 1385 days.

AG122	1.396E 13	SB122	4.130E 14	IN122	1.549E 15	SN122	1.155E 22	SB122M	3.270E 13
		SC122	6.085E 16	TE122	1.504E 19				
IN123M	3.707E 15	IN123	4.630E 14	SN123M	4.070E 17	SN123	1.547E 20	SB123	1.200E 22
		TE123M	0.0	TE123	0.0	*SB124M1	1.999E 12	*SB124	7.258E 18
		*TE124	4.569E 19						
IN124	4.797E 14	SN124	1.434E 22	SB124M2	0.0	SB124M1	1.696E 14	SB124	1.690E 19
		TE124	2.112E 20						
IN125M	1.901E 14	IN125	1.333E 15	SN125M	7.801E 16	SN125	1.128E 20	SB125	1.314E 22
		TE125M	1.757E 20	TE125	7.173E 21	*SN126	1.122E 17	*TE126	1.174E 19
IN126	4.942E 14	SN126	4.841E 22	SB126M	3.525E 16	SB126	3.755E 19	TE126	3.987E 21
		I126	0.0	XE126	0.0				
IN127	1.680E 15	SN127M	1.814E 17	SN127	5.557E 18	SB127	5.320E 20	TE127M	2.568E 21
		TE127	5.239E 19	I127	1.061E 23	*I128	2.898E 16		
IN128	3.023E 15	SN128	9.632E 18	SB128	1.949E 18	SB128M	1.638E 19	TE128	2.766E 23
		I128	8.340E 14	XE128	3.563E 19	*XE129	2.659E 17		
IN129	6.342E 14	SN129M	3.502E 17	SN129	1.042E 18	SB129	1.104E 20	TE129M	3.704E 21
		TE129	2.833E 19	I129	5.470E 23	XE129	4.381E 16	*I130	2.355E 19
IN130	3.831E 14	SN130	1.482E 18	SB130M	2.437E 18	SB130	1.547E 19	TE130	1.084E 24
		I130M	4.547E 15	I130	7.000E 17	XE130	1.056E 21		
IN131	1.339E 14	SN131	3.689E 17	SB131	2.191E 19	TE131M	2.634E 20	TE131	2.518E 19
		I131	1.287E 22	XE131M	2.902E 20	XE131	1.388E 24		
SN132	1.624E 17	SB132	3.625E 18	TE132	7.490E 21	I132	2.219E 20	XE132	2.185E 24
		CS132	0.0	BA132	0.0	*XE133M	5.653E 17	*XE133	1.940E 19
		CS133	1.506E 21						
SN133	2.046E 15	SC133	2.724E 18	TE133M	4.831E 19	TE133	1.709E 19	I133	2.824E 21
		XE133M	1.668E 20	XE133	1.714E 22	CS133	2.772E 24	*CS134	2.290E 23
		*CS135	2.002E 22						
SB134	1.066E 17	TE134	8.922E 19	I134M	8.946E 17	I134	1.367E 20	XE134	3.662E 24
		CS134	9.736E 19	BA134	3.263E 19				
SB135	5.834E 15	TE135	4.162E 17	I135	8.942E 20	XE135M	5.876E 18	XE135	3.020E 20
		CS135	7.959E 23	BA135M	0.0	BA135	3.588E 17	*XE136	2.351E 24
		*CS136	6.612E 20						
TE136	2.676E 17	I136M2	6.740E 17	I136M1	1.370E 18	I136	6.308E 17	XE136	3.096E 24
		CS136	1.159E 20	BA136	6.487E 21				
TE137	2.098E 16	I137	6.110E 17	XE137	8.054E 18	CS137	2.852E 24	BA137M	4.344E 17
		BA137	1.298E 23						

TABLE A.2.3.

Fractional Yields of Tellurium Isotopes.

Mass no.	Nuclide (subsequent to Te in chain)	Fractional independent fission yield from ^{235}U	∴ Factor to calculate yield via tellurium nuclide
123	^{124m}Sb	0.0	1.00
	^{124}Sb	via neutron capture	
125	^{126}Sn	0.0 via neutron capture	1.00
126	I	0.0	1.00
	Xe	0.0	1.00
127	I	0.0	1.00
128	I	0.0001	0.9999
	Xe	0.0	0.9999
129	I	0.0001	0.9999
	Xe	0.0	0.9999
130	I	0.0003	0.9997
	Xe	0.0	0.9997
131	I	0.0050	0.9950
	Xe	0.0	0.9950
132	I	0.0045	0.9955
	Xe	0.0	0.9955
	Cs	0.0	0.9955
	Ba	0.0	0.9955
133	I	0.0147	0.9853
	Xe	0.0	0.9853
	Cs	0.0	0.9853
134	I	0.1549	0.8451
	Xe	0.0029	0.8426
	Cs	0.0	0.8426
	Ba	0.0	0.8426
135	I	0.3658	0.6342
	Xe	0.0363	0.6112
	Cs	0.0004	0.6109
	Ba	0.0	0.6109
136	I	0.5522	0.4478
	Xe	0.0822	0.4110
	Cs	0.0009	0.4106
	Ba	0.0	0.4106
137	I	0.5248	0.4752
	Xe	0.2602	0.3550
	Cs	0.0214	0.3474
	Ba	0.0003	0.3473

ACKNOWLEDGEMENTS.

I gratefully acknowledge the help and encouragement of Dr.D.A.Hilton and Dr.G.B.Briscoe during the course of this work and to Dr.R.C.Lobb for valuable discussions during the preparation of Chapter 5.

The study was undertaken at the Berkeley Nuclear Laboratories of the Central Electricity Generating Board and I am indebted to Dr.B.Edmondson for permission to publish this work in thesis form.

REFERENCES.

Adams, M.D., 1967, ANL 7399.

Adamson, M.E., Rand, M.H., 1969, AERE R 6034.

Aitken, E.A., Evans, S.K., Rosenbaum, H.S., Rubin, B.F., 1971, Trans. Amer. Nucl. Soc. 14. 1. 176.

Allen, G.C., 1972, Private Communication.

Allen, G.C., 1973, Private Communication.

Andriessen, H., Hoppe, N., Tavernier, W.de, Soenen, M., 1970, Proc. Int. Meeting on Fast Reactor Fuel and Fuel Elements, Kernforschungszentrum, Karlsruhe.

Antill, J.E., Peakall, K.A., Smart, E.F., 1975, J. Nucl. Mater. 56. 47.

Auger, P., 1925a, Compt. Rand. 180. 65.

Auger, P., 1925b, J. Phys. Rad. 6. 205.

Bagnell, K.W., 1966, The Chemistry of Selenium, Tellurium and Polonium, Elsevier Publishing Co. Amsterdam.

Bailey, W.E., Zebroski, E.L. 1970, GEAP 10028-34.

Barney, W.K., Wemple, B.D., 1958, KAPL 1836.

Batey, W., Bagley, K.Q., 1974, J. Brit. Nucl. Energy Soc. 13. 1. 49.

Beraha, E., 1968, Pract. Metallography 5. 443.

Blackburn, P.E., Johnson, C.E., Battles, J.E., Johnson, I., Markin, A.E., Tetenbaum, M., Crouthamel, C.E. Tevebaugh, A.D., Vogel, R.C., 1971, ANL 7822.

Bober, M., Schumacher, G., 1973, in Advances in Nuclear Science and Technology Vol. 7. Academic Press, New York.

Bragg, W.L., 1912, Proc. Cambridge Phil. Soc., 17. 43.

Brookes, S.L., 1952, Amer. Chem. Soc., 74. 227.

Brown, A.F., Healey, T., 1969, CEGB report RD/B/N1374.

Calais, D., Aubert, M., Le Beuze, R., Conte, M., Mikailoff, H., 1974, IAEA Sym. on Thermodynamics of Nuclear Materials, Vienna.

Calais, D., Conte, M., Kerculas, F.de, Le Beuze, R., 1972, IAEA Panel on Behaviour and Chemical State of Fission Products in Irradiated Fuel, Vienna.

Castaing, R., 1951, Thesis, University of Paris.

Castaing, R., 1960, Advances in Electronics and Electron Physics, Vol. 13, Academic Press, New York.

Chandler, W.T., 1962, TID 7626.

Christensen, J.A., 1963, HW 76302.

Cooper, W.C., 1971, Tellurium, Van Nostrand Reinhold Co.,New York.

Coquerelle, M., Gabolde, J., Lesser, R., Werner, P., 1972, Nucl. Technol. 16. 110.

Cowen, H.C., Webster, S.J., 1973, BNES Conf. on Nuclear Fuel Performance, London.

Cox, C.M., Olsen, A.R., Fitts, R.B., Long, E.L.Jr., 1971, Trans. Amer. Nucl. Soc. 14. 1. 173.

Cunningham, J.E., Beaver, R.J., Thurber, W.C., Waugh, R.C., 1958, TID 7546.

Debye, P., Scherrer, P., 1916, Physik. 17. 277.

Debye, P., Scherrer, P., 1917, Physik. 18. 291.

Dulgeroff, C.R., Seele, G.D., 1960, AFOSR-TR-60-112.

Duncumb, P., Jones, E.M.(Mrs.), 1969, TIRL report 260.

Eadie, A., 1975, Atom 228. 185.

Elkins, H.B., 1950, The Chemistry of Industrial Toxicology, John Wiley and Sons Inc. New York.

Ephrain, F., 1949, Inorganic Chemistry, 5th. Edition, Gurney.

Evans, H.E., Hilton, D.A., Holm, R.A., 1976 CEGB report RD/B/N3416.

Findlay, J.R., 1972, IAEA Panel on Behaviour and Chemical State of Fission Products in Irradiated Fuels, Vienna.

Fish, R.L., Holmes, J.J., Leggett, R.D., 1970, BNWL 1323.

Fitts, R.B., Long, E.L.Jr., Cuneo, D.R., 1970, ORNL 4589.

Fitts, R.B., Long, E.L.Jr., Leitnaker, J.M., 1971, ORNL-TM-3385.

Francis, J.M., Curtis, M.T., Hilton, D.A., 1971, J. Nucl. Mater. 41. 2. 203.

Gibbs, G.B., Hales, R., 1973, CEGB report RD/B/N2706.

Glassner, A., 1965, ANL 5750.

Götzmann, O., Thümmler., F., 1968, KFK 1081.

Götzmann, O., 1969, KFK 1086.

Götzmann, O., Hofmann, P., 1972, KFK 1546.

Götzmann, O., Hofmann, P., Thümmler, F., 1974, J. Nucl. Mater. 52. 33.

Gurinsky, D., 1964, NASA-SP-41.

Gurinsky, D.H., Weeks, J.R., Klamut, J.R., Rosenblum, L., DeVan, J.H., 1965, 3rd. Int. Conf. on the Peaceful Uses of Atomic Energy, Vol.9, Geneva.

Hampel, C.A., (Ed.), 1961, Rare Metals Handbook (2nd. Edition), Chapman and Hall, London.

Harris, L.A., 1968a, J. Appl. Phys. 39. 3. 1419.

Harris, L.A., 1968b, J. Appl. Phys. 39. 3. 1428.

Hoechel, J., 1971, Statement at Amer. Nucl. Soc., Fast Reactor Fuel Element Technology, New Orleans.

Hofmann, P., Thümmler, F., Wedemeyer, H., 1969, KFK 979.

Hull, A.W., 1917a, Phys. Rev. 9. 84. 564.

Hull, A.W., 1917b, Phys. Rev. 10. 661.

Johnson, C.E., Crouthamel, C.E., Chen, H., Blackburn, P., 1969, Trans. Amer. Nucl. Soc., 12. 2. 565.

Johnson, C.E., Crouthamel, C.E., 1970, J. Nucl. Mater. 34. 101.

Johnson, C.E., Crouthamel, C.E., 1971a, Trans. Amer. Nucl. Soc. 14. 1. 173.

Johnson, C.E., Crouthamel, C.E., 1971b, Trans. Amer. Nucl. Soc. 14. suppl. 1. 17.

Jones, K.W., 1972, Private Communication.

Keroulas, F.de, Le Beuze, R., Calais, D., Marcon, J.P., 1971, Fall Meeting of the French Soc. of Metallurgy.

Keroulas, F.de, Le Beuze, R., Calais, D., Van Craeynest, A., Conte, M., 1972, J. Nucl. Mater. 43. 313.

Kluch, R.L., Jansen, D.H., 1967, ORNL-TM-1813.

Kwast, H., 1971, RCN 144.

Lander, J.J., 1953, Phys. Rev. 91. 6. 1382.

Lauritzen, T.A., Novak, P.E., Davies, J.H., 1966, GEAP 4466.

Lauritzen, T.A., Comprelli, F.A., 1976, Trans. Amer. Nucl. Soc. 10. 2. 459.

Lauritzen, T.A., 1968, GEAP 5633.

Lawson, R.L.J., 1969, MSc. Thesis, University of Aston in Birmingham.

Levinson, D.W., 1964, IIPRI-B215-22.

Lobb, R.C., Jones, R.B., 1973, Int. Conf. on Phys. Metallurgy of Fuel Elements, Berkeley.

Lobb, R.C., 1976, To be published.

Long, J.V.P., Cosslet, V.E., 1957, in X-ray Microscopy and Microradiography, Academic Press, New York.

Maiya, P.S., 1971, Trans. Amer. Nucl. Soc. 14. 2. 599.

Maiya, P.S., Busch, D.E., 1972, J.Nucl. Mater. 44. 96.

Maiya, P.E., Busch, D.E., 1975, Met. Trans. 6A. 409.

Martin, P.M., Poole, D.M., 1971, Met. Rev. 16. 19.

McCarthy, W.H., Bennett, J.W., Hull, G.R., Perry, K.J., 1971, GEAP 13735.

McCarthy, W.H., Perry, K.J., Hull, G.R., Bennett, J.W., 1972, Nucl. Technology 16. 1. 171.

McCoy, H.E., 1965, Corrosion 21. 84.

Mead, L.D., Gies, W.J., 1900, Am. J. Physiol. 3. 20.

Morgan, W.W., Hart, R.G., Jones, R.W., Edwards, W.J., 1961, CRDC 1027.

Moseley, H.G.J., 1913, Phil. Mag. 26. 1024.

Moseley, H.G.J., 1914, Phil. Mag. 27. 703.

Neimark, L.A., Brown, F.L., 1969, ANL 7606.

Neimark, L.A., Brown, F.L., Natesh, R., Petkus, E.J., Murphy, W.F., 1969, ANL 7577

Neimark, L.A., Lambert, J.D.B., 1971, ANL 7753

Ohse, R.W., Schlechter, M., 1972, EUR 4893e

Perry, K.J., Craig, C.N., 1969, Trans. Amer. Nucl. Soc. 12. 2. 564.

Perry, K.J., Melde, G.F., Duncan, R.N., Trans. Amer. Nucl. Soc. 14. suppl. 1. 17.

Perry, K.J., Melde, G.F., McCarthy, W.H., Duncan, R.N., 1971, Proc. of Conf. of Amer. Nucl. Soc. on Fast Reactor Fuel Element Technology, New Orleans.

Philips, J.R., Waterbury, G.R., Vanderbough, N.E., 1974, J. Inorg. Nucl. Chem. 36. 1. 17.

Pritchard, W.C., Johnson, K.A., Leary, J.A., 1963, LA 2828.

Ramsdale, J.K.(Mrs.), Hilton, D.A., 1972, CEGB report RD/B/N2337.

Rand, M.H., Markin, T.L., 1967, AERE-R-5560.

Reed, D., Ramsdale, J.K.(Mrs.), 1971, CEGB report RD/B/N2022.

Ring, P.J., Challenger, K.D., Busboom, H.J., 1972, Nucl. Technology 16. 104.

Robins, I.H., 1972, Unpublished Work.

Rosen, S., Simmons, J.M., Aitken, E.A., Frost. B.R.T., Tevebaugh, A.D., Sheely, W.F., 1971, 4th. Int. Conf. on the Peaceful Uses of Atomic Energy, Geneva.

Rubin, B.F., Perry, K.J., 1969, GEAP 5761.

Simon, R.H., Lindgren, J.R., Siltanen, J.N., Fitts, R.E., 1970, Proc. Int. Meeting on Fast Reactor Fuel and Fuel Elements, Kernforschungszentrum, Karlsruhe.

Skavdahl, R.E., Zebroski, E.L., 1967a, GEAP 5491.

Skavdahl, R.E., Zebroski, E.L., 1967b, GEAP 5522.

Skavdahl, R.E., Zebroski, E.L., 1968, GEAP 5584.

Skinner, J., Newbigging, A.W.P., 1973, BNES Int. Conf. on Nuclear Fuel Performance, London.

Smith, A.F., 1969a, Met. Sci. J. 3. 93.

Smith, F.M., 1969b, BNWL 1101.

Smith, A.F., Killeen, J.C., Wild, R.K., 1974, CEGB report RD/B/N3098.

Sparry, R.P., Pearce, R.J., 1972, CEGB report RD/B/N2385.

Stone, J.R., Carbon, P.E., 1961, in Rare Metals Handbook (2nd. Edition), Chapman and Hall, London.

The Times, 1976, 59799. 16.

Tobias, A., 1973, CEGB report RD/B/M2669.

USAEC report, 1967, GA 8107.

Van Arkel, A.E., De Boer, J.H., 1925, Z. Anorg. Chem. 148. 345.

Weber, R.E., Peria, W.T., 1967, J. Appl. Phys. 38. 4355.

Weber, J.W., Jensen, E.D., 1971, Trans. Amer. Nucl. Soc. 14. 1. 175.

Whitlow, W.H., Hilton, D.A., 1972, Unpublished Work.

Wild, R.K., 1974, Private Communication.

Winslow, P.M., 1965, Corrosion 21. 11. 341.

Zeitz, L., Baez, A.V., 1957, in X-ray Microscopy and Microradiography, Academic Press, New York.

Notes on the abbreviations used in the references.

The report designated CRDC is issued by the Atomic Energy of Canada Ltd.

Reports designated CEGB are issued by the Central Electricity Generating Board.

Reports designated EUR, KFK, RCN are issued by the Commission of the European Communities.

The report designated TIRL is issued by Tube Investments Research Laboratories.

Reports designated AERE are issued by the United Kingdom Atomic Energy Authority.

The report designated AFOSR is issued by the United States Air Force Office of Scientific Research.

Reports designated ANL, BNWL, GA, GEAP, HW, IITRI, KAPL, LA, NASA, ORNL, TID are issued by the United States Atomic Energy Commission (USAEC).